

AD-A189 579



EXPERIMENTAL INVESTIGATION OF A CO-H_2
DIFFUSION FLAME USING HIGH-FREQUENCY
THERMOMETRY

THESIS

Moisés Fernández Alvaro, Major SAF

AFIT/GEP/ENP/87D-7

DTIC
ELECTE
MAR 02 1988
S
H

DEPARTMENT OF THE AIR FORCE
AIR UNIVERSITY

AIR FORCE INSTITUTE OF TECHNOLOGY

Wright-Patterson Air Force Base, Ohio

DISTRIBUTION STATEMENT A

Approved for public release;
Distribution Unlimited

88 3 01 05 4

EXPERIMENTAL INVESTIGATION OF A CO-H₂
DIFFUSION FLAME USING HIGH-FREQUENCY
THERMOMETRY

THESIS

Moisés Fernández Alvaro. Major SAF

AFIT/GEP/ENP/87D-7

DISTRIBUTION STATEMENT A

Approved for public release;
Distribution Unlimited

DTIC
ELECTE

MAR 02 1988

H

AFIT/GEP/87D-7

EXPERIMENTAL INVESTIGATION OF A CO-H₂ DIFFUSION
FLAME USING HIGH-FREQUENCY THERMOMETRY

THESIS

Presented to the Faculty of the School of Engineering
of the Air Force Institute of Technology

Air University

In Partial Fulfillment of the
Requirements for the Degree of
Master of Science

Moisés Fernández Alvaro, M.S.

Major. SAF

December 1987

Approved for public release; distribution unlimited

Preface

The purpose of this study was to measure the temporal-spatial temperature distributions in a non-sooting CO-H₂ diffusion flame at high repetition rates. The observations of such a flame at $Re = 857$ revealed the existence of both low frequency oscillations associated with large scale buoyancy-driven vortices and relatively high frequency oscillations believed to be a characteristic of the internal cold jet fuel core of the flame. Other H₂-CO:N₂ gas mixtures (using the N₂ as diluent) were investigated up to $Re = 2264$, and similar high frequency oscillations were found.

For this research the novel thin filament pyrometry (TFP) technique, developed by Goss, Villimpoc and Sarka, was employed: this technique relies upon the blackbody emission of a thin ceramic filament (SiC) in a combustng flowfield. Radial temperature profiles were taken by the TPF technique in the H₂-CO flames at 10 mm axial increments.

A laser-sheet lighting technique consisting of two perpendicular sheets was used to visualize the flame structure: this technique involves seeding both the central fuel jet and co-annular air with TiCl₄ vapor.

In performing the experiments and writing this thesis, I have had a great deal of help from others. I wish to thank my thesis sponsor Sigmund W. Kizirnis, for his continuous interest, support and counselling. Dr. Viroj

tion For

GRA&I

IB

nced

ation

ution/

Availability Codes

Avail and/or
Special

Dist

A-1



Villimpoc for this guidance through this study, and Dr. Larry P. Goss for his help on computer programing. A word of thanks is also owed to Dr. W.M. Roquemore and Dr. L-D. Chen for their help in the theoretical aspects of the combustion phenomena.

Moisés Fernández Alvaro

Table of Contents

	Page
Preface	ii
List of Figures	vi
List of Tables	viii
Abstract	ix
I. Introduction	1
Background	1
Objective and Approach	10
II. Theory	13
Thin Filament Pyrometry Technique	13
Laser-Sheet Lighting Technique	20
III. Experimental Apparatus	22
Experimental Setup for the TFP Technique	22
Rotating Mirror	22
Diode Detector	24
Digitizer	24
Triggering Laser	25
Experimental Setup for the L-S Lighting technique	25
IV. Experimental Procedure	28
Experimental Procedure for the TFP technique	28
Calibration Procedure	28
Data Analysis	30
V. Results and Discussion	34
Flow Visualization Studies	34
TFP technique	37
Temperature Profiles	38
Frequency Analysis	55
VI. Conclusions and Recomendations	63
Bibliography	66

Appendix A: Temperature Profiles of N ₂ -CO-H ₂ Diffusion Flame and Intensity Contour Lines at Various Axial Locations; Re = 857	71
Appendix B: Temperature Profiles of N ₂ -CO-H ₂ Diffusion Flame and Intensity Contour Lines at Various Axial Locations; Re = 2264	83
Appendix C: Temperature Profiles of N ₂ -CO-H ₂ Diffusion Flame and Intensity Contour Lines at Various Axial Locations; Re = 2099	95
Appendix D: Temperature Profiles of N ₂ -CO-H ₂ Diffusion Flame and Intensity Contour Lines at Various Axial Locations; Re = 1717	99
Vita	102

List of Figures

Figure		Page
1.	Bi-dimensional Visualization of a Flame in two Perpendicular Planes	11
2.	Experimental Arrangement for Measuring Emissivity of SiC Filament by Reflectance . . .	17
3.	Relative Emission Curve from SiC Thin Filament as Detected by InGaAs Detector . . .	19
4.	Spectral Responsivity Characteristic of InGaAs Detector	19
5.	Thin Filament Pyrometry Optical Set-up	23
6.	Experimental Set-up of Jet Diffusion Flame Visualization Technique	26
7.	Image of CO-H ₂ Diffusion Flame at Re=857 H ₂ /CO=3.391 and f=4 & 5.6	35, 36
8.	Temperature Profiles of CO-H ₂ Diffusion Flame and Intensity Contour Lines at 0 mm Axial Location	39
9.	Temperature Profiles of CO-H ₂ Diffusion Flame and Intensity Contour Lines at 20 mm Axial Location	40
10.	Temperature Profiles of CO-H ₂ Diffusion Flame and Intensity Contour Lines at 40 mm Axial Location	41
11.	Temperature Profiles of CO-H ₂ Diffusion Flame and Intensity Contour Lines at 60 mm Axial Location	42
12.	Temperature Profiles of CO-H ₂ Diffusion Flame and Intensity Contour Lines at 80 mm Axial Location	43
13.	Temperature Profiles of CO-H ₂ Diffusion Flame and Intensity Contour Lines at 100 mm Axial Location	44
14.	Temperature Profiles of CO-H ₂ Diffusion Flame and Intensity Contour Lines at 130 mm Axial Location	45

15.	Temperature Profiles of CO-H ₂ Diffusion Flame and Intensity Contour Lines at 140 mm Axial Location	46
16.	Temperature Profiles of CO-H ₂ Diffusion Flame and Intensity Contour Lines at 160 mm Axial Location	47
17.	Temperature Profiles of CO-H ₂ Diffusion Flame and Intensity Contour Lines at 180 mm Axial Location	48
18.	Temperature Profiles of CO-H ₂ Diffusion Flame and Intensity Contour Lines at 200 mm Axial Location	49
19.	Detail of Intensity Contour Lines at 40 mm Axial Location	54
20.	Frequency Distribution Profiles of CO-H ₂ Diffusion Flame at 0 mm and 10 mm Axial Location	56
21.	Frequency Distribution Profiles of CO-H ₂ Diffusion Flame at 20 mm and 30 mm Axial Location	57
22.	Frequency Distribution Profiles of CO-H ₂ Diffusion Flame at 40 mm and 60 mm Axial Location	58
23.	Frequency Distribution Profiles of CO-H ₂ Diffusion Flame at 80 mm and 90 mm Axial Location	59
24.	Frequency Distribution Profiles of CO-H ₂ Diffusion Flame at 110 mm and 160 mm Axial Location	60
25.	Frequency Distribution Profiles of N ₂ -CO-H ₂ Diffusion Flame at 0 mm and 40 mm Axial Location, experiment A	62

List of Tables

Table		Page
I.	Comparison Between Various Optical Techniques for Thermometry	7
II.	Test Conditions for Temperature Measurements of H ₂ -CO-N ₂ and H ₂ -CO Flames	29

Abstract

The purpose of this investigation was to measure the radial temperature profiles as a function of time in a non-sooting CO-H₂ diffusion flame at high repetition rates. Measurements were taken from the nozzle exit up to 200 mm above the nozzle in 10 mm increments. The results of such an analysis at $Re = 857$ revealed the existence of low frequency (25-30 Hz) oscillating structures in the outside reaction layer associated with the dynamics of large scale buoyancy-driven vortices, and high frequency (300-325 Hz) oscillations believed to be associated with local instabilities of the internal jet core of the flame.

Other H₂-CO:N₂ gas mixtures (at $Re = 1717$, 2099 and 2264) were investigated and similar high frequency oscillations were found.

In this research the novel thin filament pyrometry technique, developed by Goss, Villimpoc and Sarka was employed; this technique relies upon the blackbody emission of a thin ceramic filament (SiC) in a combustng flowfield.

A limited Fourier Transform frequency analysis was carried out. However, due to the limited number of sampled intervals an exact correlation between the different harmonics that appeared in the spectra can not be made.

EXPERIMENTAL INVESTIGATION OF A CO-H₂ DIFFUSION FLAME USING HIGH-FREQUENCY THERMOMETRY

I. Introduction

Background

Combustion processes applied to propulsion, energy conversion, manufacturing and heating are vital to modern day civilization. Despite the century-long use of combustion, there are a number of areas that are not currently well understood. Many of the current limitations in the knowledge base of combustion can be attributed to the inability to experimentally probe these processes. These difficulties arise due to both the hostility and interactivity of combustion phenomena which makes physical probing quite difficult. Optical techniques have long been recognized for their potential to non-intrusively interrogate combustion processes. With the advent of lasers, the capabilities of optical techniques have been greatly enhanced. Perhaps more importantly, an array of new methods has emerged which previously was not possible to implement or was yet undiscovered. Most laser-based techniques fall in this latter category and the measurements of combustion temperature, chemical composition and flow

velocity are frequently based upon the interpretation of radiative emission spectra which follows the interaction of laser light with the specific internal energy states of atoms or molecules.

Since combustion problems requiring theoretical analysis are primarily concerned with the flow of reacting and diffusing gases, one must understand (in addition to chemical thermodynamics) the conservation equations of fluid dynamics, including transport properties and chemical kinetics. In diffusion flames, infinitely fast chemical reaction rates are assumed and the global flame properties are determined primarily by transport effects.

A diffusion flame may be defined as any flame in which the fuel and oxidizer initially are separated; with this usage, the term is synonymous with non-premixed combustion. In a restricted sense, a diffusion flame may be defined as a non-premixed, quasi-steady, nearly isobaric flame in which most of the reaction occurs in a narrow zone that can be approximated as a surface (flame sheet or reaction-sheet). In the laminar flame regime, all the mixing and transport is achieved by molecular processes, while in the turbulent flame regime these processes are aided by macroscopic eddy motion.

The most fundamental question in turbulent combustion concerns the applicability of a continuum description. It is customary to assume that the full Navier-Stokes equations

(that is, the Navier-Stokes equations augmented by chemical-kinetics laws) govern turbulent combustion; Navier-Stokes turbulence, characterized by fluctuations of velocities and state variables in space and time, occurs when the inertial forces are sufficiently large in comparison with the viscous forces (that is, at sufficiently large values of a representative Reynolds number, Re) (1:374). Turbulence develops from fluid-mechanical local instabilities of flow (2:443-473) when Re is large enough to prevent viscous damping from suppressing fluctuations. The Navier-Stokes equations, combined with a proper set of initial and boundary conditions, are deterministic in that they are believed to possess a unique solution. However, at high Re , the solution is strongly sensitive throughout most of the flow field to the initial and boundary conditions, and in reality the conditions cannot be specified accurately enough to obtain the deterministic solution, either theoretically or experimentally. It then becomes reasonable to introduce statistical methods and seek only probabilistic aspects of the solutions.

For initially non-premixed reactants, two limiting cases may be visualized, namely, the limit in which the chemistry is rapid compared with the fluid mechanics and the limit in which it is slow. The primary combustion reactions in ordinary turbulent diffusion flames encountered in the laboratory and in the industry appear to lie closer to the

fast-chemistry limit. Some of the specific questions asked are: What is the flame length or flame height? What is the average local volumetric rate of heat release? What are the initial conditions for a turbulent-jet diffusion flame to be lifted off the fuel duct? What are the radiant energy fluxes emitted by the flame? How complete is the combustion? What is the rate of production of oxides of nitrogen? What is the rate of production and liberation of smoke and of unburnt hydrocarbons?.

In order to test the theoretical models of combustion, one needs to be able to measure local temperatures, flow velocities, and concentrations of major and minor species at rates that are in excess of the time scales of turbulence. An "ideal" technique should satisfy the following criteria: It should (i) be capable of making in situ and real-time measurements, (ii) be non-perturbing, (iii) have a high sensitivity, (iv) have a high degree of spatial resolution, and (v) have a high degree of temporal resolution. In addition, a truly ideal technique should (vi) measure several combustion parameters simultaneously and (vii) be affordable (3:1339). In general, optical techniques satisfy the first two criteria and many optical techniques have been investigated which satisfy the criteria enumerated above to varying degrees. A few of the techniques have been quite successful.

Temperature and majority species are usually determined

by means of Raman techniques (4:1521; 5:175), while radical intermediates in a much lower concentration are often probed using laser-induced fluorescence (LIF) (6:568; 7:145; 8:511). Raman methods, however, [with the exception of electronically enhanced Raman techniques (9:121; 10:39)] are insensitive to trace minority species since their signal strength is proportional to the concentration; and LIF techniques often suffer from collisional quenching of the fluorescence in high-pressure combustion environments (8:511) whose effect can be overcome partially by using saturated-LIF (11:445; 6:568).

Newly developed techniques include photoacoustic spectroscopy (PAS) (12:118; 13:2133), photoacoustic deflection spectroscopy (PADS) (14; 15:781), and photothermal deflection spectroscopy (PTDS) (16:1333).

After Patel and Tam (17:467) demonstrated in 1979 a highly sensitive pulsed photoacoustic spectroscopy technique involving the use of pulsed lasers, has this technique received attention in the area of combustion diagnostic.

In the last few years there has been extensive interest in the techniques of the PTDS and PADS. Since the initial work of Davis (18:515) and of Boccara, Fournier, Amer and co-workers (19:130; 20:377; 21:519), extensive new applications have been developed by Tam and co-workers (22:457; 23:436; 24:280; 25) and by others (26:381). Gupta and co-workers have demonstrated the usefulness of these

techniques for combustion diagnostics (27:2663; 28:3873; 29:303; 30:672; 31:4626). The two techniques are closely related to each other and satisfy most of the criteria enumerated above for an "ideal" technique.

Besides the widely used laser-Doppler anemometry (LDA) (32; 33:473) and laser-enhanced ionization (LEI) (34:168) techniques applied to the flow velocity measurements in a flame, other techniques such as PTDS (35:532) which overcomes the difficulty associated with LDA for low velocities, and image processing (IP) (36:1420) have been demonstrated.

As a matter of fact, no ideal technique seems to exist and all of the techniques have relative advantages and disadvantages over each other. Table I shows some of these characteristics for comparison in temperature measurements of flame environment.

The extension of the non-linear techniques to high frequencies (essential to an understanding of turbulence phenomena) has suffered from the lack of high repetition-rate, high peak-power laser sources. High-frequency thermometry has, to date, been carried out using fine-wire thermocouples, Rayleigh scattering (although both methods are extremely difficult to apply to a practical flame system), and the PTDS technique (37; 38).

A novel technique capable of high-frequency thermometry along a line is the thin filament pyrometry (TFP) technique

TABLE I
Comparison Between Various Optical
Techniques for Thermometry

Tech nique	Advantages	Disadvantages
CARS	High spatial resolution. High sensitivity.	High peak-power pulsed laser needed. Expensive instrumentation. Susceptibility to environmental disturbances. No applicable to minority species.
LIF	High spatial resolution. High sensitivity. Simple instrumentation.	Need to know quenching rates
SLIF	High spatial resolution. High sensitivity.	Lower sensitivity with molecules with long-lived excited states. High laser power needed. Not applicable to molecular species with transitions in the UV or violet region.
PAS	2-D resolution.	Resolution limited by microphone bandwidth. Poor sensitivity using PZT transducer. Interference by the acoustic wave passing through the flame sheet.
PADS	High 2-D spatial resolution. High temporal resolution. Applicable in sooting flames.	Lower sensitivity than PTDS, but increasing as T decrease.

TABLE I (Cont'd)
Comparison Between Various Optical
Techniques for Thermometry

Tech nique	Advantages	Disadvantages
PTDS	High 2-D spatial resolution. High sensitivity. Applicable in sooting flames. High temporal resolution.	

that has been recently applied successfully by Villimpoc et al. to the study of diffusion and premixed flames to obtain time resolved temperature profiles (39; 40). This technique relies upon the blackbody emission of a thin ceramic filament (SiC) placed in a combusting flow field. The major attributes of this method are the high-frequency response, good spatial resolution, and the ability to make point temperature measurements along the line of the ceramic filament with flames in the range 1000°K-2600°K. The technique is limited to non-sooting flames since the emission from soot can interfere with the filament emission.

Finally, the flow visualization is an essential part in the combustion study. It is used (i) to identify the scales of processes taking place in different regions of combusting flows, (ii) as an aid in interpreting measurements from any diagnostic technique, and (iii) to provide insights into the dynamics of the mixing and transport processes inside of flames. A new laser-sheet lighting technique has recently been demonstrated (41:159-174; 42; 43); it involves seeding the central fuel jet with $TiCl_4$ vapor, as the fuel is mixed with air the $TiCl_4$ reacts spontaneously and nearly instantaneously with the water vapor in the flame to form micro size TiO_2 particles and HCl . The Mie scattering from the TiO_2 particles, observed at right angles to the plane of the laser-sheet, provides a planar view of the flow field inside the flame. The combination of two perpendicular

laser-sheets, as is shown in Fig. 1, has given two bi-dimensional views of the flame structure .

Objective and Approach

The main purpose of this study was to obtain an experimental characterization on temperature at high repetition rates for a CO-H₂ diffusion flame using the thin filament pyrometry technique. The present measurement has been limited to the near field, e.g. the region within 20 diameters downstream from the burner exit.

There are two main reasons for selecting a CO-H₂ diffusion flame in this study: (i) the pyrolysis of high hydrocarbons constituents of common fuels produces CO and H₂ which react with the ambient air in a fast oxidation in the flame, and (ii) using CO and H₂ one can easily control the chemistry of the flame and obtain accurate predictions for other fuels.

Since the TFP technique has been used in a N₂ diluted H₂ diffusion flame (39; 40) this study was undertaken by using a N₂-CO-H₂ mixing as a previous step to the thermometry in CO-H₂ mixing. On the other hand, the fact that both CO and N₂ have the same molecular weight and practically the same thermal conductivity and viscosity coefficients leads one to expect a similar flame structure for these flames judging from the fluid mechanics point of view, although the chemistry is quite different.

Measurements were taken at various axial locations of

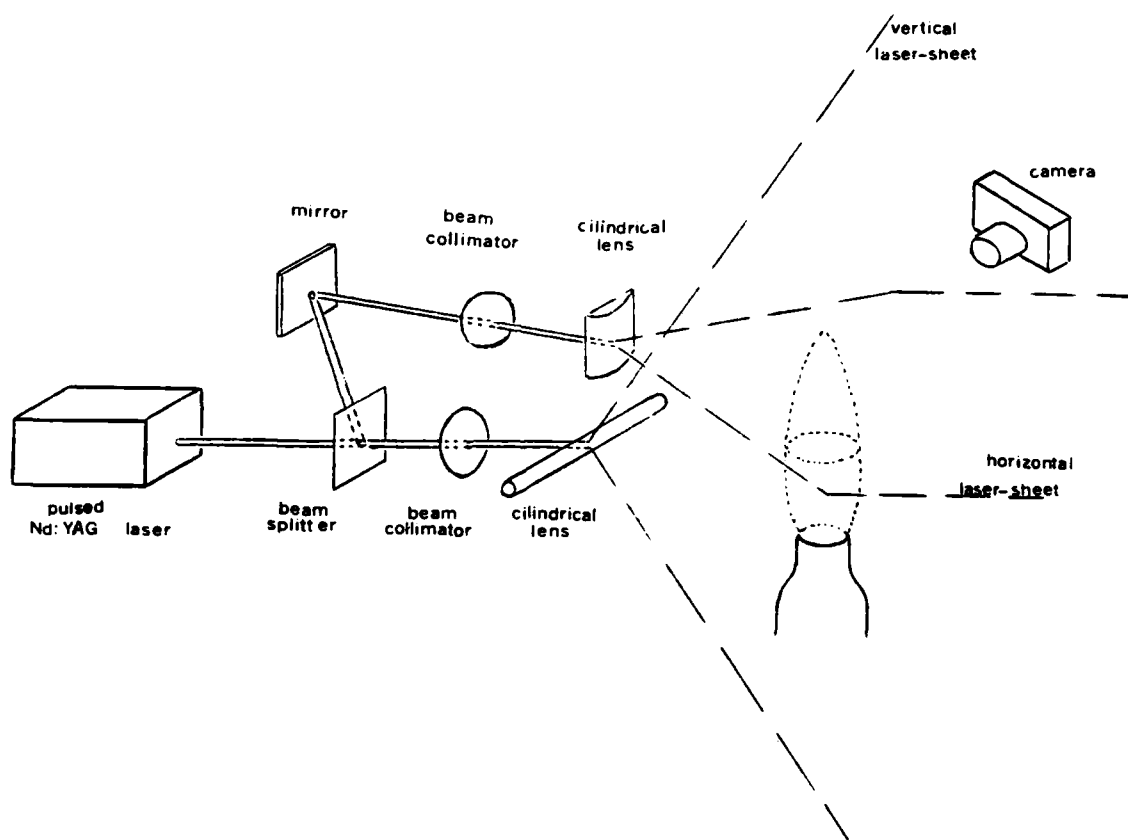


Fig. 1 Bi-dimensional visualization of a flame in two perpendicular planes.

the flame with a step resolution of 10 mm using different gas mixtures as the way to get the temporal-radial temperature profiles at several fluid dynamics regimes.

Furthermore, the two perpendicular laser-sheets lighting technique was used to visualize the flow as an aid to the understanding of the dynamic flame structure.

11. Theory

Thin Filament Pyrometry Technique

This technique relies upon the blackbody emission (radiation resulting from the thermally excited molecular oscillations of the source) of a ultrafine β -SiC (with excess carbon) filament available commercially (44). The filament diameter ranges from 10 to 20 μm (nominally 15 μm), and the thermal conductivity is 10 Kcal/m hr $^{\circ}\text{C}$ along the filament axis at room temperature. Because of its small size, the convective heat transfer coefficient of the filament is quite large and it can respond almost instantaneously to temperature changes in its surroundings; estimates of fiber response to a transient heat pulse are between 1 ms and 2 ms, i.e. $\sim 700\text{Hz}$.

The thermal conductivity of the filament is approximately forty times lower than that of a Pt-PtRh wire which drastically reduces the spread in the temperature profile along the filament, resulting in high spatial resolution. Because the emissivity (ratio of the excitance of the actual source at each temperature to the ideal blackbody excitance at the same temperature) of the filament is large (0.88) and constant with respect to wavelength, the fiber can be considered as a graybody in radiometric terms, and its spectral excitance, M_e , (radiation flux emitted per unit area, per unit wave length in all directions) can be directly related to the flame temperature.

Quantitative measurements with the filament require that its temperature response be calibrated in order to establish a relationship between filament emission intensity and adiabatic temperature. The equations describing the blackbody emission from such a filament are well established. The Planck equation which describes the spectral distribution of excitance for an ideal blackbody at each wavelength, λ ,

$$M_e(\lambda) = \frac{2\pi hc^2}{\lambda^5} \frac{1}{\exp(hc/k\lambda T) - 1} \quad (1)$$

is used in conjunction with the Gouffé equation to determine the total spectral flux which is emitted from the surface of the filament

$$M_e(\lambda_0, T) = \frac{a \epsilon_0(\lambda_0, T) C_1}{\lambda_0^5 [\exp(C_2/\lambda_0 T) - 1]} \quad (\text{Watt/m}) \quad (2)$$

where a is the filament surface area, ϵ_0 the apparent emissivity of the filament, C_1 the first radiation constant, C_2 the second radiation constant, λ_0 the wavelength in vacuum, and T the filament temperature. If Eq.(1) is to be used for quantitative measurement of the temperature of the filament, the emissivity of the filament must be known as a function of temperature. The conventional approach to

calibrating the emissivity of a material is to heat the given material to a known temperature, measure its excitance, and compare it to that of a blackbody at the same temperature, but due to the small size filament employed, this approach is impractical. Therefore, as established by Goss et al. (45) an alternative approach of measuring the reflectance (ratio of the power reflected to the power incident) of the filament as a function of temperature can be used.

The reflectance can be related to the directional emissivity, $\epsilon(\theta, \phi)$, by Kirkoff's relationship

$$\epsilon(\theta, \phi) = 1 - \rho(\theta, \phi) \quad (3)$$

where $\rho(\theta, \phi)$ is the directional hemispherical reflectance for the spherical coordinates θ and ϕ . In general, the required accuracy in reflectance for a desired accuracy in emissivity accuracy is given by the following relation

$$\frac{\Delta \rho}{\rho} = \frac{\epsilon}{1 - \epsilon} \frac{\Delta \epsilon}{\epsilon} \quad (4)$$

where $\Delta \rho$ and $\Delta \epsilon$ represent the corresponding errors. For a highly emissive sample such as the SiC filament, with emissivity of 0.88, the error in the emissivity measurement based on a 1% error in the reflectance is 0.13%. Thus,

reflectance measurements (if carried out correctly, i.e. measuring the bi-directional reflectance distribution function at all collection angles) can be very accurate measure of emissivity. The concern with the SiC fiber is not to measure the absolute value of the emissivity at all temperatures but rather to establish whether the emissivity remains constant in the range of interest. This requires that the change in the emissivity (not the absolute value) be monitored as a function of temperature. This can be accomplished with the experimental setup shown in Fig. 2. The chopped output from a HeNe laser is monitored by a photomultiplier tube, PMT, and lock-in amplifier. The bundle of filaments are heated by a flame to a maximum temperature of $\sim 2200^{\circ}\text{K}$. Since the filament is a graybody and since no measurable change is observed in the emissivity at the HeNe wavelengths, it can be concluded that the emissivity of the filament indeed remains constant over the temperature range of interest. This implies that the excittance of the filament can be predicted by the blackbody equations. In practice, however, a detector of limited spectral bandwidth is used to detect the excittance and, thus, the blackbody results must be convolved over the detector response curves to predict the measured response of the filament.

The equation (2) must be multiplied by the detector response and integrated over this region. Thus, the

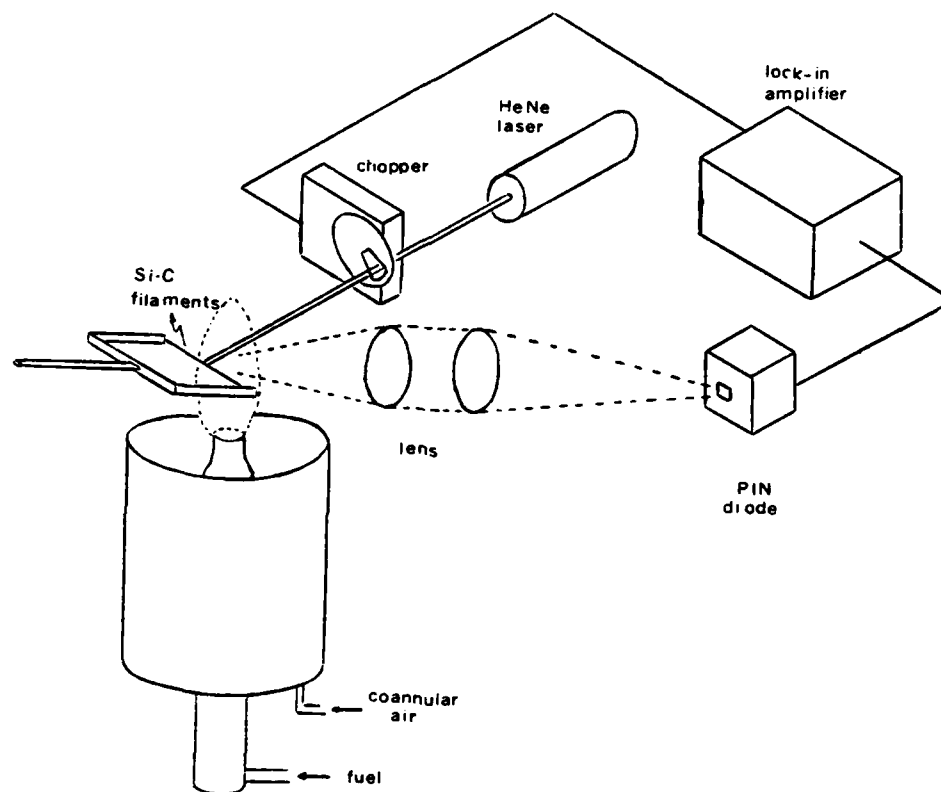


Fig. 2 Experimental Arrangement for Measuring Emissivity of SiC Filaments by Reflectance

detected signal is given by

$$I_{exp} = k_{exp} \int_{\lambda_1}^{\lambda_2} Me(\lambda, T) R(\lambda) Tr(\lambda) d\lambda \quad (5)$$

where $Me(\lambda, T)$ is the graybody function, $R(\lambda)$ the response function of the InGaAs photodiode, $Tr(\lambda)$ the transmission characteristics of the optics employed in the experiment, and k_{exp} an experimental constant which takes into account the collection efficiency of the optical system.

To simplify the calibration procedure, the emission from the filament at a known temperature is measured, and all measurements are referenced to this value. This allows experimental factors (alignment, collection efficiency, fiber diameter, etc.) to be normalized. Moreover, the normalization between the different filaments used through the same experiment is provided by ratioing the measurements at an axial location in the flame where the emission from the filament does not change in time.

Finally, the intensity data are converted to temperature using a calibration curve. This curve, shown in Fig. 3 (45), is calculated by convolving the detector response over the blackbody excitance; the curve is fit by a mathematical power series expansion of intensity to determine the temperature and normalized to the emission at a known temperature and axial location.

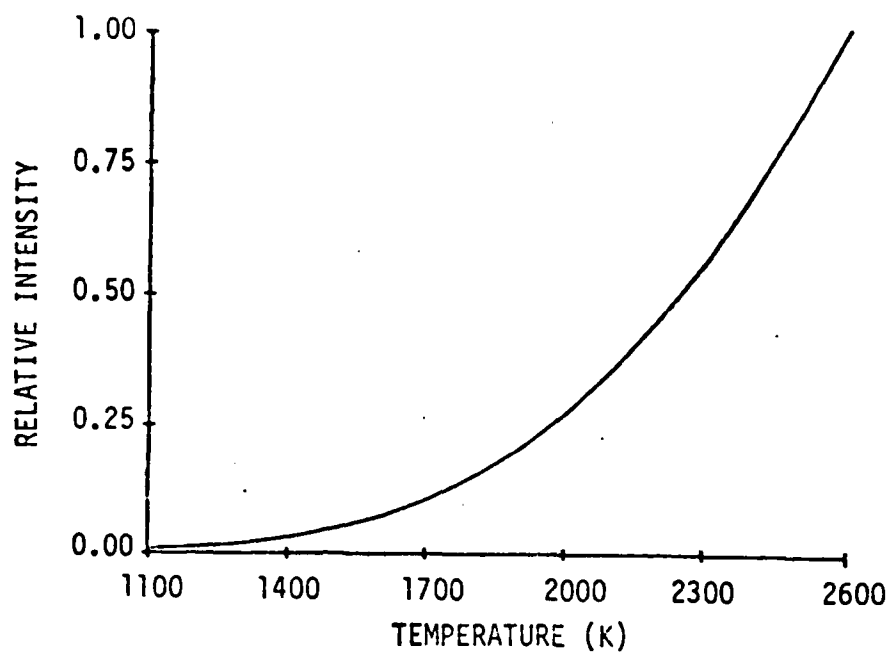


Fig. 3 Relative Emission Curve From SiC Thin Filament as Detected by InGaAs Detector.

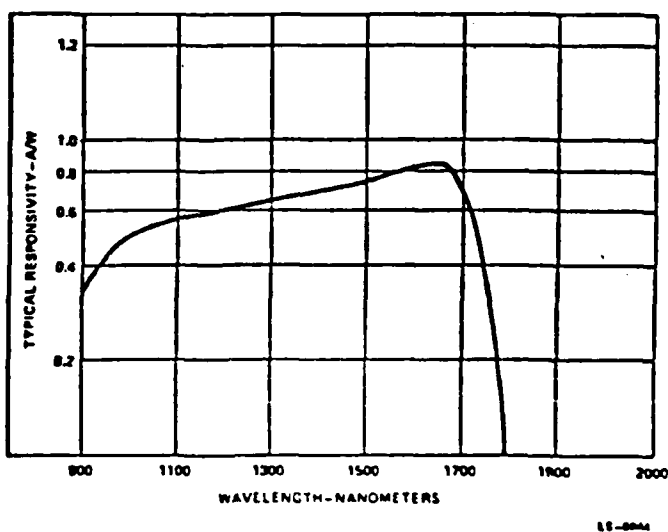


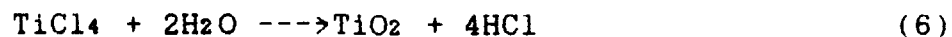
Fig. 4 Spectral Responsivity Characteristic of InGaAs Detector.

Because the temperature of the filament may be different from that of the surrounding gas due to radiation losses, a detailed heat-balance analysis must be conducted for accurate prediction of the gas temperature. The results of such an analysis for the flame conditions reported by Goss et al. (45) indicated that the radiation correction varies from 20°K at 1000°K to 300°K at 2600°K.

As can be seen from Fig. 3, the detected emission from the filament varies greatly with temperature. Because of this variance along with the limited dynamic range of the digitization system (255 to 1), the temperature uncertainty can be large (especially at low temperature). Assuming a 1% uncertainty in the intensity measurements, the temperature uncertainty at 1100 °K is ~80 °K and at 2300 °K is ~8 °K.

Laser-Sheet Lighting Technique

The laser-sheet lighting technique involves seeding the central fuel jet with TiCl_4 vapor. As the fuel is mixed with the air, the TiCl_4 reacts with the water vapor formed in the combustion process to form TiO_2 particles and HCl according with the stoichiometry



The Mie scattering from the TiO_2 particles is observed as a green color at right angles to the planes of the green Nd:YAG laser-sheets which are passed vertically through the

center of the flame and horizontally at the desired axial location. The technique is simple and easy to implement requiring only a laser and camera.

The introduction of TiCl_4 to the flow does not disturb the combustion process since the reaction of TiCl_4 vapor and H_2O vapor occurs nearly isothermally and the amount of TiCl_4 added to both the dry air and the dry central fuel is negligible.

III. Experimental Apparatus

Experimental Setup for the TFP Technique

The optical arrangement employed in this technique is shown in Fig. 5. An axisymmetric fuel nozzle of 10 mm diameter was mounted at the center of a co-axial air jet of 254 mm diameter; the low velocity (16 SCFM, ≈ 5 cm/s) air is introduced through the outer tube about the fuel tube to reduce the effect of room air disturbances. The burner was mounted on a motor-driven translation stage to permit vertical movements. A brief description of the main instruments employed in this technique and their principal characteristics follows.

Rotating mirror

In the thin filament pyrometry technique the light from the filament is imaged by a 44 cm focal length lens onto a rotating mirror, which sweeps the image of the filament across a single detector through a 50 cm focal length lens. This mirror-detector combination converts a spatial scan into a temporal one.

The Lincoln Laser Corp., model S-225-030-XLIM, rotating mirror scanner (RMS) is actually a wheel consisting of ten different faces which rotates at speeds up to 500 Hz. The wheel in these experiments rotated at a 100 Hz rate driven by a variable frequency motor control Lincoln Laser Corp. model VFC-2; with the ten faces, the image was swept by the detector at an effective rate of 1000 Hz.

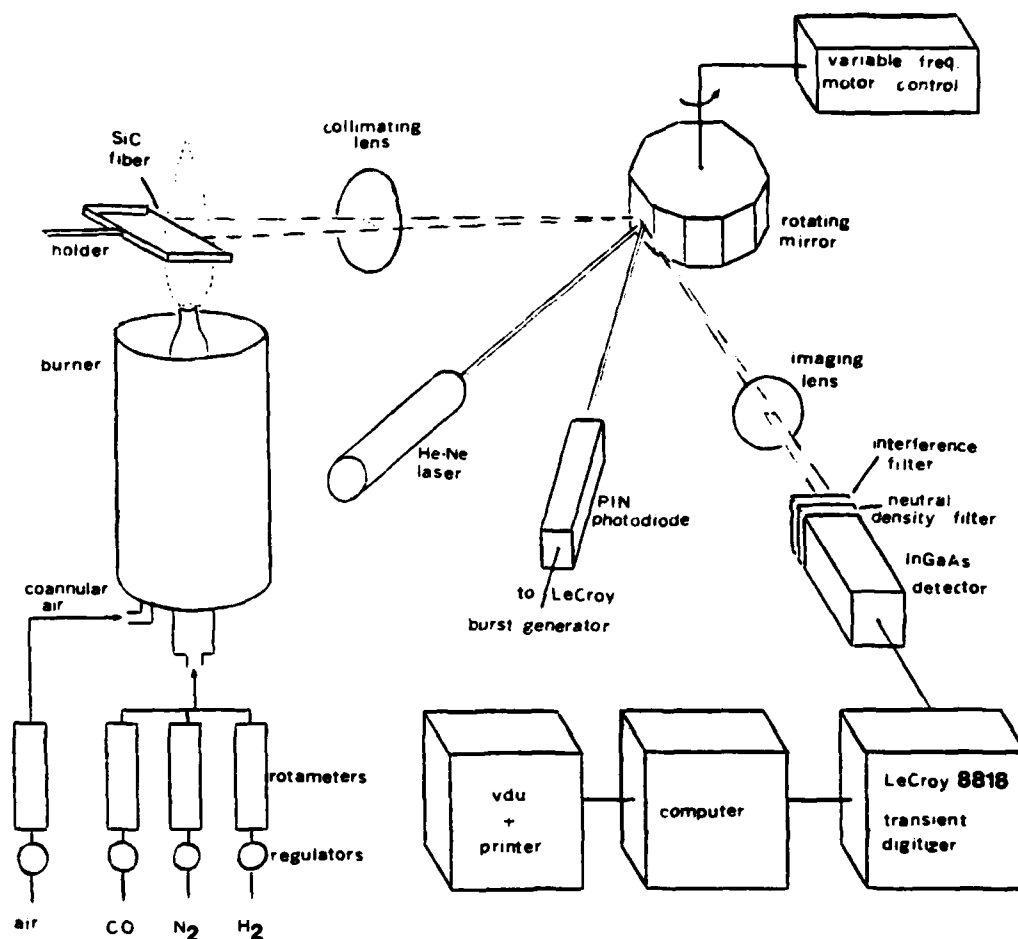


Fig. 5 Thin Filament Pyrometry Optical Set-up

Diode Detector

The image from the rotating mirror is swept across a In-Ga-As photodiode, RCA model C30980E, whose spectral response is shown in pg. 19, and whose principal technical specifications are:

- quantum efficiency at 1300 nm and 1550 nm, 70% typ.
- total dark current (I_d), 150 nA typically.
- noise current (I_n) at $f = 10$ kHz, 0.3 pA/Hz^{1/2} typ.

Due to the spectral response which is limited to the near IR, only temperatures in excess of 1100°K could be measured. However, with a suitable choice of IR detector and optics, this lower temperature limit could be extended.

Digitizer

A Lecroy TR8818 Transient Recorder is used to digitize the analog signal from the detector and store it in MM8103 ECL memory units (32 K each one) for subsequent transmission through a custom built interface to a ModComp 7870 Classic computer, for storage and data analysis (in which the 8 bit data from the LeCroy are unpacked into 16 bit data for the ModComp). The synchronization pulse from the PIN-diode is delayed and used to open a 200 μ s window centered on the sweep of the filament image; this delay allows the image signal to be located at the optimum point inside the 200 μ s window. The image of a 6 cm length along the filament is recorded in 512 discrete samples during the 200 μ s window at the rate of 2.56 MHz, giving an effective spatial resolution

of 120 μm per sample point. A pulse generator (General Radio model 1340), was used to provide the 512 pulses which carry at the leading edge the signal from the In-Ga-As detector.

The model TR8818 digitizer is optimized for digitizing and recording high frequency signal, evidenced by its wide bandwidth (DC to >100 MHz), fast sampling rate and its high dynamic accuracy even for signal frequencies approaching the Nyquist limit. The signal to be digitized is connected via an amplifier (Lecroy 6102) for gain control. Once armed by programmed command through computer keyboard, the unit digitizes the input signal, with 8-bit resolution and up to 200 MS/s digitization rate, and loads its memory.

Triggering Laser

A HeNe laser (Spectra Physics, model 145-01) and a PIN-photodiode providing the necessary synchronization signals were used for proper scanning and digitization of the image. The laser was used with the power supply Spectra Physics model 248.

Experimental Setup for the L-S Lighting Technique

The experimental arrangement for this technique is shown in Fig. 6. A pulsed frequency doubled Nd:YAG laser (Quanta-Ray DCR) was used as the laser source to produce the horizontal and vertical laser beam sheets. The principal characteristics of this laser are:

- pulse width, 10 ns.

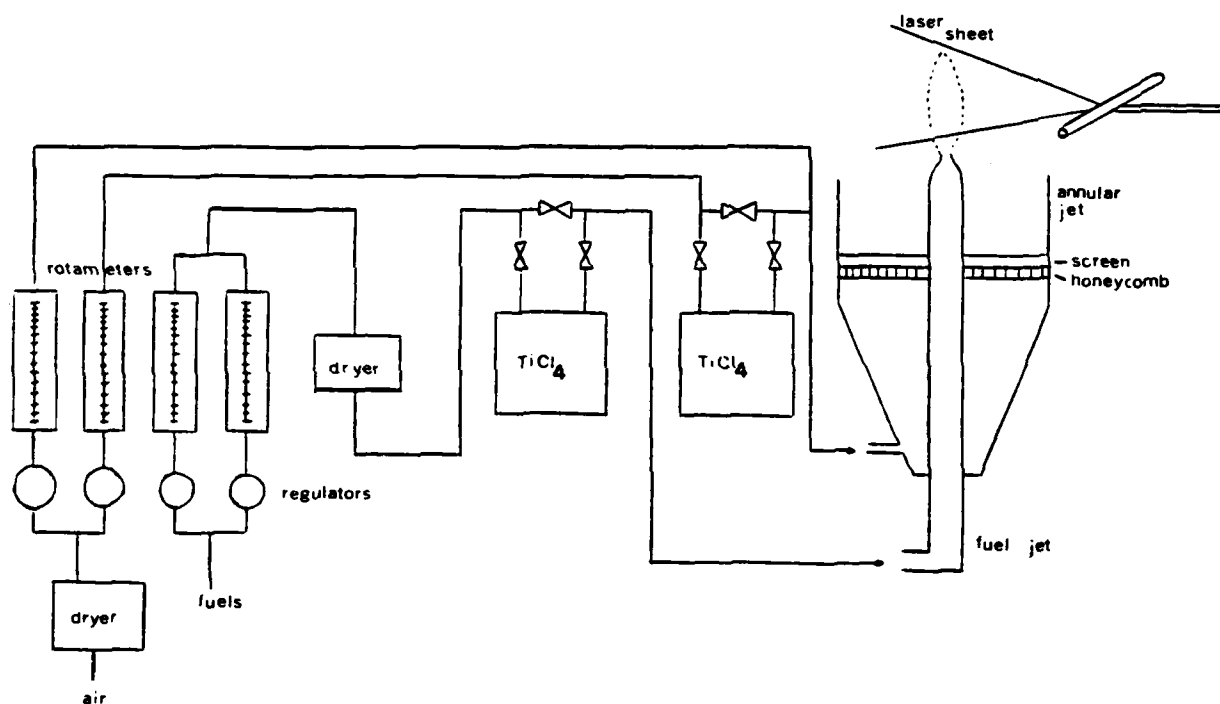


Fig. 6 Experimental Set-up of Jet Diffusion Flame Visualization Technique

- pulse energy, 70 mJ/pulse with amplifier oscillator.
- optimum pulse repetition rate, 10 pulses/s.

Although the power of the Nd:YAG is adjustable, the higher range of operation was used to provide better illumination to the internal structure of the flame and obtain the best definition on the photo.

A Hasselblad 500 camera was used whose shutter was triggered by the laser firing using an exposure time of 1/500 s and a diaphragm aperture, f#, of 4 and 5.6.

In this experiment both the laser's oscillator and amplifier were used to generate the required output energy. A burner with similar geometry to the one used in the TFP technique was employed in this experiment.

Since HCl is formed in the TiCl_4 reaction with the water vapor, some precautions must be taken when applying the technique. Since an extremely small amount of TiCl_4 is used to seed the flow, the concentration of the HCl formed is very small. However, care must be taken to vent the exhaust products from the laboratory.

IV. Experimental Procedure

Experimental Procedure for the TFP Technique

In the thin filament pyrometry technique, using the optical arrangement shown in pg. 23, radial temperature profiles of the flame as a function of time were made at different axial locations, from the nozzle exit to 200 mm above the nozzle in 10 mm increments. The test conditions are summarized in TABLE II.

The filament was suspended on the centerline of the diffusion jet by a holder which supplies just enough tension to keep the filament from mechanical oscillations (probable at relatively high jet velocities) but not too much as to decrease drastically its survivability at high temperatures where its tensile strength is reduced. The emission from the filament was swept across the photodetector by the spinning mirror and sent to the computer after the signal is digitized. The digitizer used in the study stores 384 images digitizing each image in 512 records. Depending on the intensity of the emission three different electronic ranges (50 mV, 100 mV and 250 mV full scale) were employed for digitization; in all ranges the full scale corresponded to 255 counts.

Calibration Procedure

The environment in which the filament is placed is harsh. Each filament could last only a few minutes (depending on axial location, Re number and gas mixture

TABLE 11
Test Conditions for Temperature Measurements
of H₂-CO-N₂ and H₂-CO Flames

Test Conditions	Experiment					
	A	B	C	D	E	F
Fuel	H ₂ - -CO-N ₂	H ₂ - -CO-N ₂	H ₂ - -CO-N ₂	H ₂ - -CO-N ₂	H ₂ - -CO-N ₂	H ₂ -CO
Re*	1717	2099	854	857	2264	857
Exit velocity V (m/s)	2.69	3.92	1.60	2.87	4.90	2.87
H ₂ / (CO+N ₂)	0.029	0.497	0.504	3.391	0.998	-
H ₂ / CO	-	-	-	-	-	3.391
H ₂ (R.l.p.m.)**	0.20	1.70	0.70	2.90	3.20	2.90
CO (R.l.p.m.)	6.40	6.40	2.60	1.60	6.00	3.20
N ₂ (R.l.p.m.)	5.80	5.80	2.40	1.50	5.40	-

(*) $Re = 4Q/\pi d\nu$; Q = volumetric flow rate in cm³/s.
d = burner diameter in cm, ν = kinematic viscosity of fuel
gas at 298 °K in cm²/s.

(**) R.l.p.m. is based on the rotameter reading in liters
per minute calibrated for C₂H₂.

employed), so several fibers were used in each experiment. The correlation between measurements made with different fibers in each experiment was accomplished by measuring at 10 mm above the nozzle with all filaments. Calibration measurements at 40 mm downstream were made for each matrix using pure H₂ flame. The flame background excittance was measured at 20 mm steps for correcting the filament measurements. The goal of this process is to obtain the excittance at the adiabatic temperature of the flame.

Data Analysis

Data analysis of the experimental data was carried out on the Modcomp Classic computer. This analysis required several steps which included:

- noise reduction by averaging six points when the difference between two consecutive records in each image is bigger than 5 counts.

- correlation of all measurements made with the different fibers, by ratioing the maximum values obtained at 10 mm above nozzle with the first to the subsequent filaments.

- conversion between the different electronic scales used in the digitizer by converting the number of counts of the digital signal to actual millivolts.

- background compensation of the signal by subtraction of averaged background from each record through all images.

- calibration with pure H₂ flame by ratioing each record

in each image to the maximum value obtained at 40 mm above nozzle, and converting the ratioed intensity to temperature using the fitted calibration curve relative to the stoichiometric temperature of a H₂ flame convolved with the detector response (45).

This process required a modification of available computer programs to include the different factors involved. The actual temperature, TEMP, was obtained from the intensity, INT, by using the calibration curve and assigning the limits

$$\begin{aligned} \text{TEMP} &= 2600 \text{ }^{\circ}\text{K when INT} = 1 \\ \text{TEMP} &= 1100 \text{ }^{\circ}\text{K when INT} \leq 0 \end{aligned} \quad (7)$$

where

$$\begin{aligned} \text{INT} &= \frac{\text{Counts}_i}{\text{Max Countscal}} \frac{\text{Fwi}}{\text{Fwcal}} \frac{(\text{mV/counts})_i}{(\text{mV/counts})_{\text{cal}}} \\ &\quad - \frac{\text{Bkg Counts}_i}{\text{Max Countscal}} \frac{(\text{mV/counts})_{\text{Bkg}_i}}{(\text{mV/counts})_{\text{cal}}} \\ &= \frac{\text{Counts}_i / (\text{counts/mV})_i}{\text{Max Countscal} / (\text{counts/mV})_{\text{cal}}} \frac{(\text{max countsw}_0 / \text{max countsw}_i)}{(\text{max countsw}_0 / \text{max countsw}_{\text{cal}})} \\ &\quad - \frac{\text{Bkg Counts}_i / (\text{counts/mV})_{\text{Bkg}_i}}{\text{Max Countscal} / (\text{counts/mV})_{\text{cal}}} \end{aligned}$$

$$= \frac{[(\text{Counts}_i / (\text{counts/mV})_i) / \text{max counts}_i]}{[(\text{Max Counts}_{\text{cal}} / (\text{counts/mV})_{\text{cal}}) / \text{max counts}_{\text{cal}}]} - \frac{\text{Bkg Counts}_i / (\text{counts/mV})_{\text{Bkg}_i}}{\text{Max Counts}_{\text{cal}} / (\text{counts/mV})_{\text{cal}}} \quad (8)$$

where

Counts_i = counts at location i in each record of every image.

$\text{Max Counts}_{\text{cal}}$ = maximum counts at calibration measurement.

$(\text{mV/counts})_i$ = millivolts per count of digitizer scale at location i .

$(\text{mV/counts})_{\text{cal}}$ = millivolts per count of digitizer scale in calibration measurement.

$(\text{mV/counts})_{\text{Bkg}_i}$ = millivolts per count of digitizer scale at location i in background measurement.

F_{wi} = conversion factor of fiber at location i to location at 0 mm (ratio of maximum counts at 10 mm above nozzle with the fibers used at locations 0 mm to i mm).

$F_{w\text{cal}}$ = conversion factor of fiber in calibration measurement to location at 0 mm (ratio of maximum counts at 10 mm above nozzle with the fiber used at location 0 mm to calibration measurement fiber).

Bkg Counts_i = counts at location i in each record of

every image in background measurement.

As has been pointed out by Goss (45) the measured filament temperature has to be corrected by radiation losses to obtain the surrounding gas temperature. As the temperature increases the blackbody emission increases as T^4 (according with the Stefan-Boltzmann formula) while the convective heat transfer increases only as T , thus the correction term becomes large as the temperature increases, and its magnitude depends on the flow conditions and constituents as well as the temperature itself (through the influence of temperature on the heat transfer coefficient). So, the correction term has to be evaluated each time the flow conditions or fuel types are changed. This correction factor was not introduced in the three-dimensional plots.

A graphic printer, Tektronix model 4012, was used to plot the temporal variation of the temperature across the radial direction of the flame, and the intensity contours in a time-versus-radial distance plot.

Because of the nature of the plots obtained, the excitance data were spectrally analyzed by using a Fourier Transform analysis computer program, to show the distribution of the temperature variation in the frequency domain along the radial direction in the flame.

V. Results and Discussion

Flow Visualization Studies

Yule et al. have made detailed studies of the structure of a transitional/turbulent propane jet flame with a burner setup very similar to the present studies (46). They identified two regions containing organized structures. One region located outside of the flame surface, consisted of large slow moving vortices that occurred at a frequency of about 30 Hz. They referred to this zone as the outer preheat zone. Another zone, referred to as the inner preheat zone, was located inside the flame at the potential core interface. These types of structures shown in Fig. 7a & 7b. are clearly identified in the visualizations of the H₂-CO flame investigated in this study. The structures inside the visible flame surface mark the fuel and H₂O combustion product interface, and the large structures outside the flame surface mark the air and H₂O product interface.

Studies by Roquemore et al. (47) have shown that at low and intermediate velocities, the toroidal vortices observed outside the visible flame surface play a dominating role in determining the flame structure. The rotation of the toroidal vortices can pull the flame radially outward forming a flame bulge. The frequency of the outer vortices corresponds to the flame flicker frequency of ~12 Hz. and is relatively independent of the fuel type and central nozzle



Fig. 7a Image of CO-H₂ Diffusion Flame at $Re = 857$.
 $H_2/CO = 3.391$ and $f\# = 4$



Fig. 7b Image of CO-H₂ Diffusion Flame at $Re = 857$,
 $H_2/CO = 3.391$ and $f\# = 5.6$

design for a wide range of fuel velocities. The outer structures are believed to be established by a buoyancy driven shear layer.

The turbulent characteristics of the jet diffusion flame are most clearly demonstrated by the fuel/water product interface occurring inside the flame surface. An initial instability wave forms in the potential core region of the jet at very low fuel flow rates. This inner instability can develop into coherent vortices as the fuel velocity increases. The flame spreading angle increases at the axial location where the vortices start to coalesce much like a non-reacting shear layer grows when vortices coalesce. At the low flow rates of the flame investigated in this study, the inner vortices are not well formed as illustrated in Fig. 7a & 7b.

The sheet lighting technique illustrates the internal and external flame structures but does not show the temperature field. The TFP technique is well suited for this purpose as discussed below.

TFP Technique

The development of the present experiments has indicated the necessity for enhancing the performance of the filament. The low survivability of the filament under the conditions used here -in contrast with the reported results using H₂-N₂ diffusion flame (38; 39)- could be due to some combined chemical effects of the CO and O₂ over the SiC

fiber. This situation leads to a lower reliability of the results and make its applicability to in situ measurements uncertain. A recently developed ceramic fiber (boron nitride coated by SiO_2 and Si_3N_4) seems to be more resistant to the oxygen action increasing its lifetime in flame environment.

The addition of extended memory to the digitizer and computer will allow an expanded frequency analysis to high frequencies, and make enough point and line measurements along the time to get averaged and probability distribution function (PDF) data as a spatial and temporal function.

Temperature Profiles

The 3-D temporal distribution of temperature profiles along the radial direction taken at various axial locations are shown from Fig. 8 to Fig. 18 corresponding to the experiment F (pure CO-H_2 flame). Included in these figures are the respective iso-intensity contour lines in a time versus radial distance graph. The reader should keep in mind that the displayed temperature fields represent the passage of the flame structure through a single axial location as a function of time, so the y-axis in these plots is time and not space as in the photograph of the flame.

The evolution of a large scale buoyancy driven structures (flame bulges) can be traced from these plots. Just above the nozzle exit the cold core of unburnt fuel is surrounded by a hot reacting flame sheet (surface) resulting

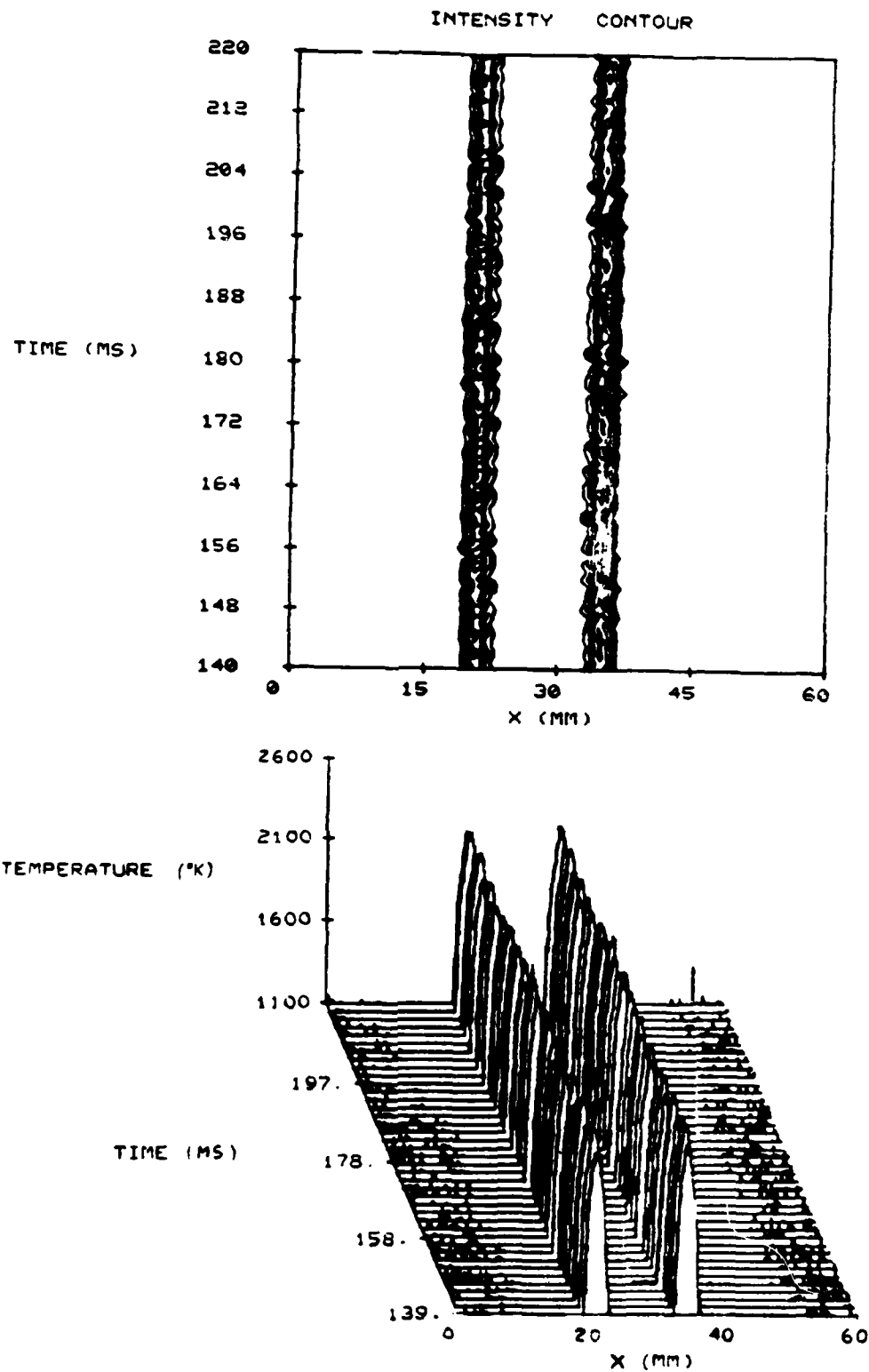


Fig. 8 Temperature Profiles of CO-H₂ Diffusion Flame and Intensity Contour Lines at 0 mm Axial Location.

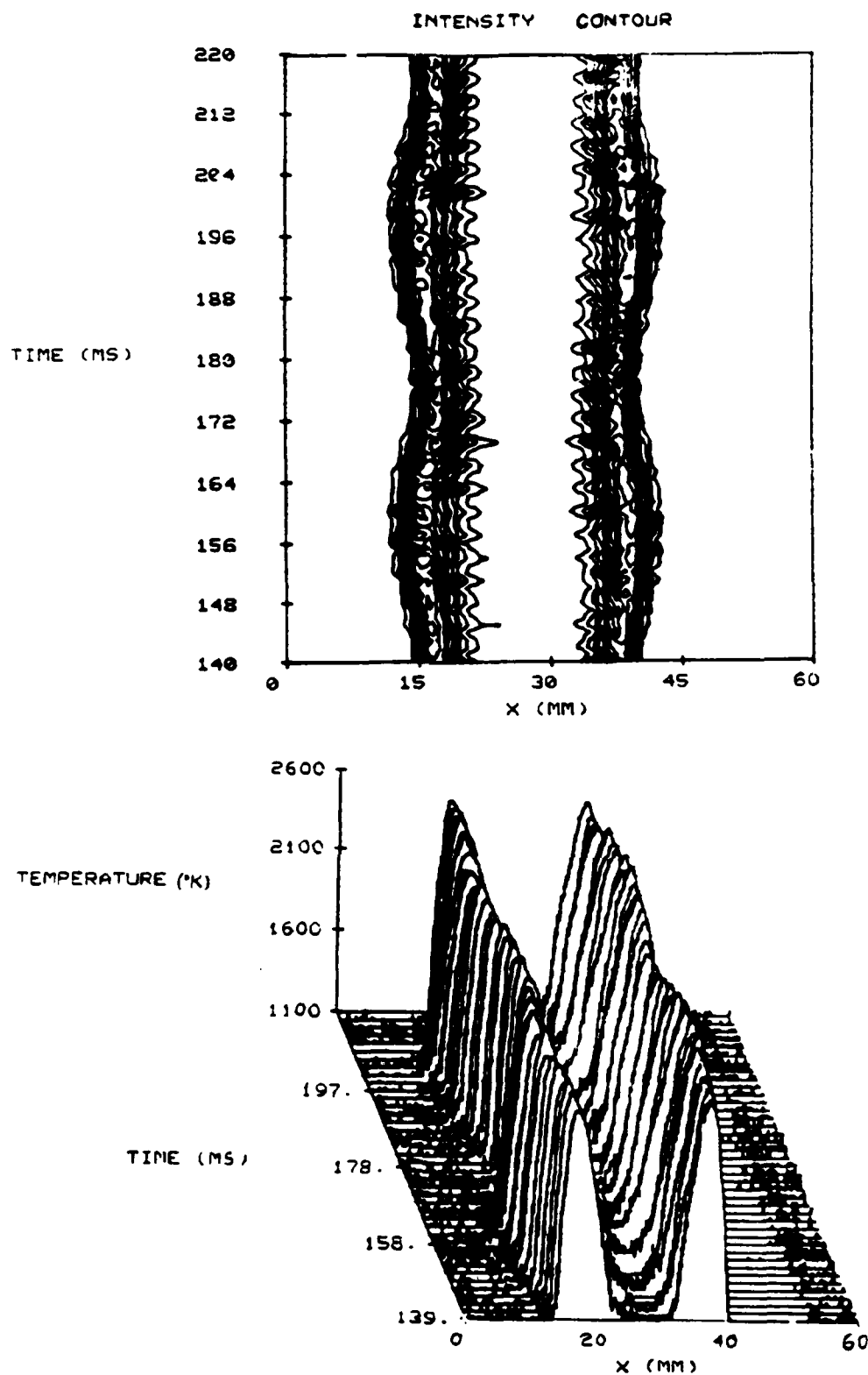


Fig. 9 Temperature Profiles of CO-H₂ Diffusion
Flame and Intensity Contour Lines at 20 mm
Axial Location.

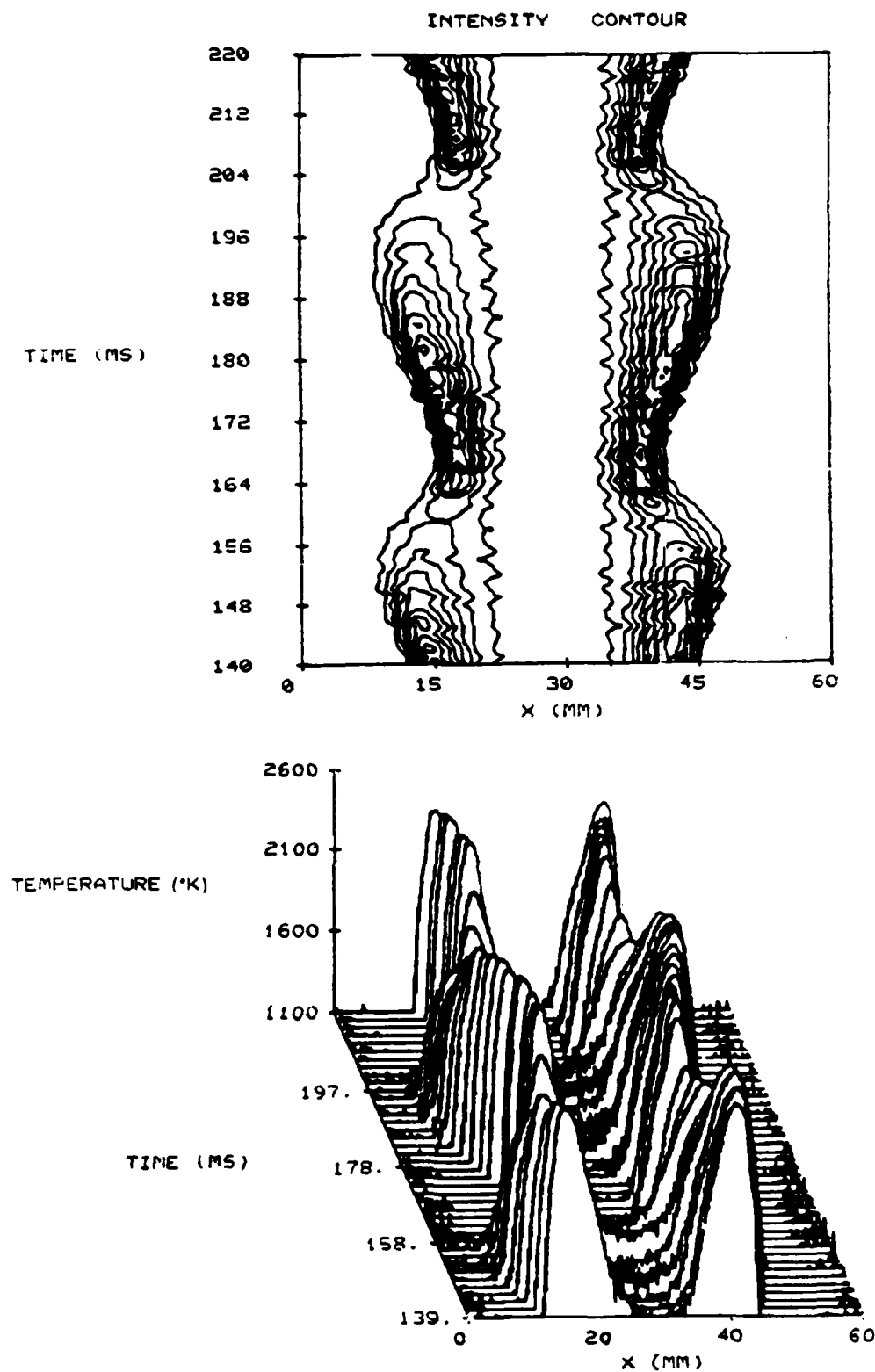


Fig. 10 Temperature Profiles of CO-H₂ Diffusion Flame and Intensity Contour Lines at 40 mm Axial Location.

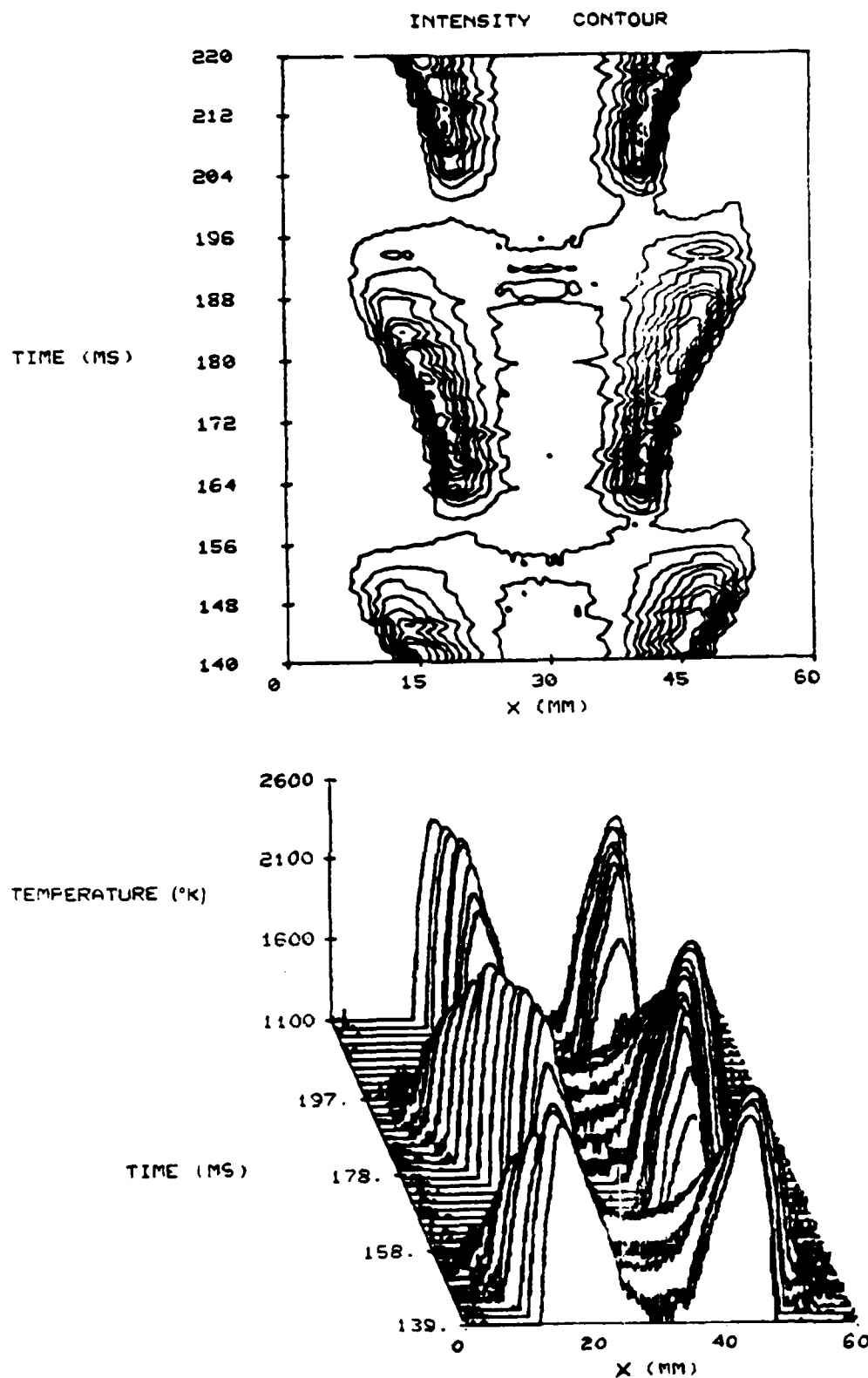


Fig. 11 Temperature Profiles of CO-H₂ Diffusion Flame and Intensity Contour Lines at 60 mm Axial Location.

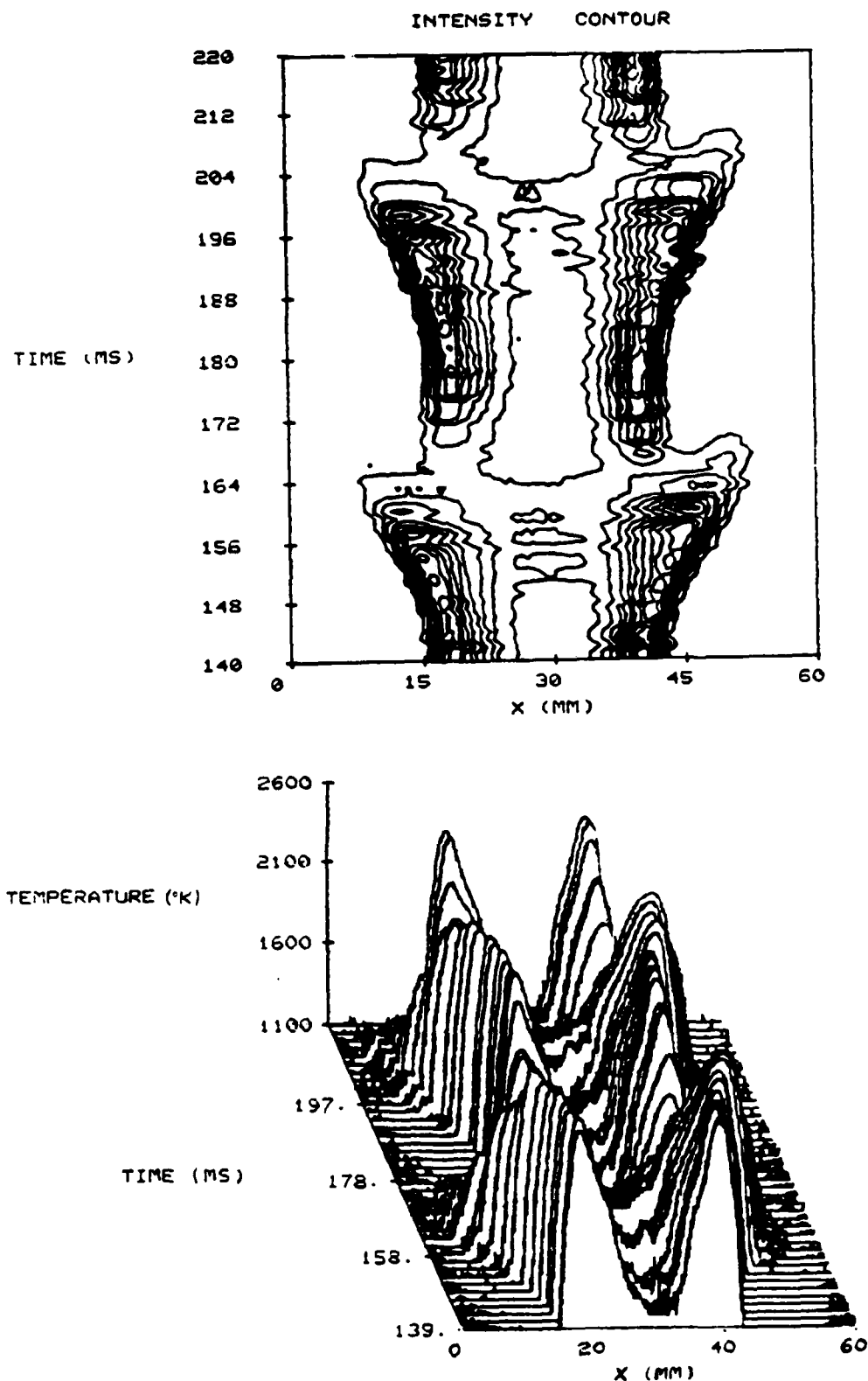


Fig. 12 Temperature Profiles of CO-H₂ Diffusion
Flame and Intensity Contour Lines at 80 mm
Axial Location.

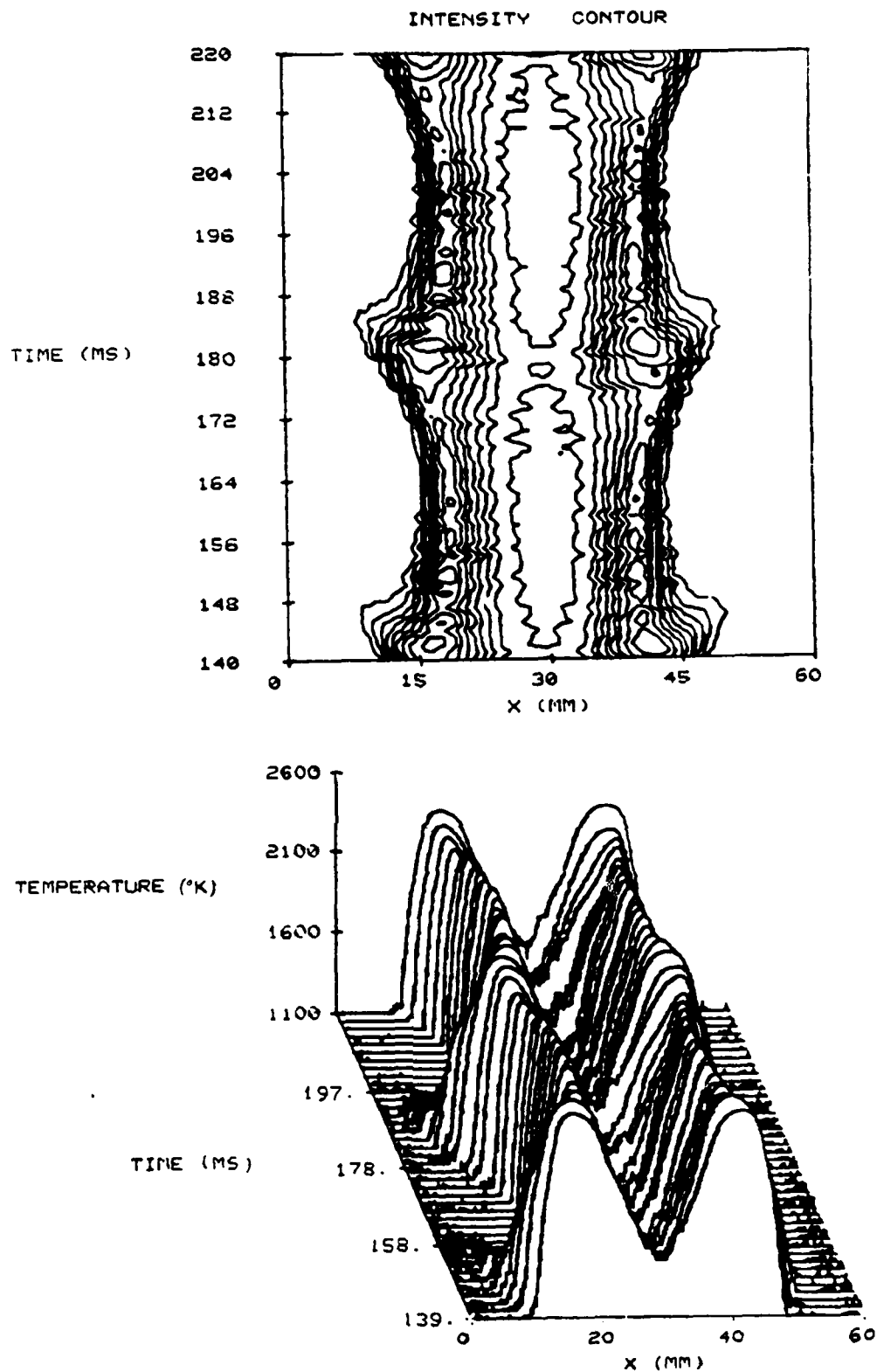


Fig. 13 Temperature Profiles of CO-H₂ Diffusion Flame and Intensity Contour Lines at 100 mm Axial Location.

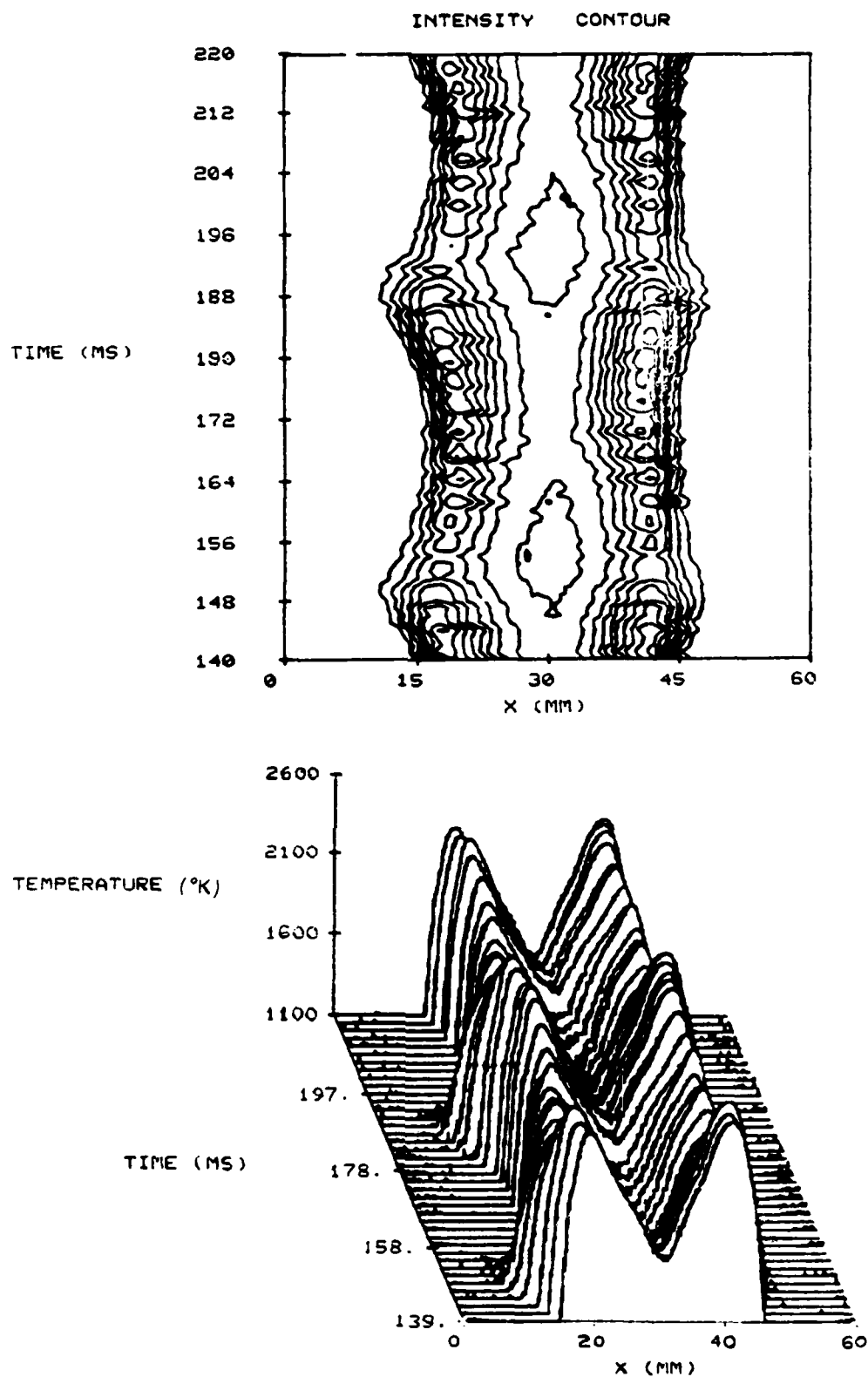


Fig. 14 Temperature Profiles of CO-H₂ Diffusion Flame and Intensity Contour Lines at 130 mm Axial Location.

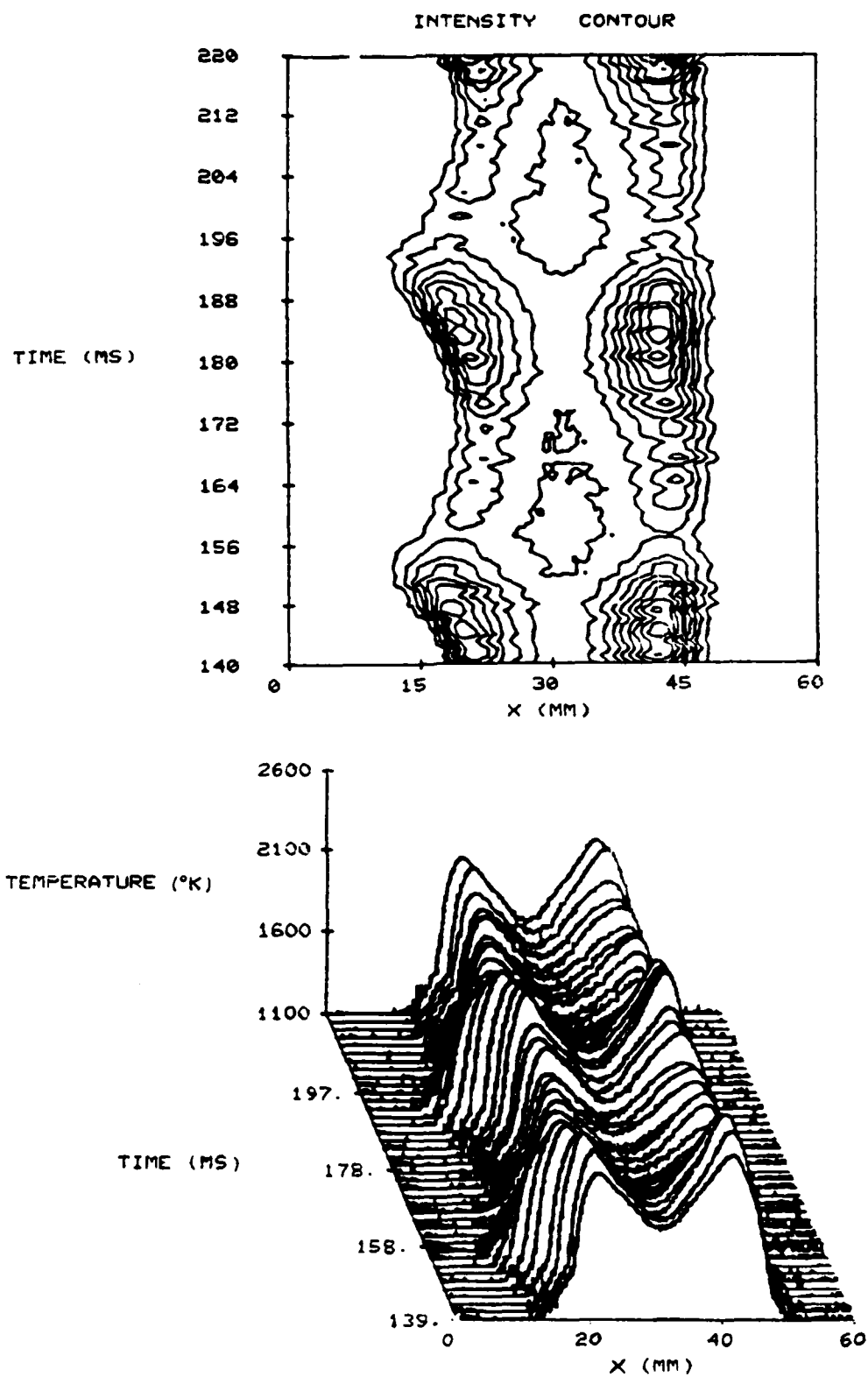


Fig. 15 Temperature Profiles of CO-H₂ Diffusion Flame and Intensity Contour Lines at 140 μ m Axial Location.

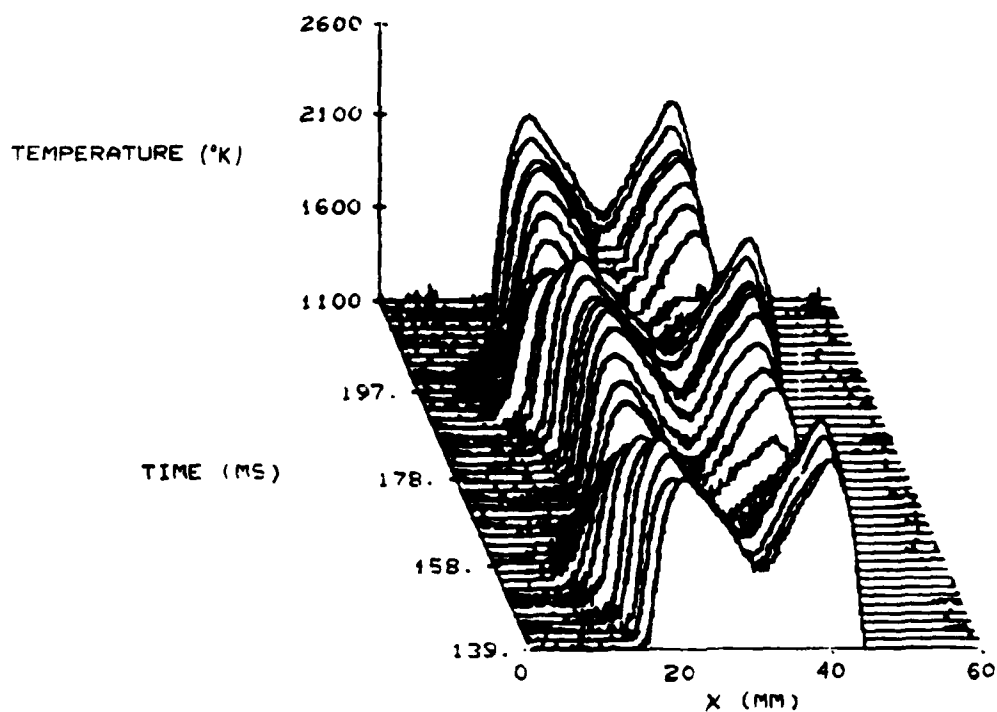
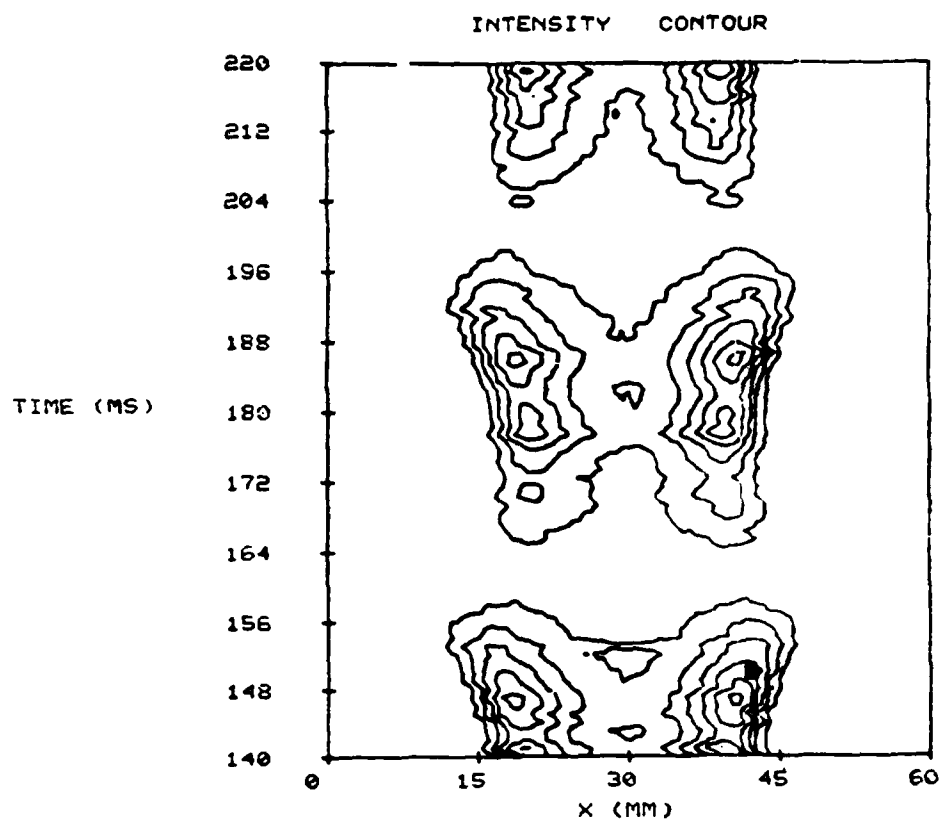


Fig. 16 Temperature Profiles of CO-H₂ Diffusion Flame and Intensity Contour Lines at 160 mm Axial Location.

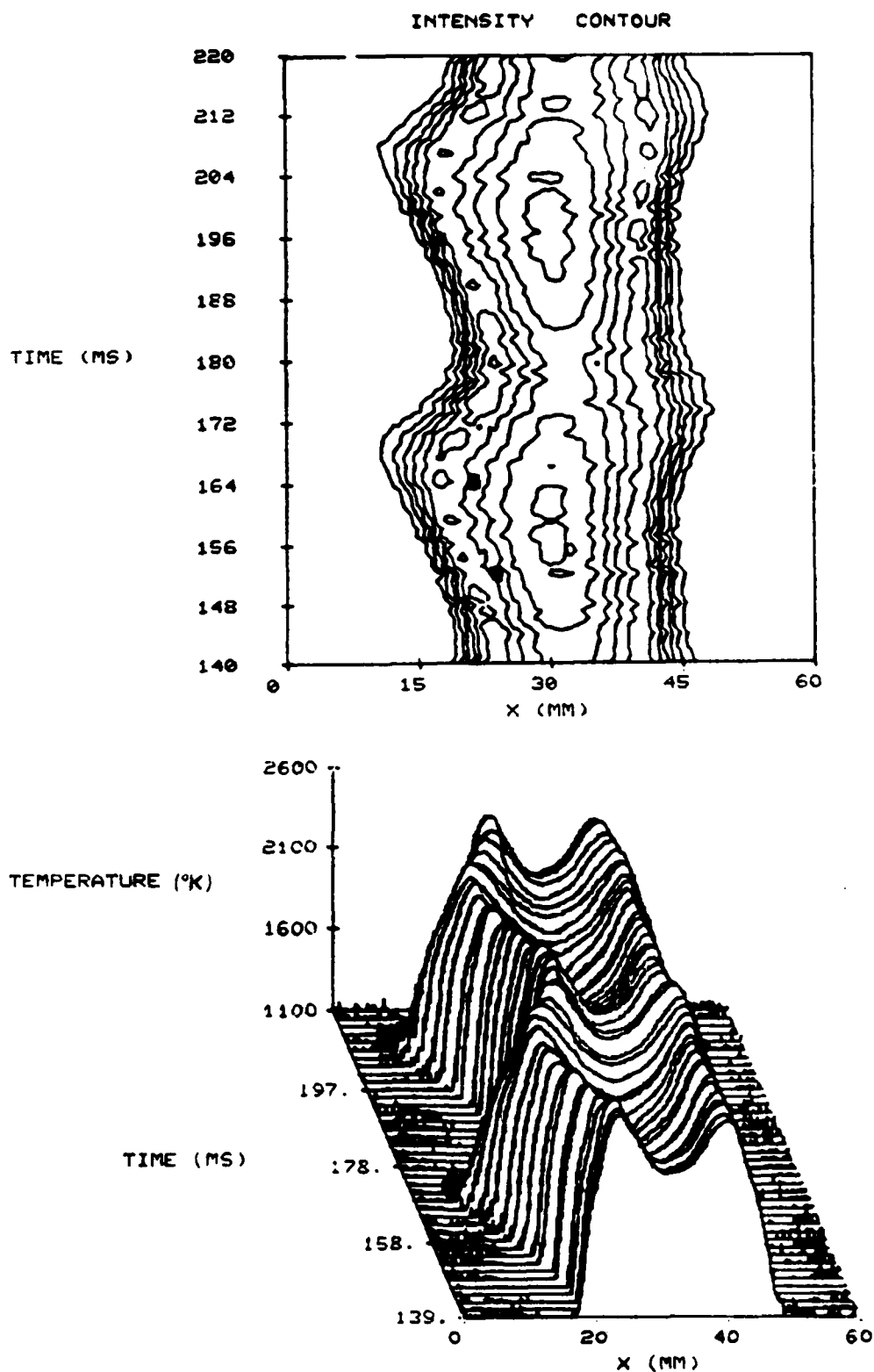


Fig. 17 Temperature Profiles of CO-H₂ Diffusion Flame and Intensity Contour Lines at 180 mm Axial Location.

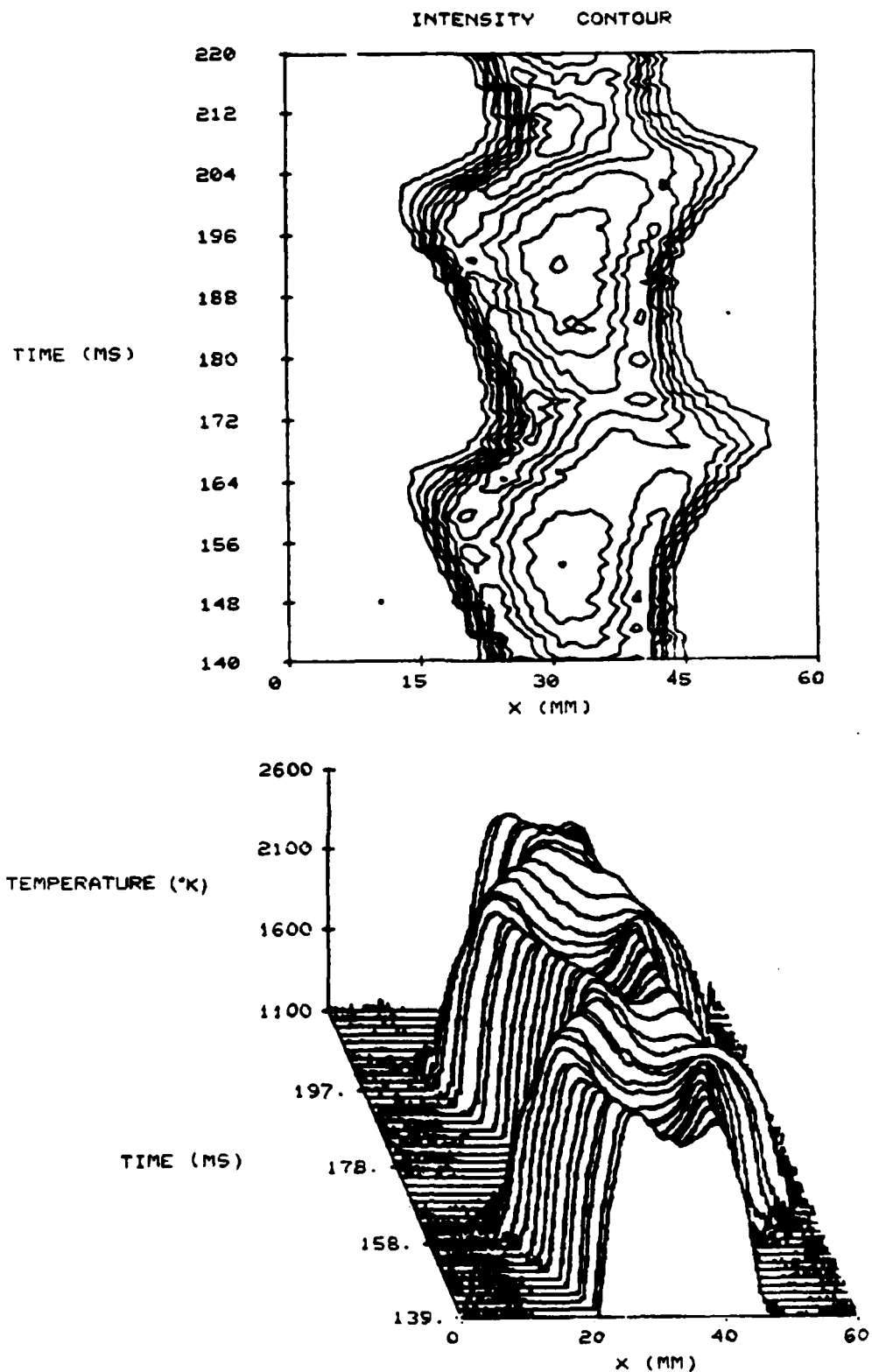


Fig. 18 Temperature Profiles of CO-H₂ Diffusion Flame and Intensity Contour Lines at 200 mm Axial Location.

from the combustion, at the stoichiometry rate, of fuel and the co-flowing air. The reaction zone is well defined and steady due to the molecular-transport nature of the mixing processes in this region. The flame structure display no indication of any low frequency oscillation but a comparatively high-frequency oscillating structure starts to be developed in the internal core affecting the external flame layer.

At 20 mm axial location, the flame has increased in size radially as well as the peak temperature. A low-frequency sinusoidal oscillation of the outer flame boundary is occurring, and the internal high frequency is fairly well developed; this high frequency seems to be in the same range of that reported by Chen (48) for the first sub-harmonic in the near field of cold round jets. The reaction sheet has doubled its width and acts as a damping wall of the frequency. Notice that the temperature gradient is sharper at the external side of the reaction sheet than at the internal one. The increase in the hot zone size is believed to be due to the high diffusivity of the H_2 molecule. The contour of the fuel jet was constructed to give a flat top velocity profile at the nozzle exit producing a very thin shear layer inside the flame surface; this is the origin of local instabilities that travel, becoming small vortices. These vortices grow and coalesce downstream producing a mixing process between the hot reacting layer and the cold

fuel core. These vortices together with the high viscosity of this flame reaction zone can be responsible for damping oscillating structure and the smoother temperature gradient outside the elastic flame surface.

At 40 mm axial location the jet has radially expanded to more than twice its initial value and the external oscillations have increased markedly in amplitude changing to a bell-like shape. Because of the difference in the velocities of the fuel and air jets, the outside shear layer tends to transport the air into the fuel jet promoting mixing. The reaction zone enlarges as more and more air is mixed with the fuel and undergoes combustion, resulting in a rise in the temperature with increasing the height from the nozzle exit. This expansion process is continued at 60 mm and 80 mm, changing to a butterfly-like shape. The flame surface wraps out over itself which results in the formation of a mushroom-like structure that engulfs the external air and forms a buoyancy driven toroidal vortex. This bulge will be reproduced at 16-17 nozzle diameters (D) downstream, as can be seen on Fig. 7 (obtained using the 2 laser-sheets lighting technique). At this bulge location the diameter reaches its maximum width of $\sim 4 D$.

At the 100 mm axial location the flame speeds up in the axial direction becoming thinner where the cold central jet is now unobservable. The mixing process drives an almost uniform increasing-decreasing process of the radial size.

with the highest temperature occurring at the maximum width point. This process continues, driving another vortex which feeds the flame surface with external air, becoming a new bulge approximately at 160 mm axial location. This interplay between the bulges and the coexisting vortex structures is responsible for the low frequency oscillations of the flame.

Above 180 mm axial location the room disturbances start to affect the flame structure giving it a three-dimensional character (flickering) with the peak temperature decreasing once the majority of fuel has been consumed and mixed. Higher axial temperature profiles were not attempted.

The height at which the toroidal vortices are formed is a strong function of the co-annular air velocity, being almost unaffected by the fuel composition (49). Rough measurements have indicated 25-30 Hz for this low frequency oscillation, while the high frequency oscillations seems to be in the 310-325 Hz range.

The graphs shown in Appendix A (from Fig. A-1 to Fig. A-11) corresponding to the experiment D, reveals a similar behavior when a H_2 -CO:N₂ diffusion flame is used. All of this means that these phenomena are predominantly driven by the fluid dynamic, and the kinetic reaction is initially confined to the flame sheet.

The Appendices B, C and D include the graphs corresponding to the experiments E, B and A respectively.

All of them show the high-frequency oscillations in the internal fuel jet.

In the experiment E for which the exit velocity is 4.9 m/s (notice that in experiment F this velocity was 2.87 m/s), the external side of the shear layer starts to develop the low-frequency oscillations at 40 mm axial location instead of 20 mm as in experiment F. The cold central jet is still observable at 200 mm and the temperature gradient is roughly equal at both sides of the shear layer. The general flame structure shows a similar behavior to the experiment F.

In the experiment B which exit velocity is 3.92 m/s the reaction zone is well defined and steady, and no indication of low frequency oscillations is displayed up to 60 mm where the radial size has increased twice. At 70 mm above nozzle, the butterfly-like structure indicates that the bulging process is being developed in the flame.

In order to check that the high-frequency oscillations were not due to the experimental fixture, a chamber (used as pressure wave filter) was settled to the fuel feeding lines using the gas mixture of experiment F. Fig. 19 clearly shows that these oscillations are an internal characteristic of the flame.

As a way to investigate if higher frequency oscillations are present at the internal structure of the flame the experiment B was performed using higher scanning

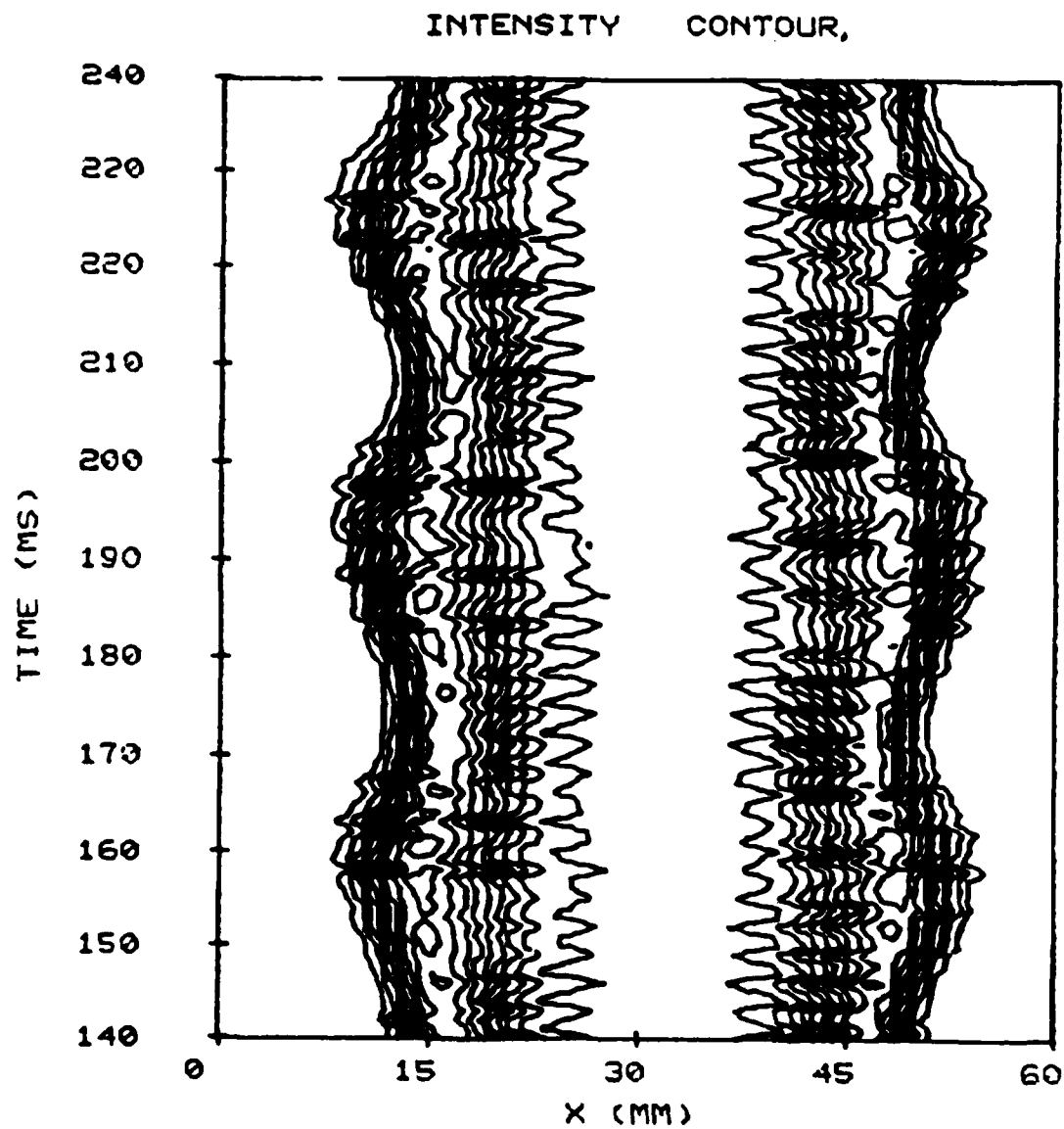


Fig. 19 Detail of Intensity Contour Lines of
CO-H₂ Diffusion Flame at 40 mm
Axial Location.

rates. Same results were obtained at different effective sweeps up to 5000 Hz.

Frequency Analysis

To determine the frequencies due to the oscillating structure obtained from the intensity contour lines, a Fourier Transform analysis of the data was carried out. The 3-D plots of the oscillation spectrum at various radial and axial locations of the flame are shown from Fig. 20 to Fig. 24 corresponding to the experiment F (pure CO-H₂ flame). As can be seen, the oscillations when developed are maintained along the axial direction.

Because of the limitation of the memory load of digitizer and computer used in the analysis, only frequencies up to 128 Hz could be determined. For that reason, it could not be established the exact meaning of the plotted frequency set around 84 Hz, and the graphs indicate only that higher frequencies occur.

At 30 mm downstream the typical low frequency associated with the buoyancy-driven structures starts to develop; at 90 mm and 160 mm axial locations the low frequency is split into two parts radially shifted. This can be associated to the bulges developed at those heights; the surface wraps out over itself forming two concentric flame sheets during a limited axial range until the bulge becomes a separate portion of the flame, and it speeds up downstream.

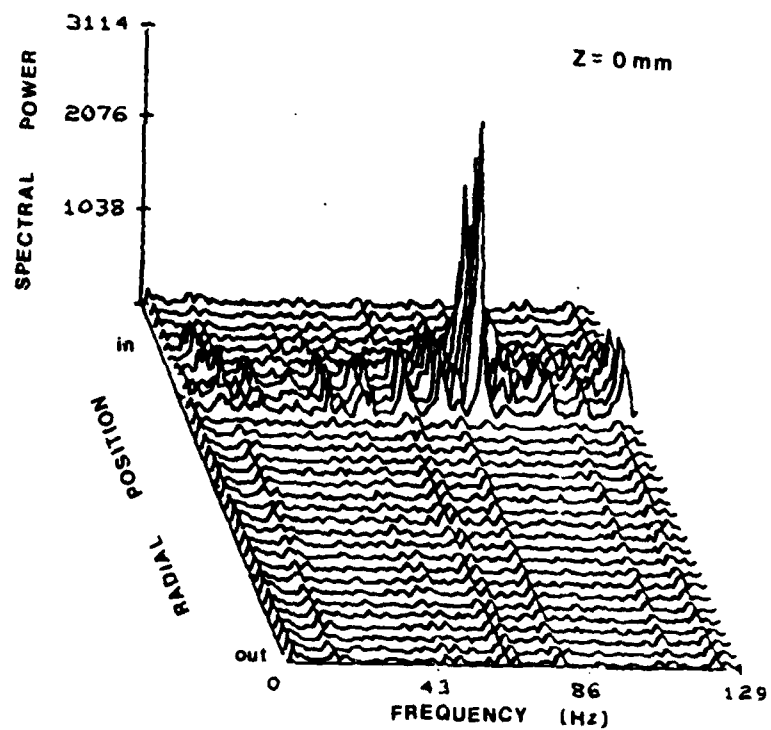
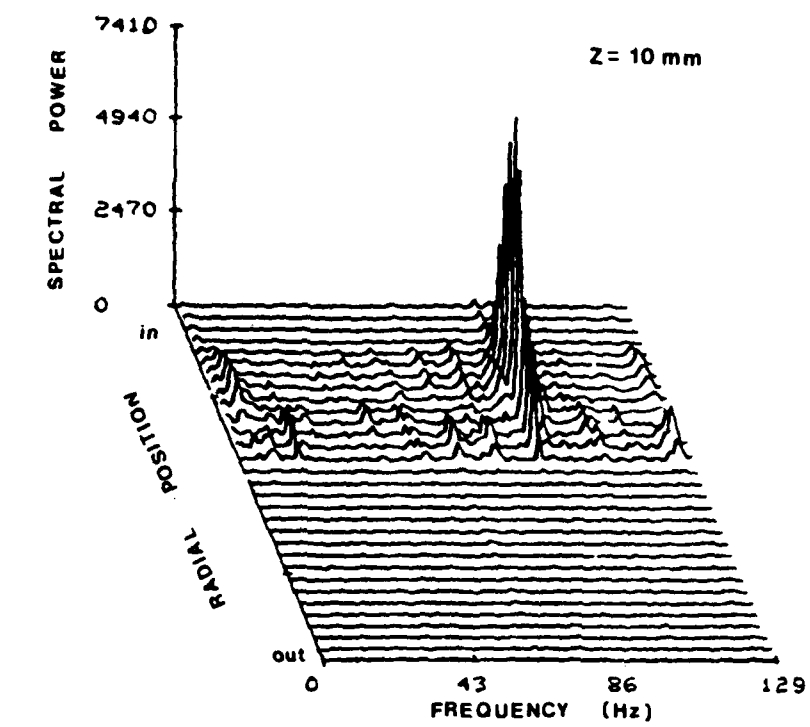


Fig. 20 Frequency Distribution Profiles of CO-H₂ Diffusion Flame at 0 mm and 10 mm Axial Location.

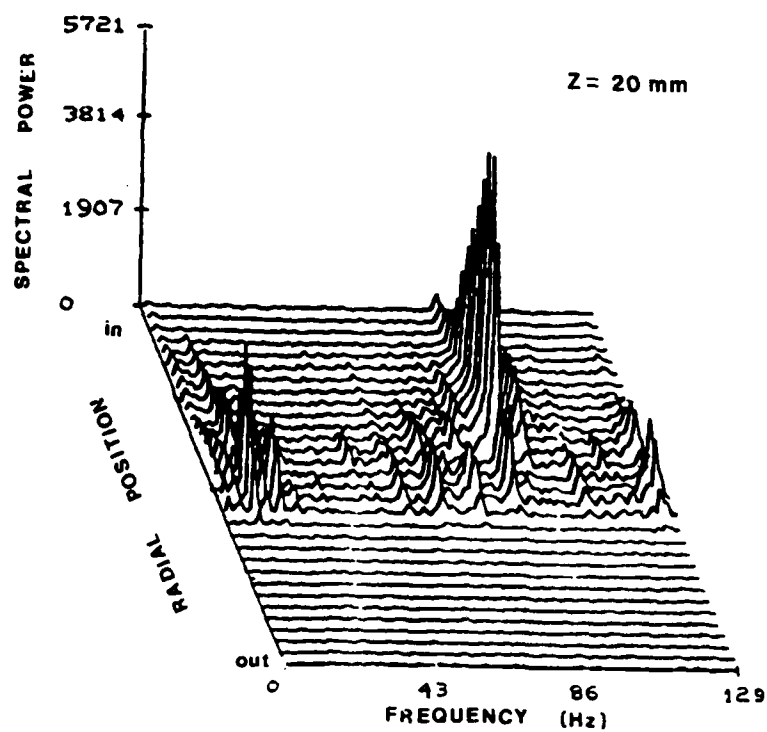
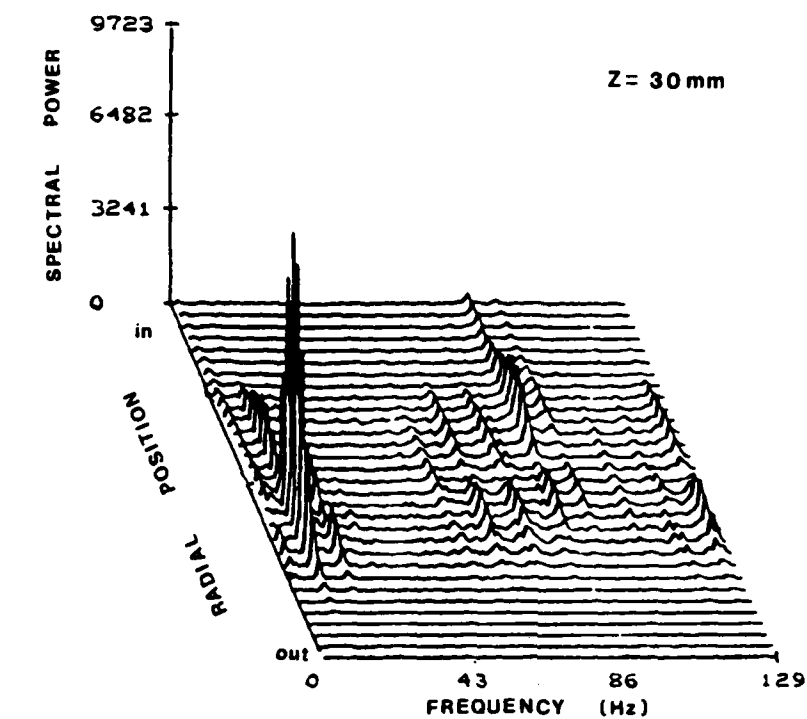


Fig. 21 Frequency Distribution Profiles of CO-H₂ Diffusion Flame at 20 mm and 30 mm Axial Location.

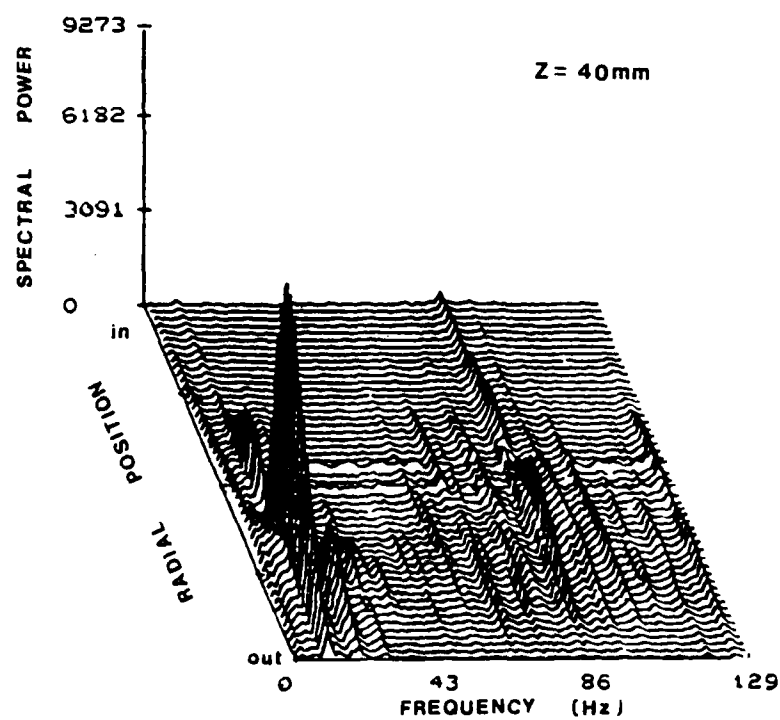
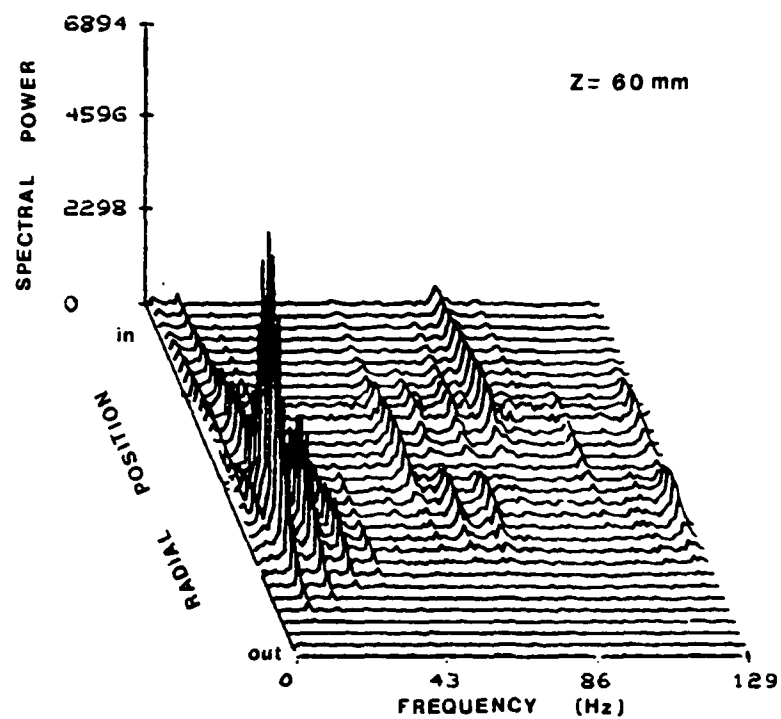


Fig. 22 Frequency Distribution Profiles of CO-H₂ Diffusion Flame at 40 mm and 60 mm Axial Location.

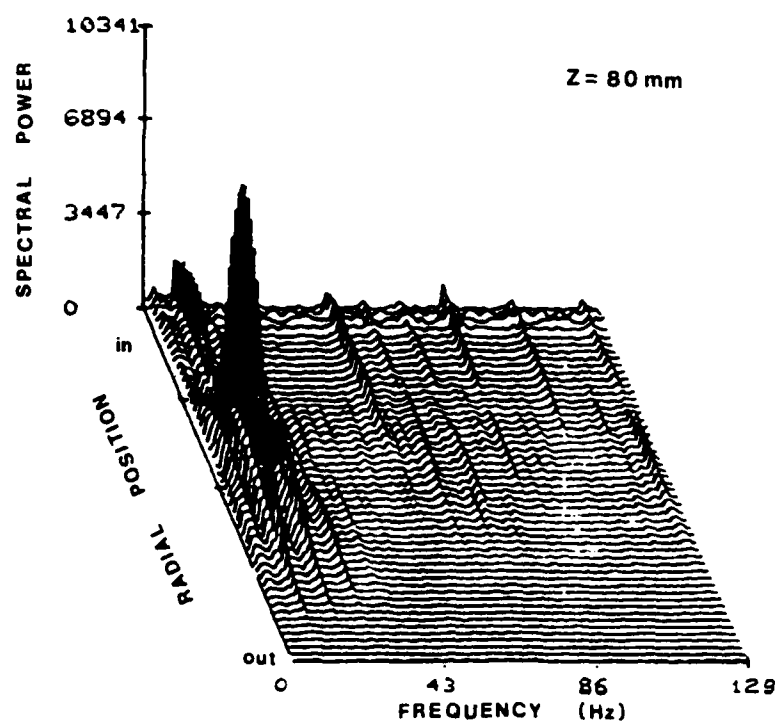
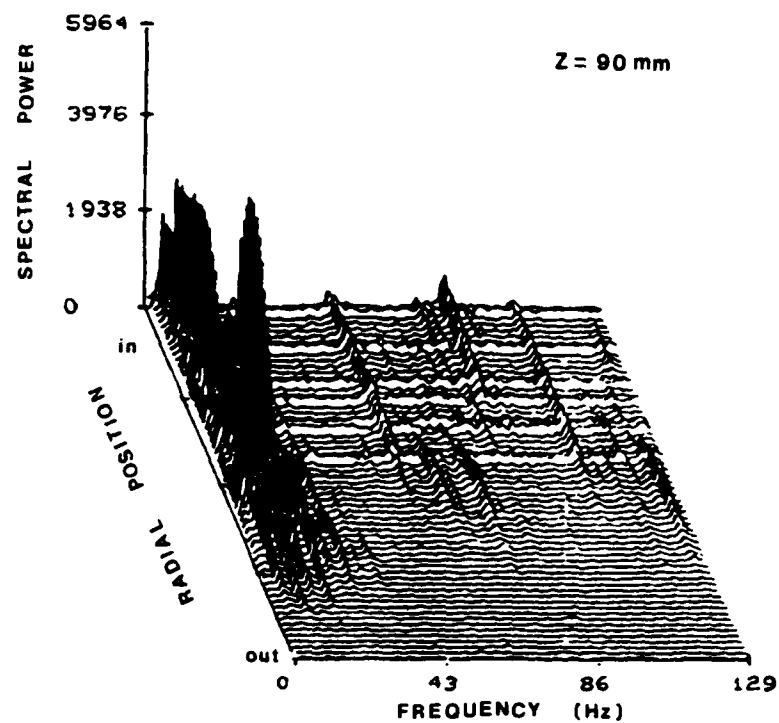


Fig. 23 Frequency Distribution Profiles of CO-H₂ Diffusion Flame at 80 mm and 90 mm Axial Location.

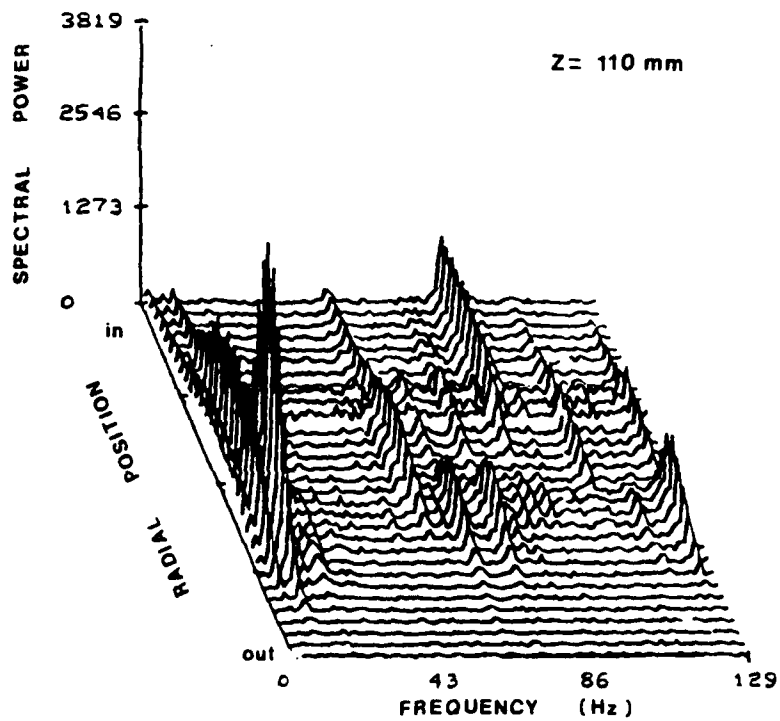
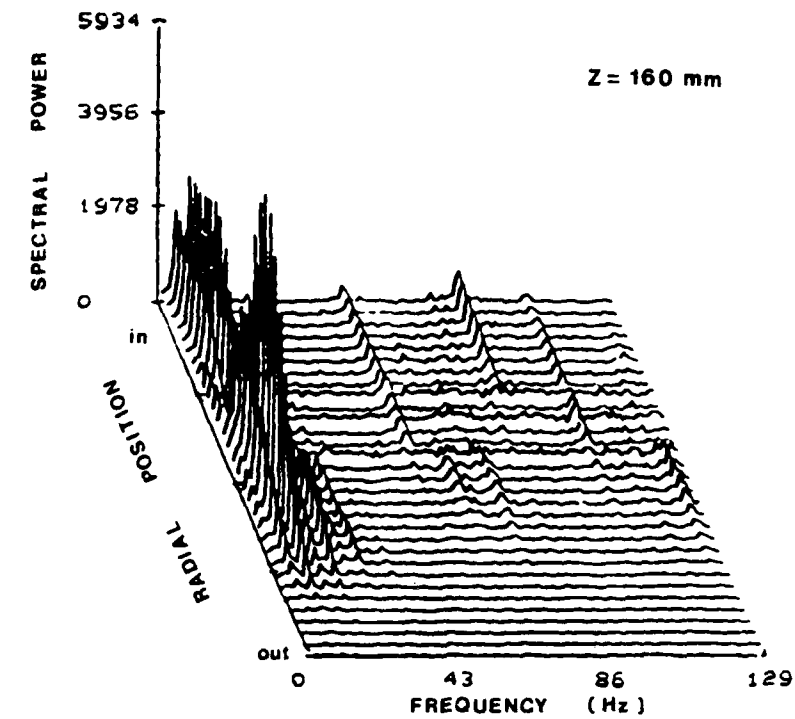


Fig. 24 Frequency Distribution Profiles of CO-H₂ Diffusion Flame at 110 mm and 160 mm Axial Location.

Fig. 25 shows a more complicated frequency behavior for the experiment A.

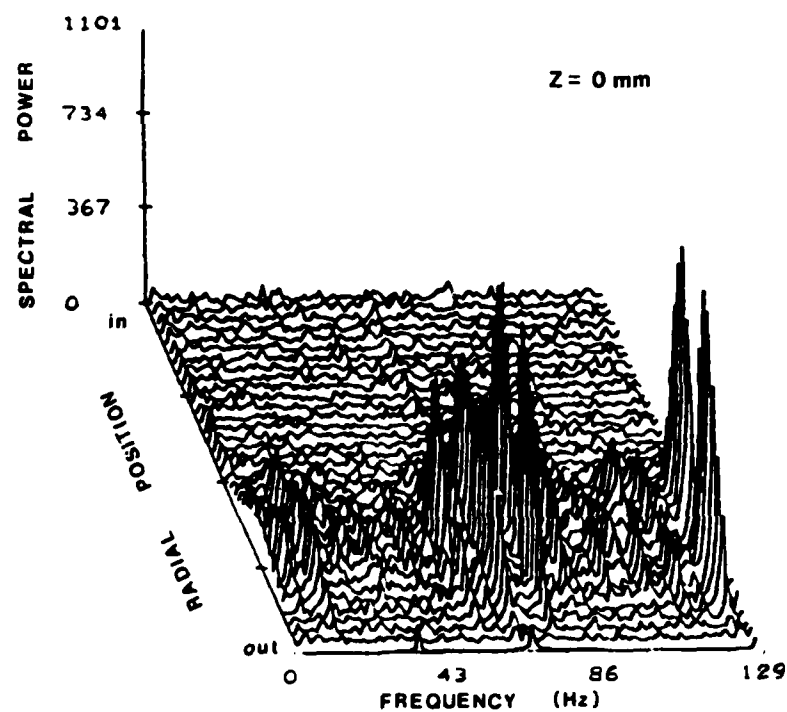
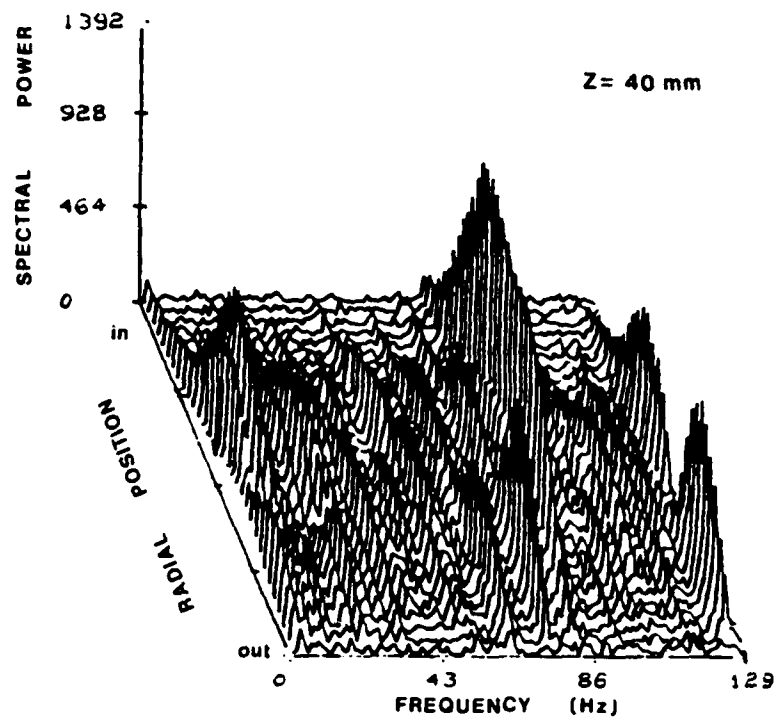


Fig. 25 Frequency Distribution Profiles of N_2 -CO- H_2 Diffusion Flame at 0 mm and 40 mm Axial Location, experiment A.

VI. Conclusions and Recommendations

The thin filament pyrometry technique has been demonstrated to be capable of measuring the temporal-spatial temperature distributions in a non-sooting CO-H₂ diffusion flame at high repetition rates up to 5000 Hz. Its high spatial and temporal resolution and its capability to make point temperature measurements along a line allows this technique to be a powerful tool for a quick qualitative characterization of the flame identifying its critical axial locations. In addition, it can provide a quantitative approach to the spatial and temporal temperature distributions as well as to the frequency spectrum of the fluid dynamic processes related with the flame.

New coated boron nitride ceramic fibers will increase its survivability under the severe combustion environment leading to a higher fiability in the quantitative measurements. A suitable choice of an IR detector and optics will extend the lower temperature measurement limit, set at 1100 °K at present.

Future improvements including radiation losses correction, and digitizer and computer loading memory increase will allow a higher precision in the temperature measurement, a higher scanning rate with the consequential wider frequency analysis, and the acquisition of sufficient amount of data to apply a statistical analysis and determine average values with its PDF along the time, radial, and

axial locations.

An intensive theoretical analysis of these results must be carried out. Questions like why the flame is not stoichiometric and what is its correlation with the local diffusion heat losses; where is the largest gradient of temperature and why, and its correlation with the temperature peaks; where are these located in the radial direction; what are the local changes of the thermal diffusion coefficient; why is the rate of temperature change different at the internal and external sides of the reaction layer, etc., need to be answered. The TFP technique needs to be increased in its quantitative precision through a detailed theoretical model of the heat balance between the filament and the surrounding gas.

Besides the low frequency associated with the dynamics of large scale buoyancy-driven vortices, a new set of higher frequencies believed associated to the internal jet core of the flame has been found in the CO-H₂ and N₂-CO-H₂ diffusion flames. Preliminary results gave a 25-30 Hz range for the low frequency and 300-325 Hz for the high. However, a more detailed Fourier Transform frequency analysis must be carried out to establish the exact correlation between the different harmonics that appear in the spectrum.

The 2-perpendicular laser-sheets lighting technique has been used as a tool to visualize the flame structure together with the TFP technique to a better understanding of

the combustion dynamics.

Bibliography

1. Williams, F.A. Combustion Theory. California: The Benjamin/Cummings Publishing Company, 1985
2. Ho, C.M. and L.S. Huang, "Subharmonic and Vortex Merging in Mixing Layers," J. Fluid Mechanics, 119: 443-473 (1982).
3. Rose, A. and R. Gupta, "Combustion Diagnostics by Photo-Deflection Spectroscopy," Twentieth Symposium on Combustion, 1339-1345 (1984).
4. Drake, M.D., M. Lapp, C.M. Penney, S. Warshaw and B.W. Gerhold, "Measurements of Temperature and Concentration Fluctuations in Turbulent Diffusion Flames Using Pulsed Raman Spectroscopy," in Proceedings, Eighteenth Symposium on Combustion. Pittsburgh, Pa.: Combustion Institute, 1521 (1981).
5. Eckbreth, A.C. and R.J. Hall, "CARS Concentration Sensitivity With and Without Nonresonant Background Suppression," Combust. Sci. Technol., 25: 175 (1981).
6. Daily, J.W., "Saturation Effects in Laser Induced Fluorescence Spectroscopy," Appl. Opt., 16: 568 (1977).
7. Lucht, R.P., D.W. Sweeney and N.M. Laurendeau, "Saturated-Fluorescence Measurements of the Hydroxyl Radical," in Laser Probes for Combustion Chemistry, Washington, D.C.: D.R. Crosley Ed. 134: 145 (1980).
8. Crosley, D.R., "Collisional Effects on Laser-Induced Fluorescence Flame Measurements," Opt. Eng., 20: 511 (1981).
9. Attal, B., K. Muller-Dethlefs, D. Debarre and J.P.E. Taran, "Resonant CARS Spectroscopy of C₂," Appl. Phys., 28: 121 (1982).
10. Attal, B., D. Debarre, K. Muller-Dethlefs and J.P.E. Taran, Rev. Phys. Appl., 18: 39 (1983).
11. Piepmeier, E.M., Spectrochim. Acta B, 27: 445 (1972).
12. Allen, J.E. Jr., W.R. Anderson and D.R. Crosley, "Optoacoustic Pulses in a Flame," Opt. Lett., 1:118 (1977).

13. Tennal, K., G.J. Salamo and R. Gupta, "Minority Species Concentration Measurements in Flames by the Photoacoustic Techniques," Appl. Opt., 21: 2133 (1982).
14. Rose, A., J.D. Pyrum, G.J. Salamo and R. Gupta, "Photoacoustic Spectroscopy and Photothermal Deflection Spectroscopy: New Tools for Combustion Diagnostics," in Proceedings, International Conference of Lasers '82 McLean, VA.: R.C. Powell Ed., (1983).
15. Rose, A., G.J. Salamo and R. Gupta, "Photoacoustic Deflection Spectroscopy: A New Specie-Specific Method for Combustion Diagnostics," Appl. Opt., 23: 781 (1984).
16. Jackson, W.B., N.M. Amer, A.C. Boccara and D. Fournier, "Photothermal Deflection Spectroscopy and Detection," Appl. Opt., 20: 1333 (1981).
17. Patel, C.K.N. and A.C. Tam, "Optoacoustic Spectroscopy of Liquids," Appl. Phys. Lett., 34: 467-470 (1979).
18. Davis, C.C. "Trace Detection of Gases Using Phase Fluctuation Optical Heterodyne Spectroscopy," Appl. Phys. Lett., 36: 515 (1980).
19. Boccara, A.C., D. Fournier and J. Badoz, "Thermo-Optical Spectroscopy: Detection by the Mirage Effect," Appl. Phys. Lett., 36: 130 (1980).
20. Boccara, A.C., D. Fournier, W.B. Jackson and N.M. Amer. "Sensitive Photothermal Deflection Technique for Measuring Absorption in Optically Thin Media," Opt. Lett., 5: 377 (1980).
21. Fournier, D., A.C. Boccara, N.M. Amer and R. Gerlach, "Sensitive in situ Trace-Gas Detection by Photothermal Deflection Spectroscopy," Appl. Phys. Lett., 37: 519 (1980).
22. Loulergue, J.C. and A.C. Tam, "Noncontact Photothermal Probe Beam Deflection Measurement of Thermal Diffusivity in a Hot Unconfined Gas," Appl. Phys. Lett., 46: 457 (1985).
23. Sontag, H. and A.C. Tam, "Time-Resolved Flow-Velocity and Concentration Measurements Using a Traveling Thermal Lens," Opt. Lett., 10: 436 (1985).
24. Tam, A.C., H. Sontag and P. Hess. "Photothermal Probe Beam Deflection Monitoring of Photochemical Particulate Production," Chem Phys. Lett., 120: 280 (1985).

25. Sontag, H. and A.C. Tam, "Characterization of Vapor and Aerosol Flows by Photothermal Methods," Can. J. Phys., Sept. (1986).
26. For a review see Tam, A.C. "Applications of Photoacoustic Sensing Techniques," Rev. Mod. Phys., 58: 381 (1986).
27. Rose, A., J.D. Pyrum, C. Muzny, G.J. Salamo and R. Gupta, "Application of the Photothermal Deflection Technique to Combustion Diagnostics," Appl. Opt., 21: 2663 (1982).
28. Kizirnis, S.W., R.J. Brecha, B.N. Ganguly, L.P. Goss and R. Gupta, "Hydroxyl (OH) Distributions and Temperature Profiles in a Premixed Propane Flame Obtained by Laser Deflection Techniques," Appl. Opt., 23: 3873 (1984).
29. Rose, A. and R. Gupta, "Application of Photothermal and Photoacoustic Deflection Techniques to Sooting Flames: Velocity, Temperature, and Concentration Measurements," Opt. Commun., 56: 303 (1986).
30. Gupta, R., "A Quantitative Investigation of Pulsed Photothermal and Photoacoustic Deflection Spectroscopy for Combustion Diagnostics," AIP Conf. Proc., 146: 672 (1986).
31. Rose, A., R. Vyas and R. Gupta, "Pulsed Photothermal Deflection Spectroscopy in a Flowing Medium: a Quantitative Investigation," Appl. Opt., 24: 4626 (1986).
32. Drain, L.E., The Laser Doppler Technique. New York: John Wiley, (1980).
33. Cheng, R.K. and T.T. Ng, Phys. Fluids, 28: 473 (1985).
34. Schenck, P.K., J.C. Travis, G.C. Turk and T.C. O'Haver, Appl. Spectrosc., 36: 168 (1982).
35. Rose, A. and R. Gupta, "Application of Photothermal Deflection Technique to Flow-Velocity Measurements in a Flame," Opt. Lett., 10: 532 (1985).
36. Sell, J.A. and R. Cattolica, "Linear Imaging of Gas Velocity using the Photothermal Deflection Effect," Appl. Opt., 9: 1420 (1986).

37. Goss, L.P., D.F. Grosjean, B. Sarka and S.W. Kizirnis, "Time-Resolved Temperature Measurements in a Premixed Flame Using the Optoacoustic Beam-Deflection Technique" AIAA Paper No. 85-1445. Monterey, CA.: AIAA/SAE/ASME 21st Joint Propulsion Conference, (1985).
38. Grosjean, D.F., B. Sarka and L.P. Goss, "Time-Resolved Temperature Measurements in a Laboratory Flame Using the Optoacoustic Beam-Deflection Method," Opt. Lett., 10: 324 (1985).
39. Villimpoc, V., L.P. Goss and B. Sarka, "Evaluation of Optical Diagnostic Techniques for High-Frequency Temperature Measurements," in Proceedings, 1987 Spring Technical Meeting of the Central States Section of the Combustion Institute, Argonne, IL., (1987).
40. Villimpoc, V., L.P. Goss and B. Sarka, "Line Temperature Measurements by the Thin-Filament-Pyrometry Technique," Opt. Lett., in press.
41. Roquemore, W.M., R.S. Tankin, H.H. Chiu and S.A. Lottes, "A Study of a Bluff-Body Combustor Using Laser Sheet Lighting," Exps. in Fluids, 4: 205 (1986).
42. Goss, L.P., W.F. Lynn, W.M. Roquemore and L-D. Chen, "Structure of Jet Diffusion Flames," in Proceedings, 1987 Spring Technical Meeting of the Central States Section of the Combustion Institute, Argonne, IL., (1987).
43. Chen, L-D., W.M. Roquemore, L.P. Goss and D.D. Trump, "The Structure of Jet Flames," in Proceedings, 21st Symposium (International) on Combustion, Munich, W. Germany, (1986).
44. NICALON NLM-202 & NLM-102, Silicon-Carbide Fiber, Dow Corning Corporation, Midland, MI., 48686-0995.
45. Goss, L.P. et al., Paper to be submitted to Appl. Opt.
46. Yule, A.J., N.A. Chigier, S. Ralph, R. Boulderstone and J. Ventura, AIAA J., 19: 752 (1981).
47. Chen, L-D., and W.M. Roquemore, Combustion Flame, 66: 1 (1986).
48. Chen, T.H. and J. Schmoll, "Development of Structures in the Near Field of Round Jets," Paper submitted to the AIAA 26th Aerospace Science Meeting, Reno, NV. (1988).

49. Roquemore, W.M., private communication.

Appendix A: Temperature Profiles of N₂-CO-H₂ Diffusion
Flame and Intensity Contour Lines at Various
Axial Locations; Re = 857

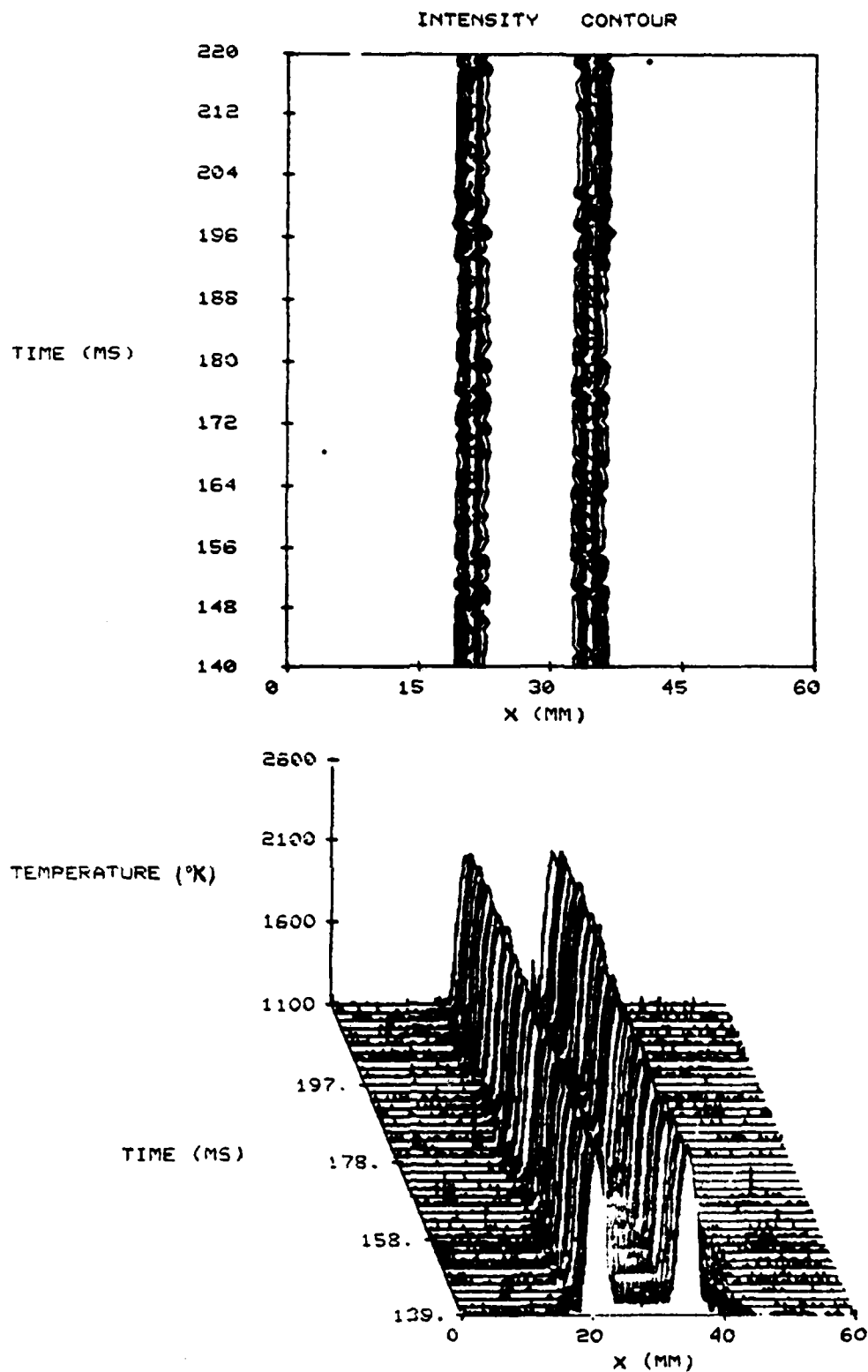


Fig. A-1 Temperature Profiles of N_2 -CO- H_2 Diffusion Flame and Intensity Contour Lines at 0 mm Axial Location. experiment D.

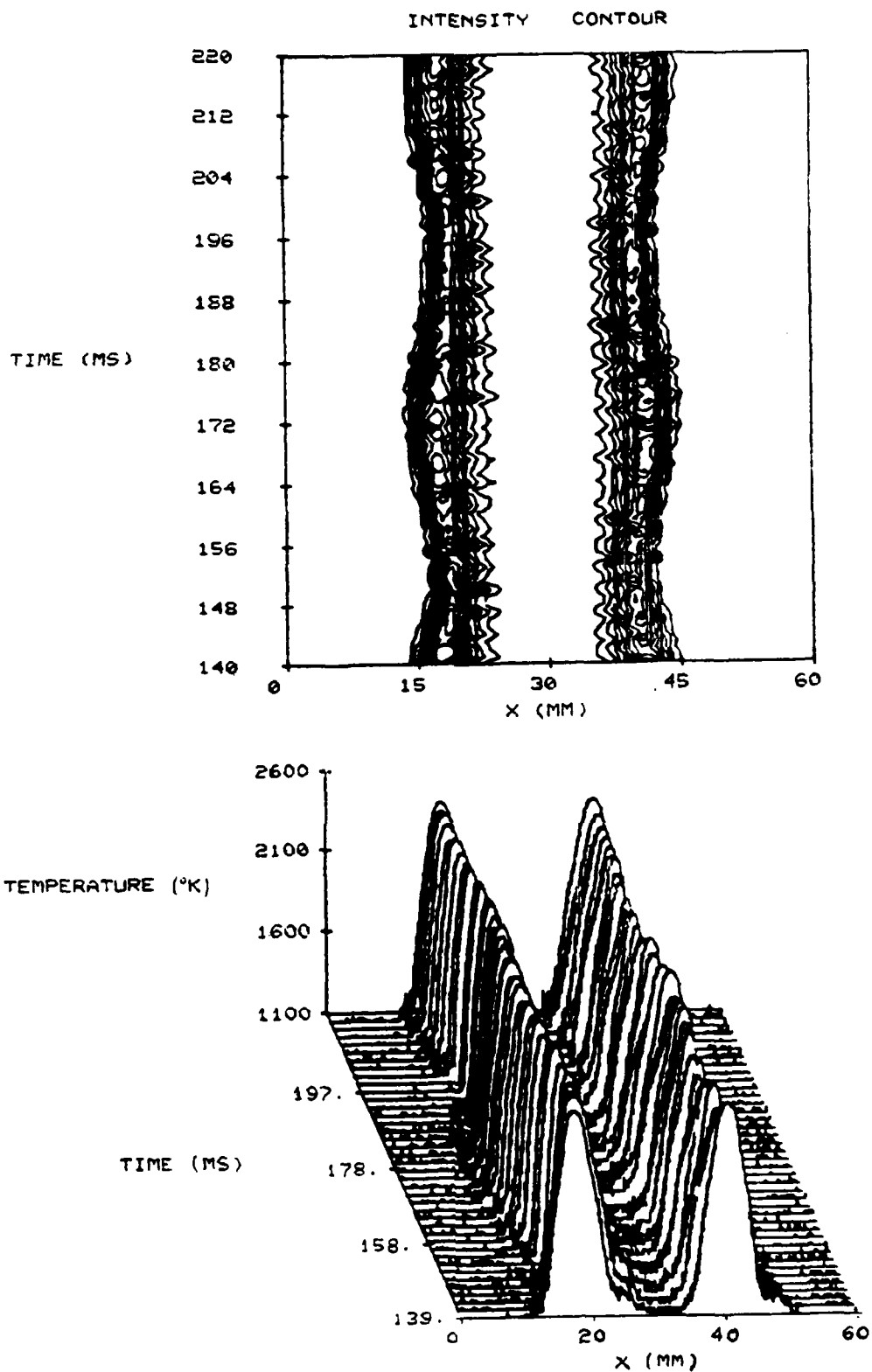


Fig. A-2 Temperature Profiles of N_2 -CO- H_2 Diffusion Flame and Intensity Contour Lines at 20 mm Axial Location, experiment D.

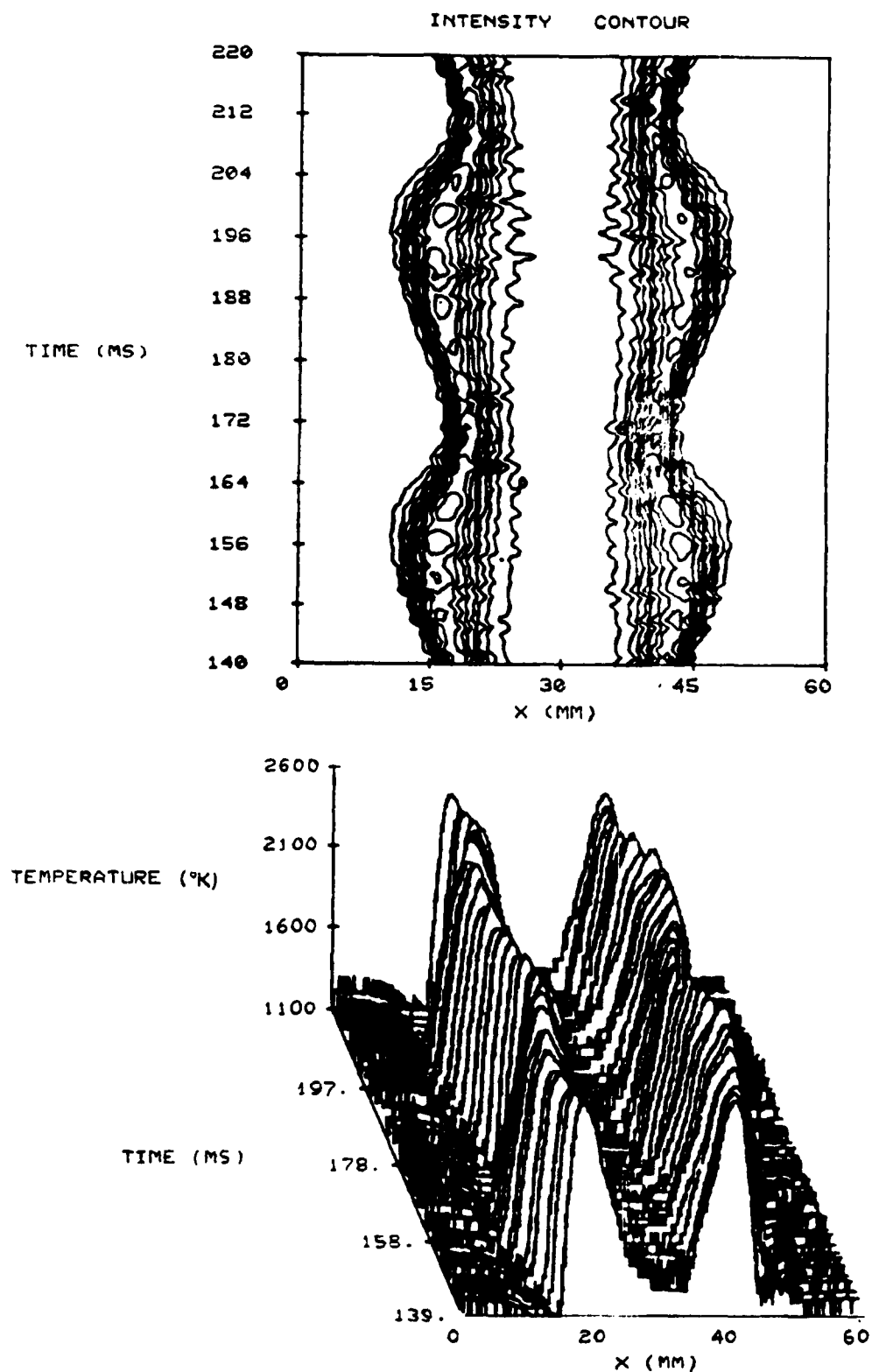


Fig. A-3 Temperature Profiles of N_2 -CO- H_2 Diffusion Flame and Intensity Contour Lines at 40 mm Axial Location, experiment D.

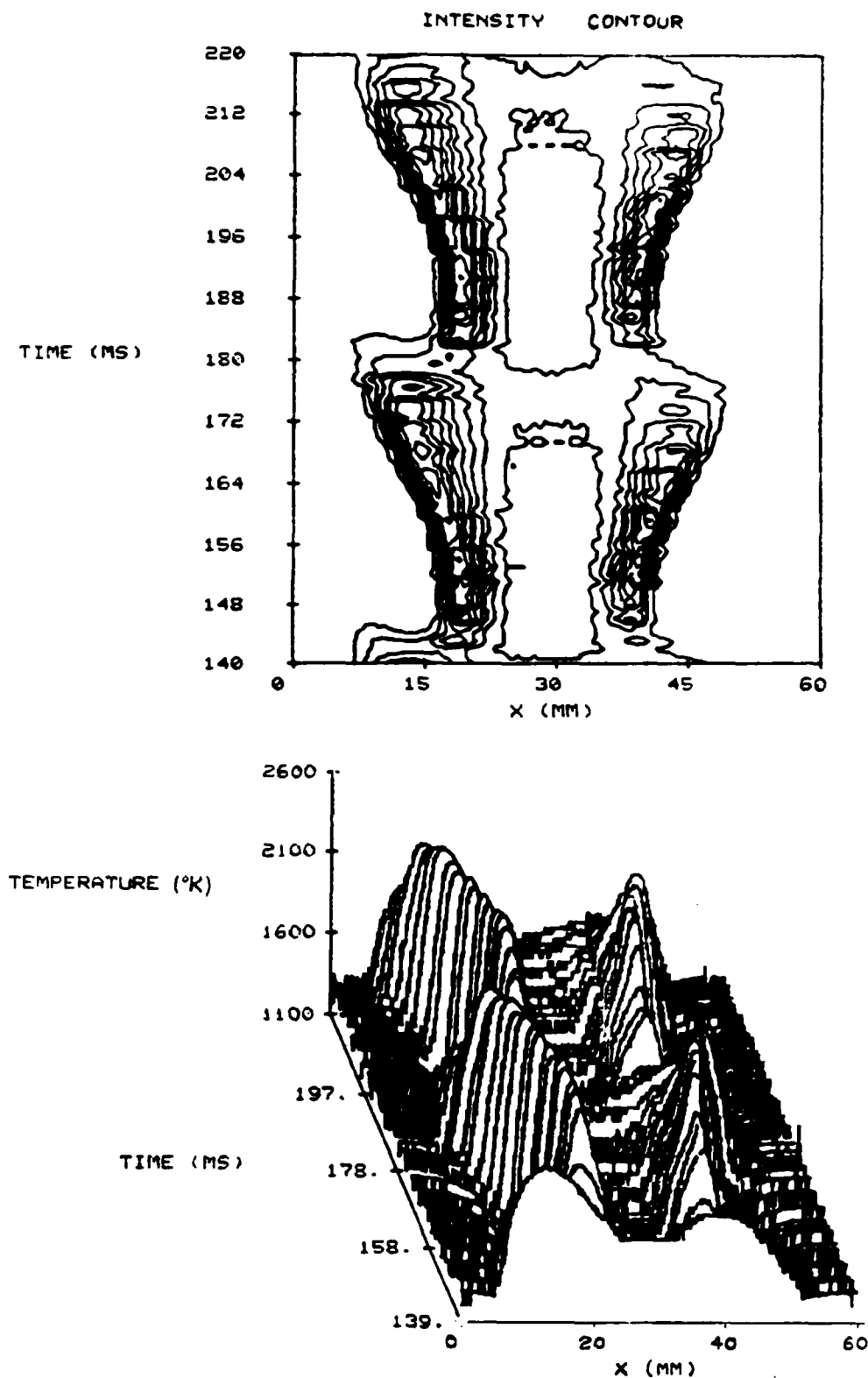


Fig. A-4 Temperature Profiles of N_2 -CO- H_2 Diffusion Flame and Intensity Contour Lines at 60 mm Axial Location, experiment D.

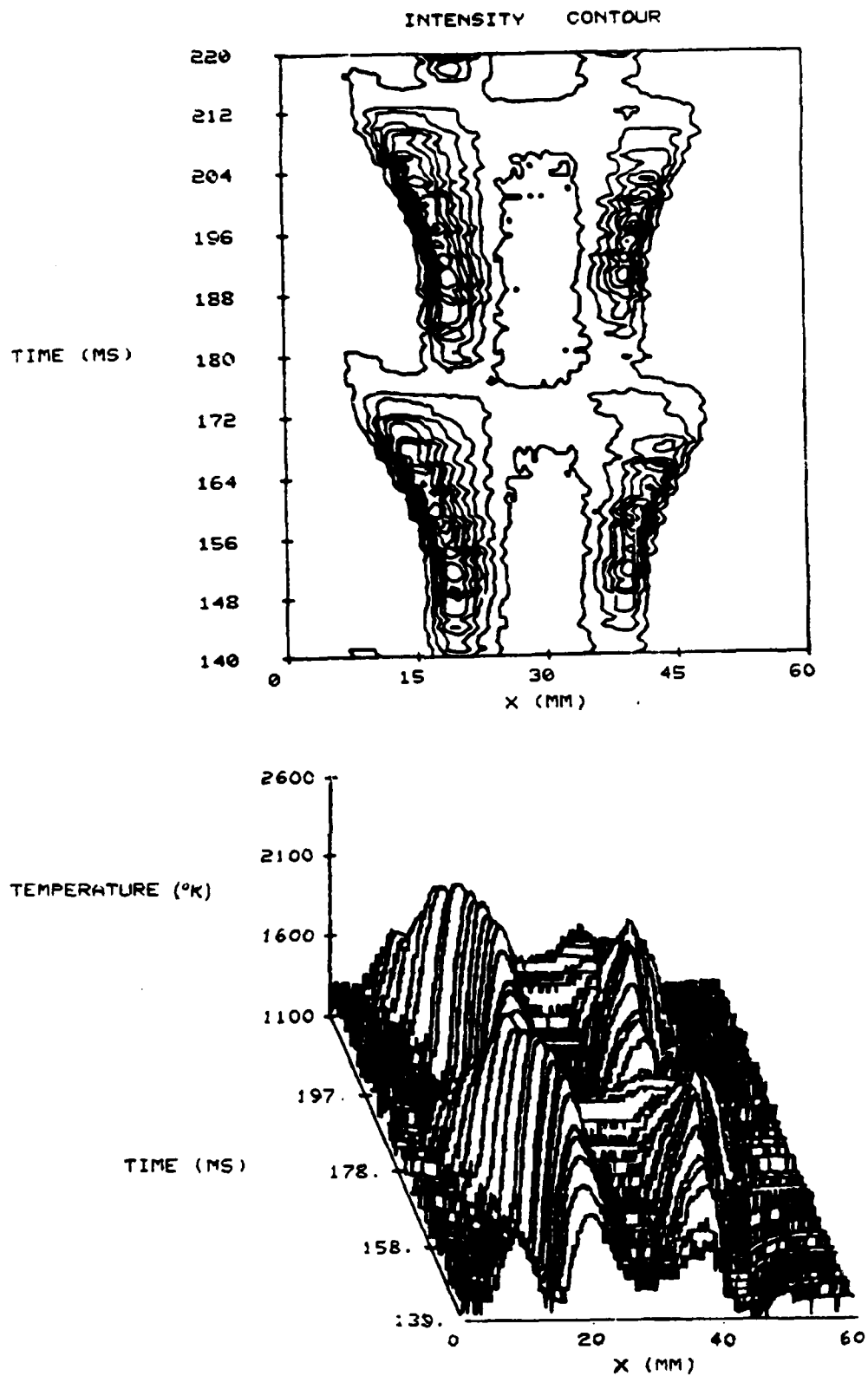


Fig. A-5 Temperature Profiles of N_2 -CO- H_2 Diffusion Flame and Intensity Contour Lines at 80 mm Axial Location, experiment D.

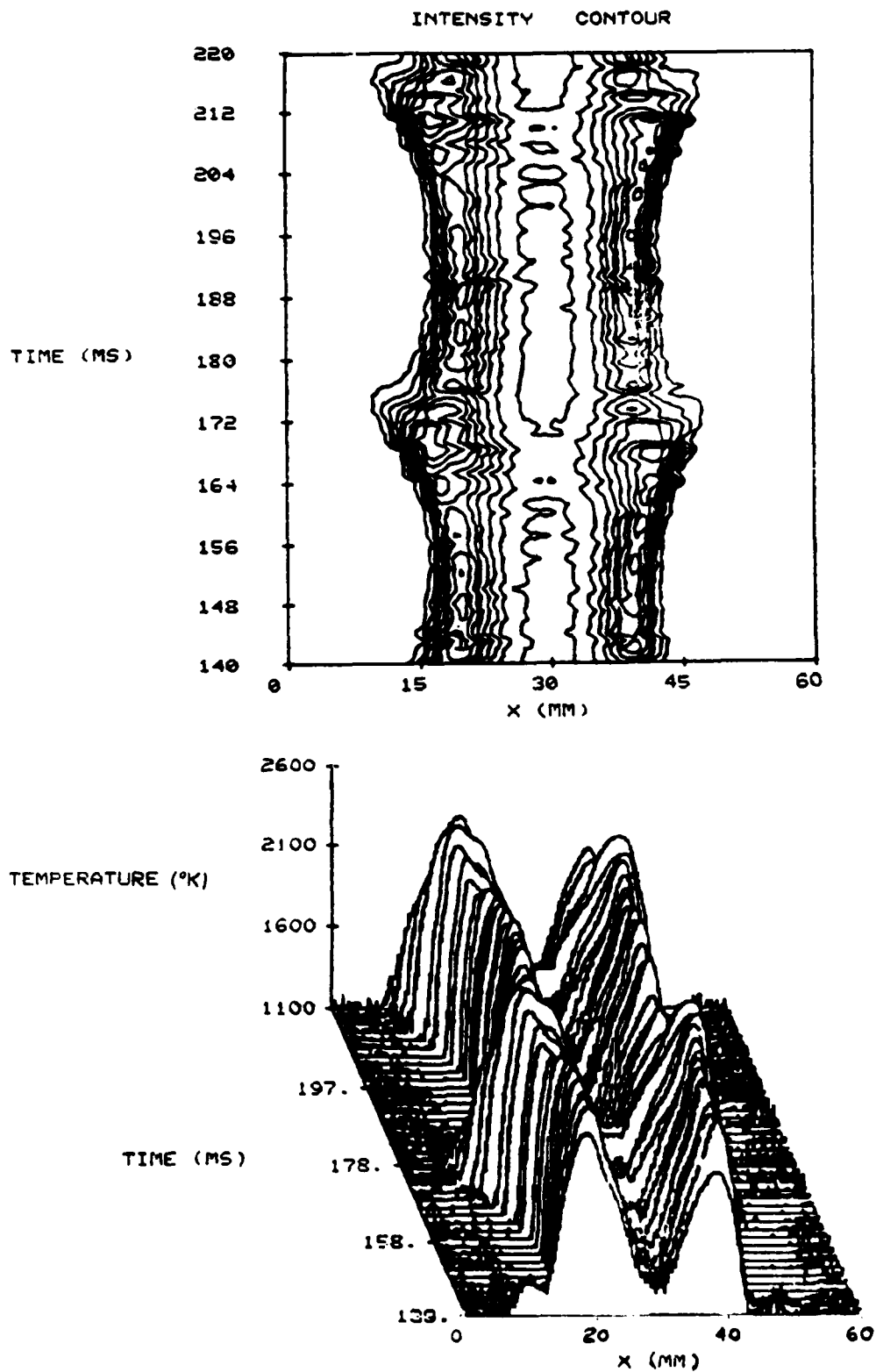


Fig. A-6 Temperature Profiles of $\text{N}_2\text{-CO-H}_2$ Diffusion Flame and Intensity Contour Lines at 100 mm Axial Location, experiment D.

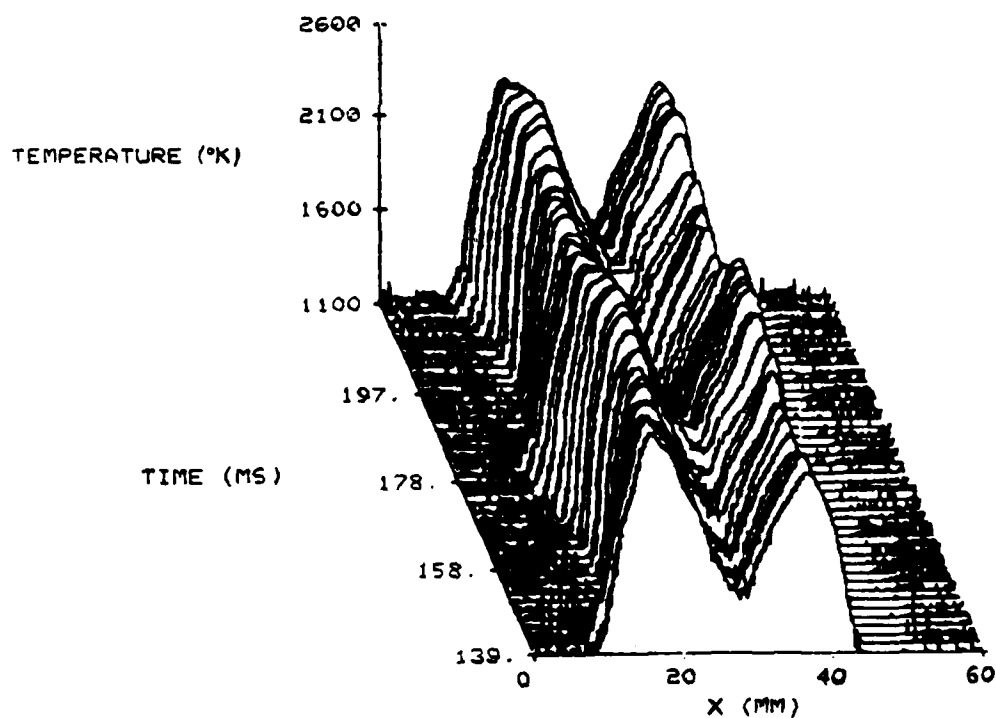
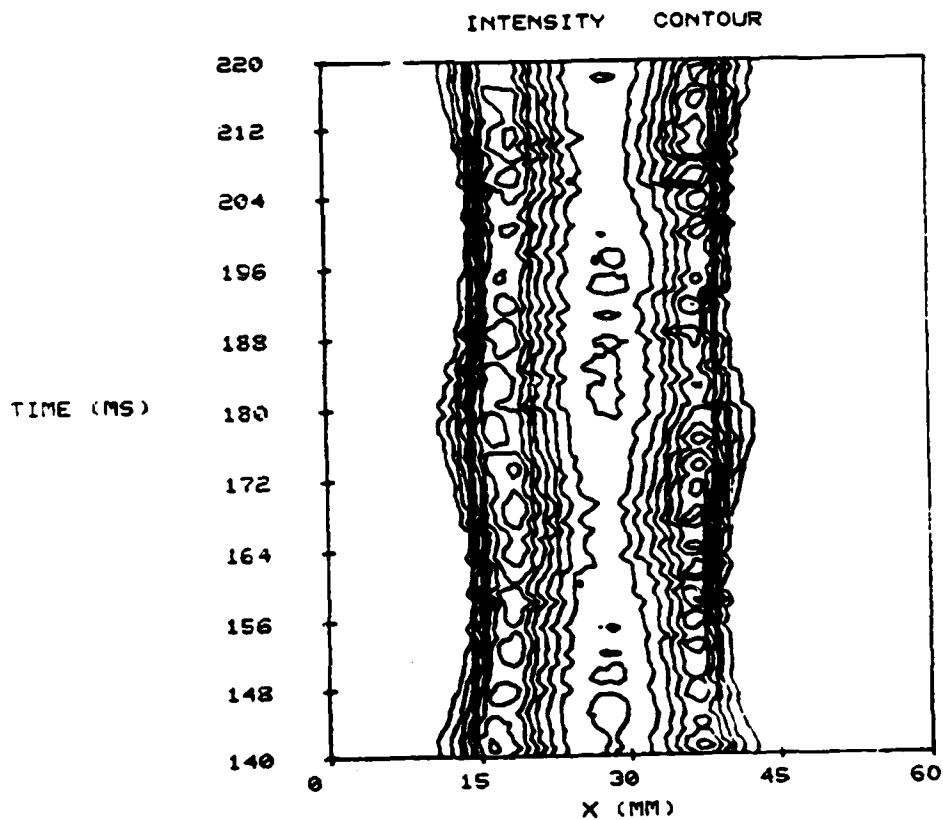


Fig. A-7 Temperature Profiles of N_2 -CO- H_2 Diffusion Flame and Intensity Contour Lines at 120 mm Axial Location, experiment D.

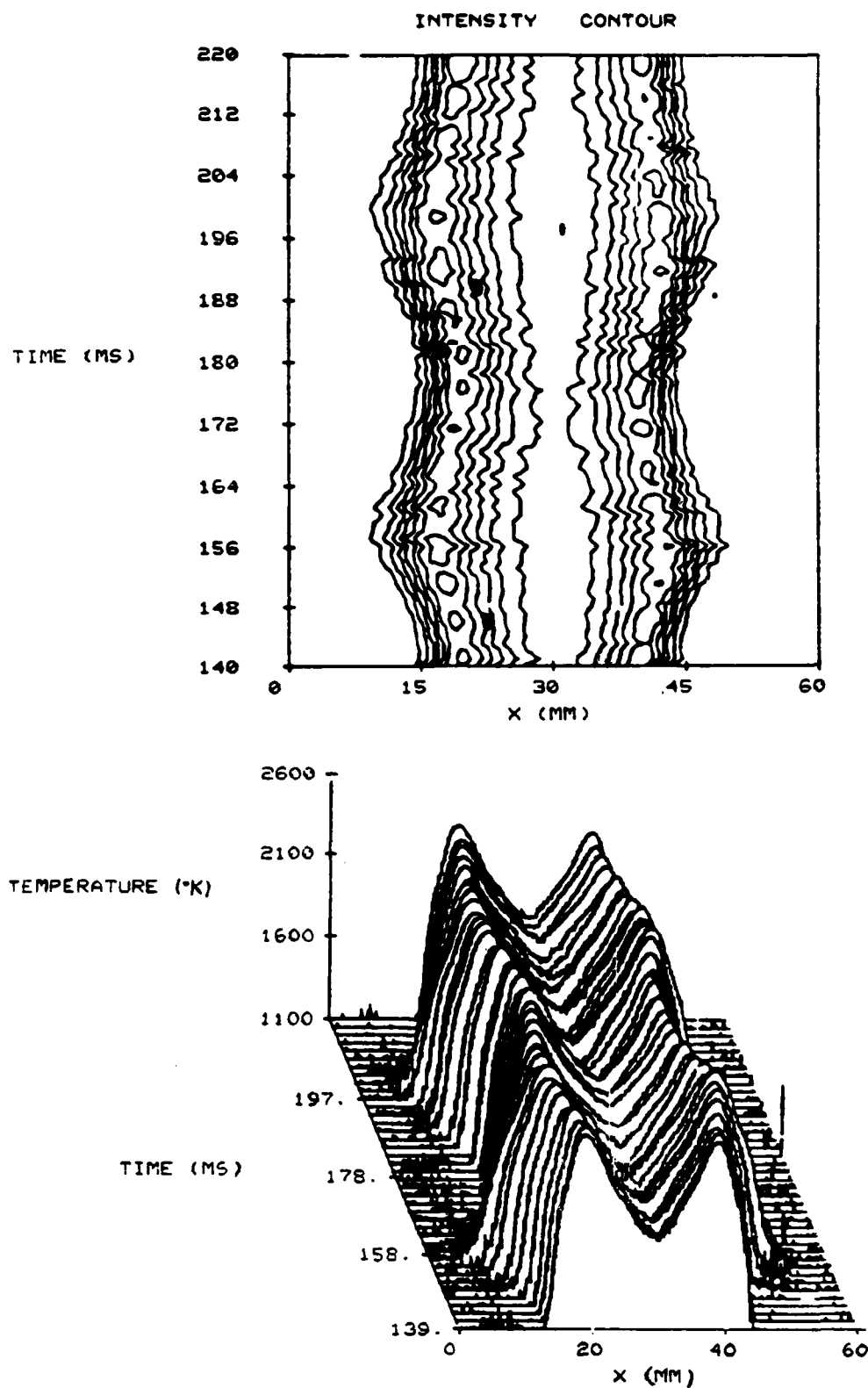


Fig. A-8 Temperature Profiles of N_2 -CO- H_2 Diffusion Flame and Intensity Contour Lines at 140 mm Axial Location, experiment D.

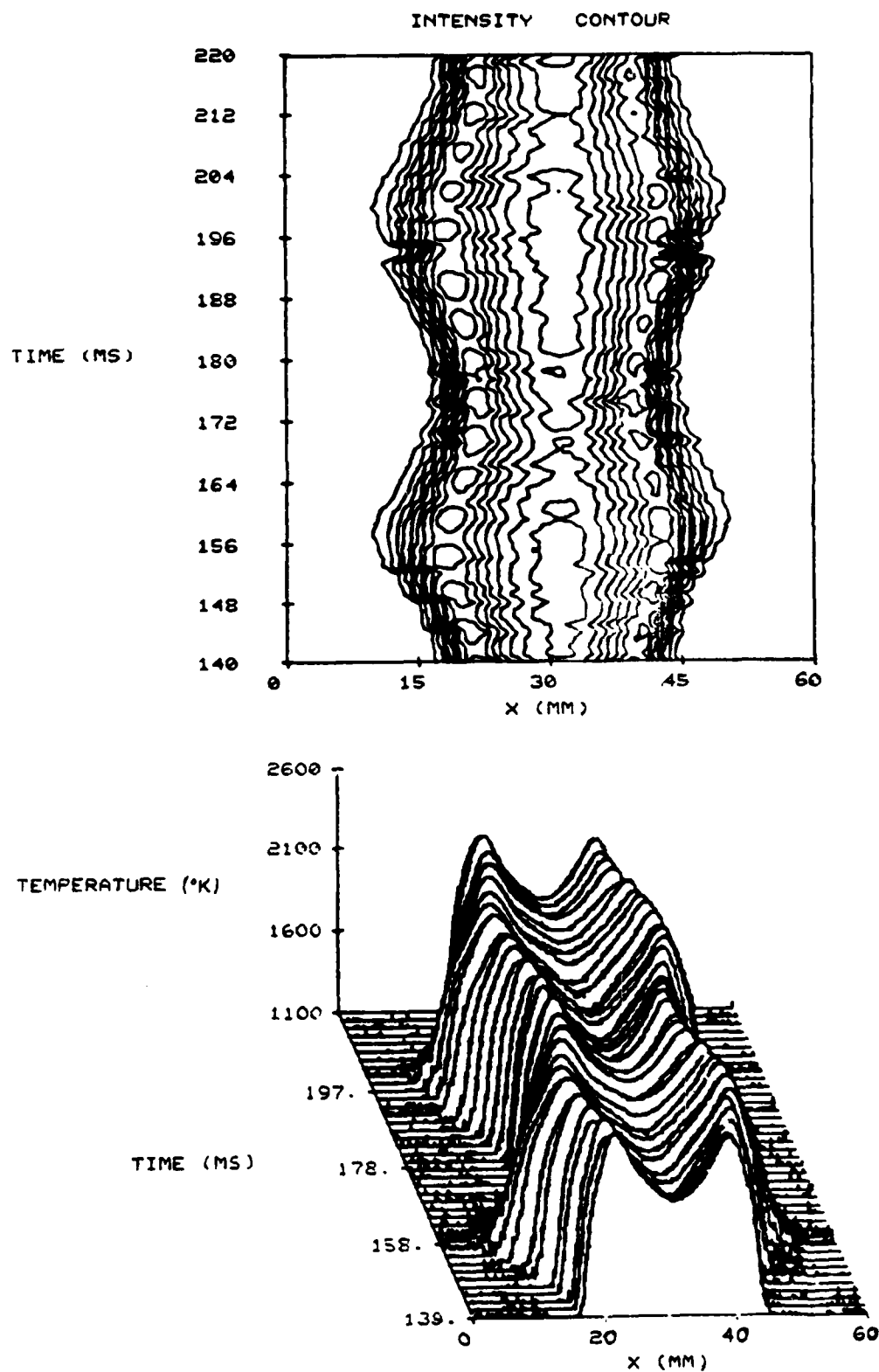


Fig. A-9 Temperature Profiles of $\text{N}_2\text{-CO-H}_2$ Diffusion
Flame and Intensity Contour Lines at 160 mm
Axial Location, experiment D.

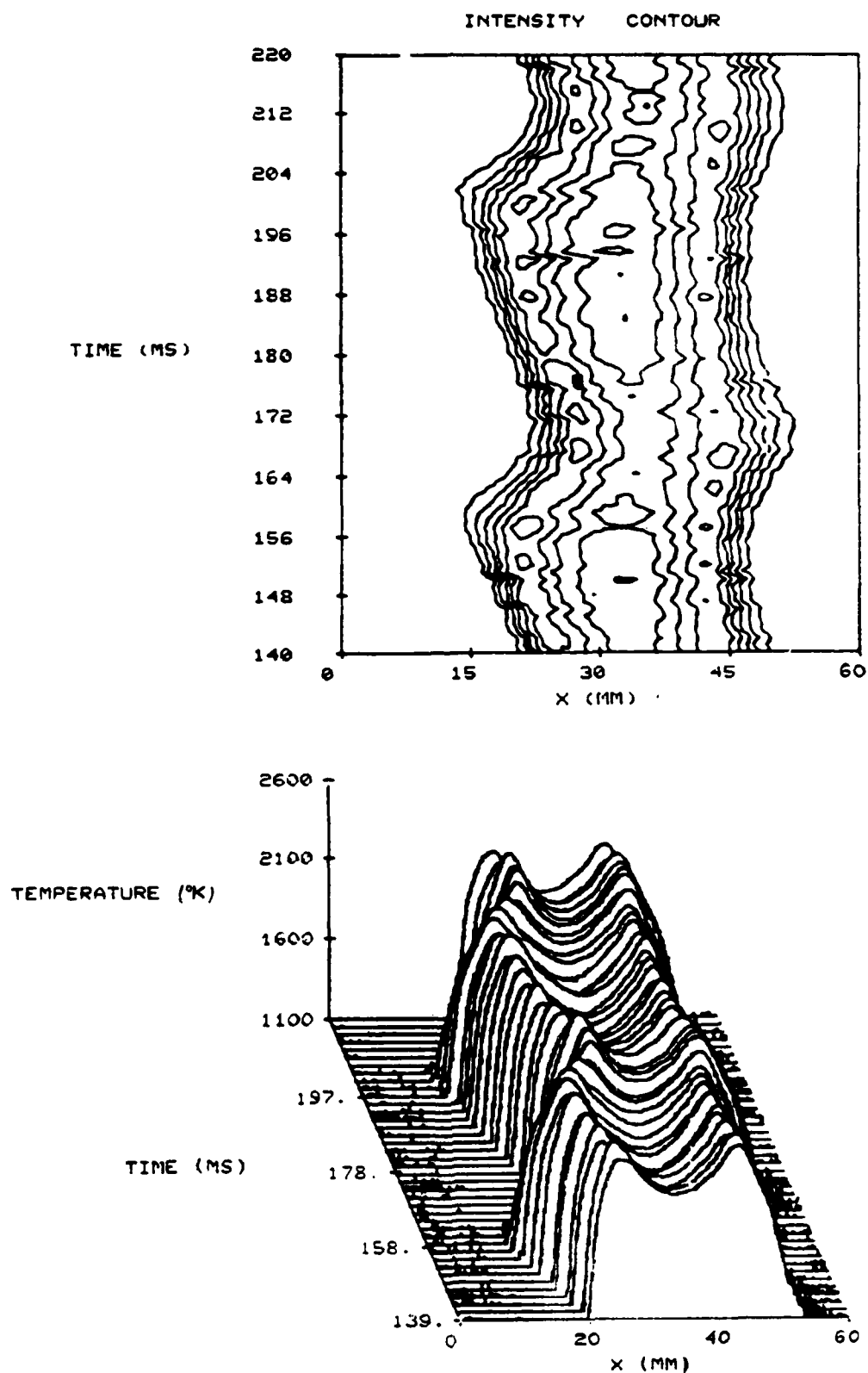


Fig. A-10 Temperature Profiles of N_2 -CO- H_2 Diffusion Flame and Intensity Contour Lines at 180 mm Axial Location, experiment D.

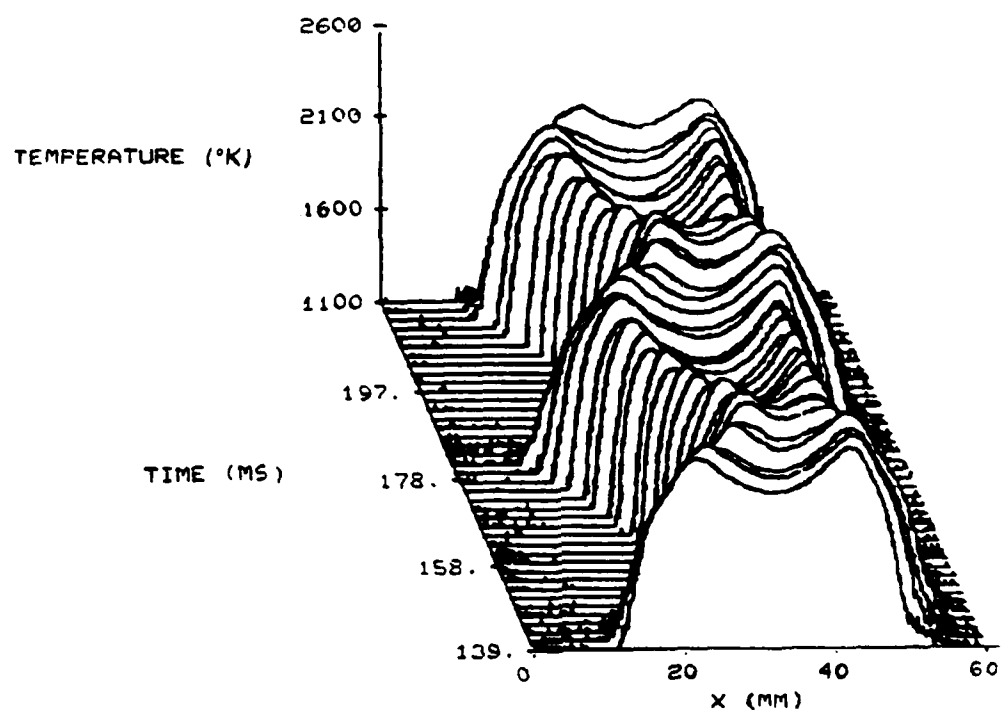
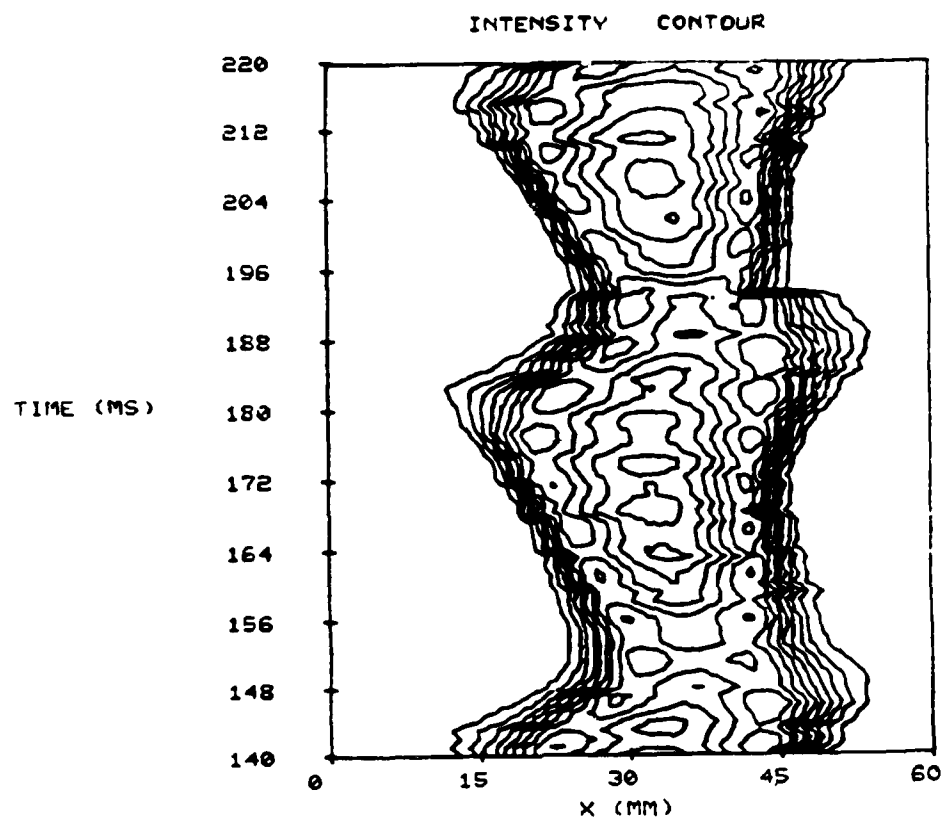


Fig. A-11 Temperature Profiles of N_2 -CO- H_2 Diffusion Flame and Intensity Contour Lines at 200 mm Axial Location, experiment D.

Appendix B: Temperature Profiles of N₂-CO-H₂ Diffusion
Flame and Intensity Contour Lines at Various
Axial Locations: Re = 2264

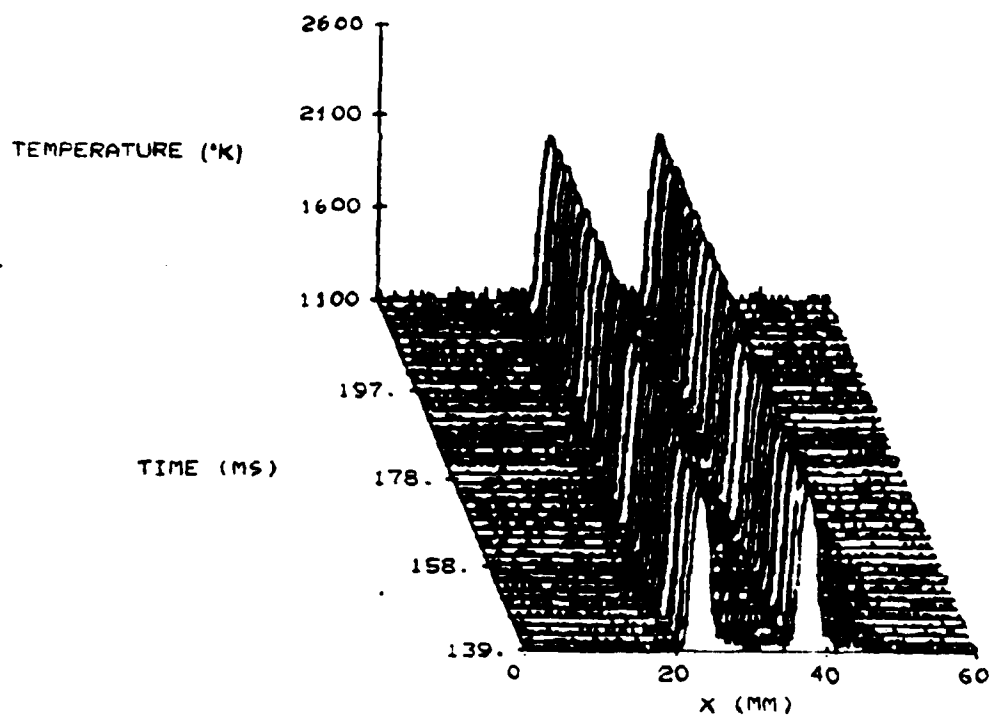
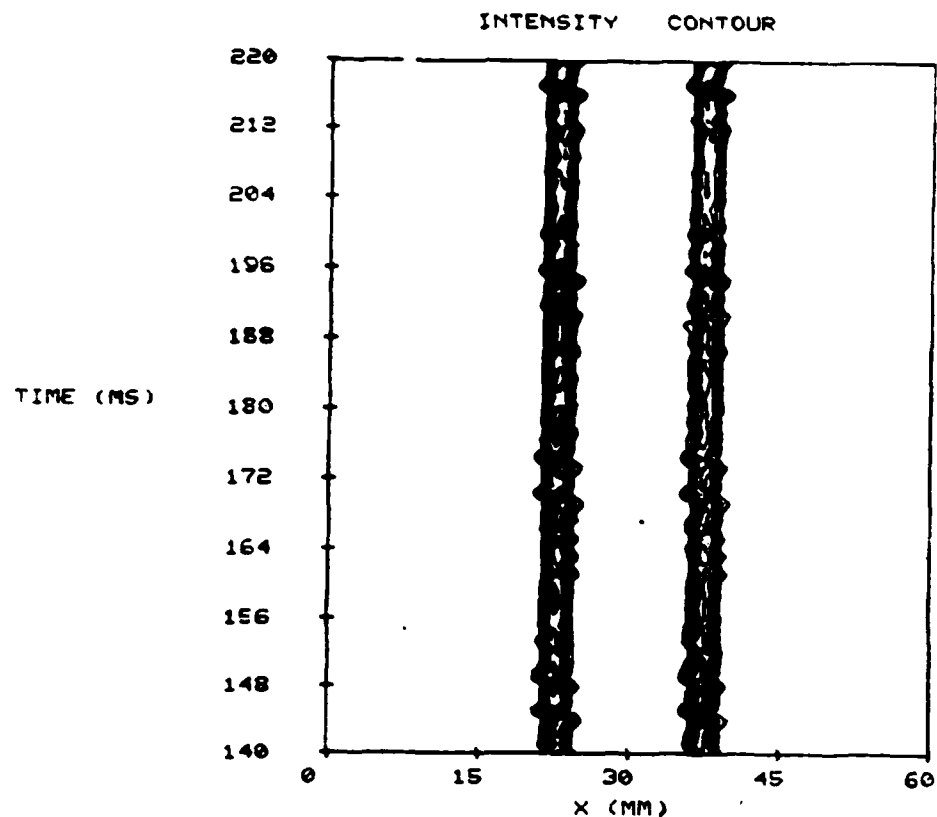


Fig. B-1 Temperature Profiles of N_2 -CO- H_2 Diffusion Flame and Intensity Contour Lines at 0 mm Axial Location, experiment E.

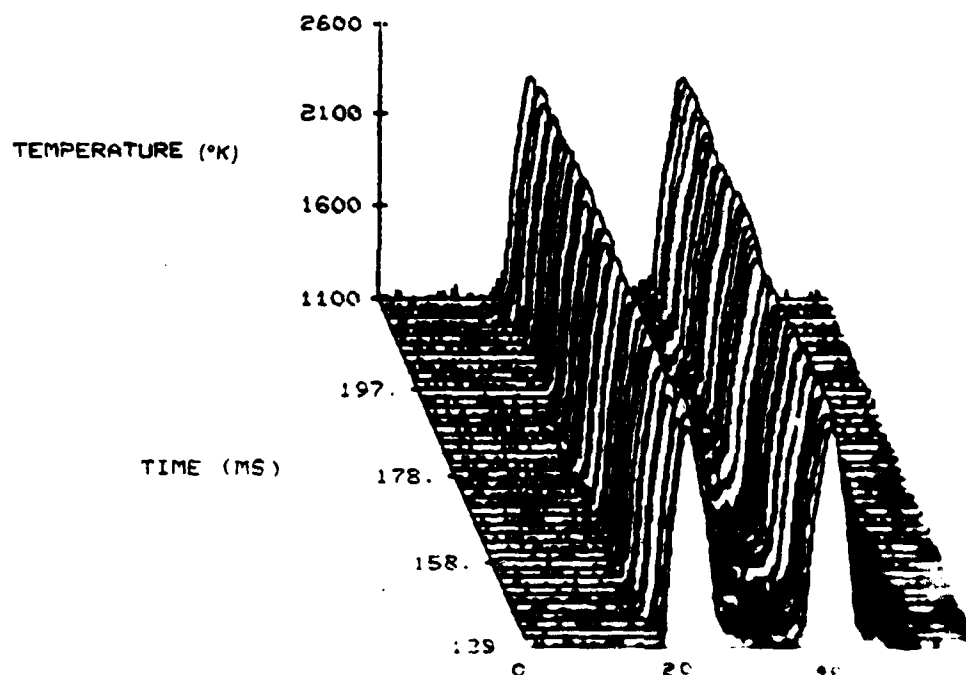
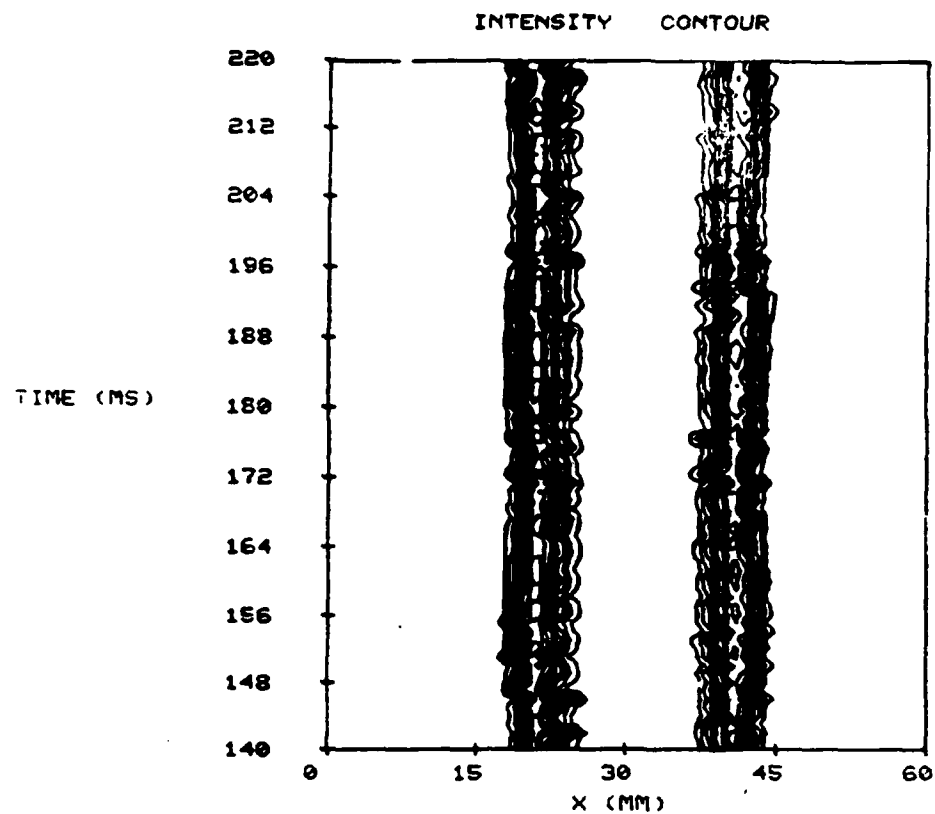


Fig. B-2 Temperature Profiles of N₂ Flame and Intensity for Axial Location experiment

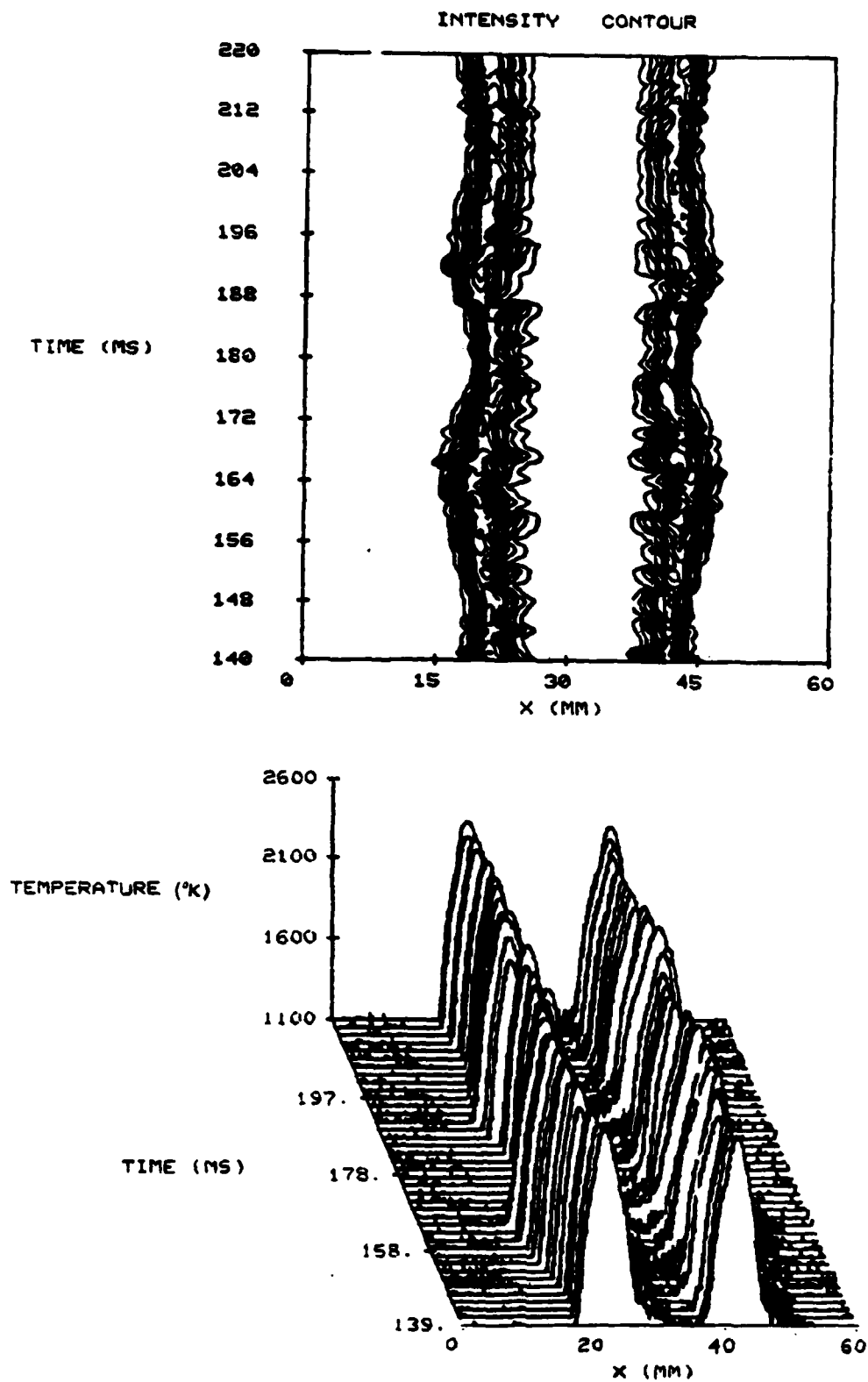


Fig. B-3 Temperature Profiles of N_2 -CO- H_2 Diffusion Flame and Intensity Contour Lines at 40 mm Axial Location, experiment E.

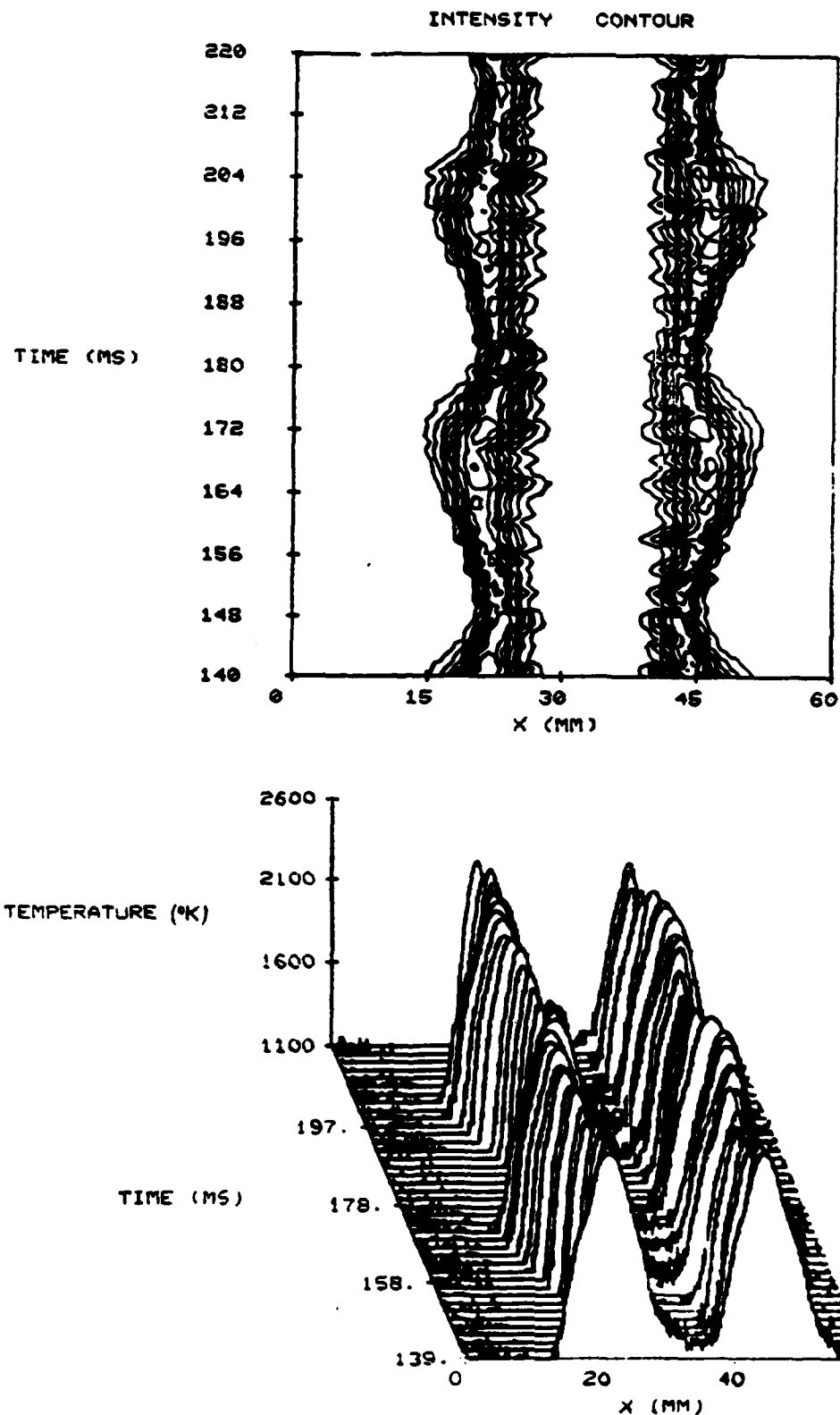


Fig. B-4 Temperature Profiles of N_2 -CO- H_2 Diffusion Flame and Intensity Contour Lines at 60 mm Axial Location. experiment E.

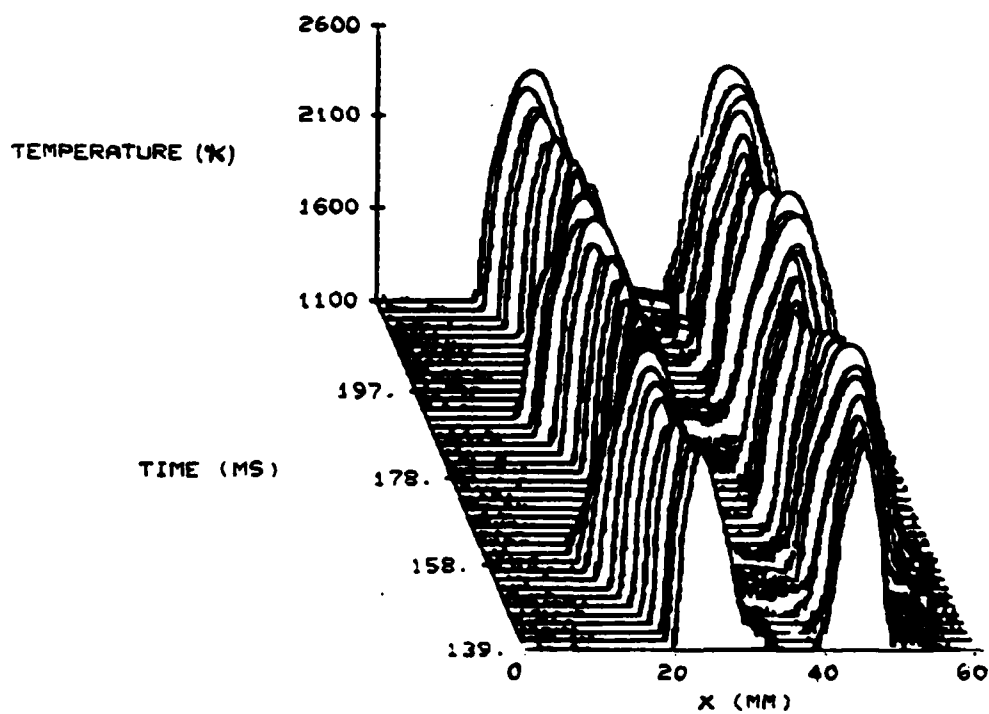
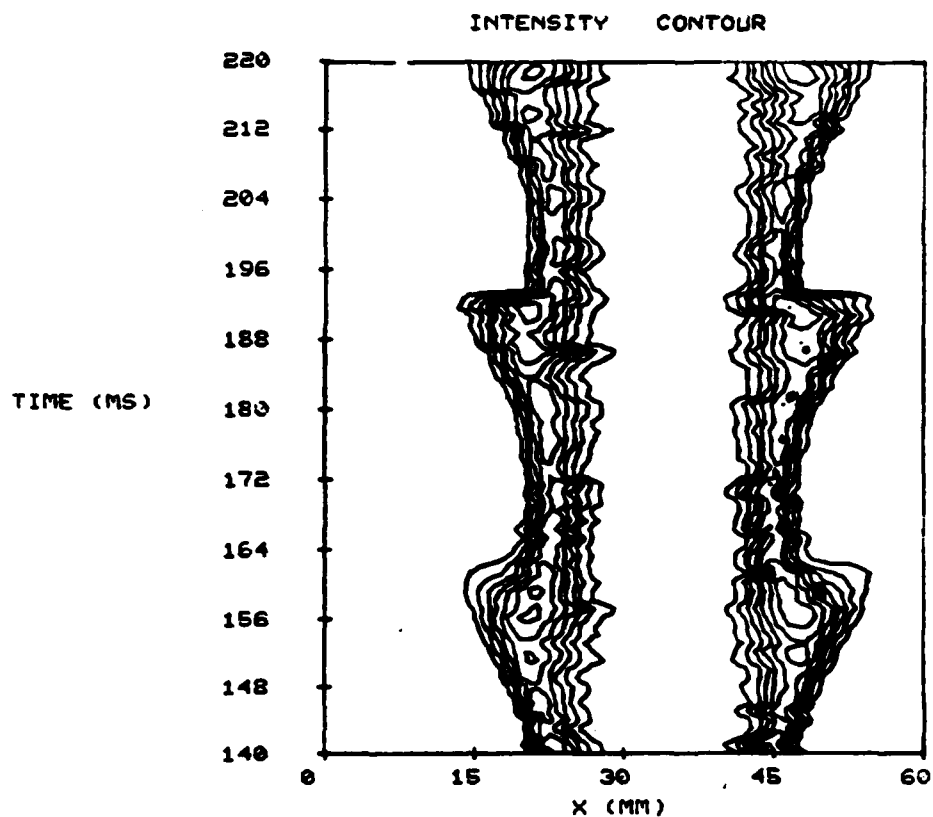


Fig. B-5 Temperature Profiles of N_2 -CO- H_2 Diffusion Flame and Intensity Contour Lines at 80 mm Axial Location, experiment E.

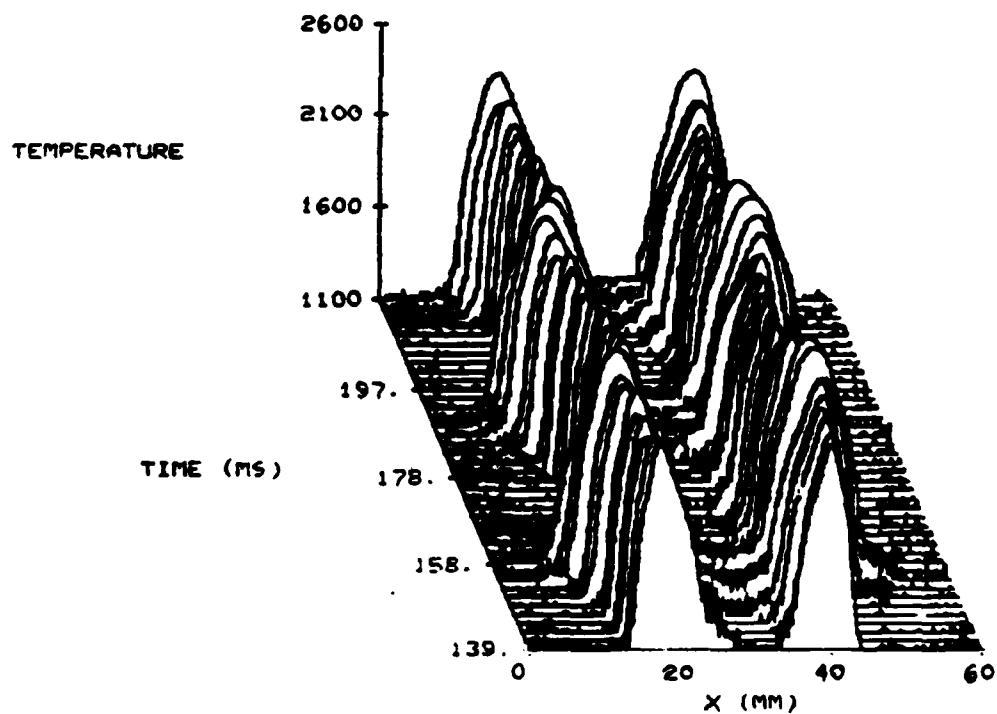
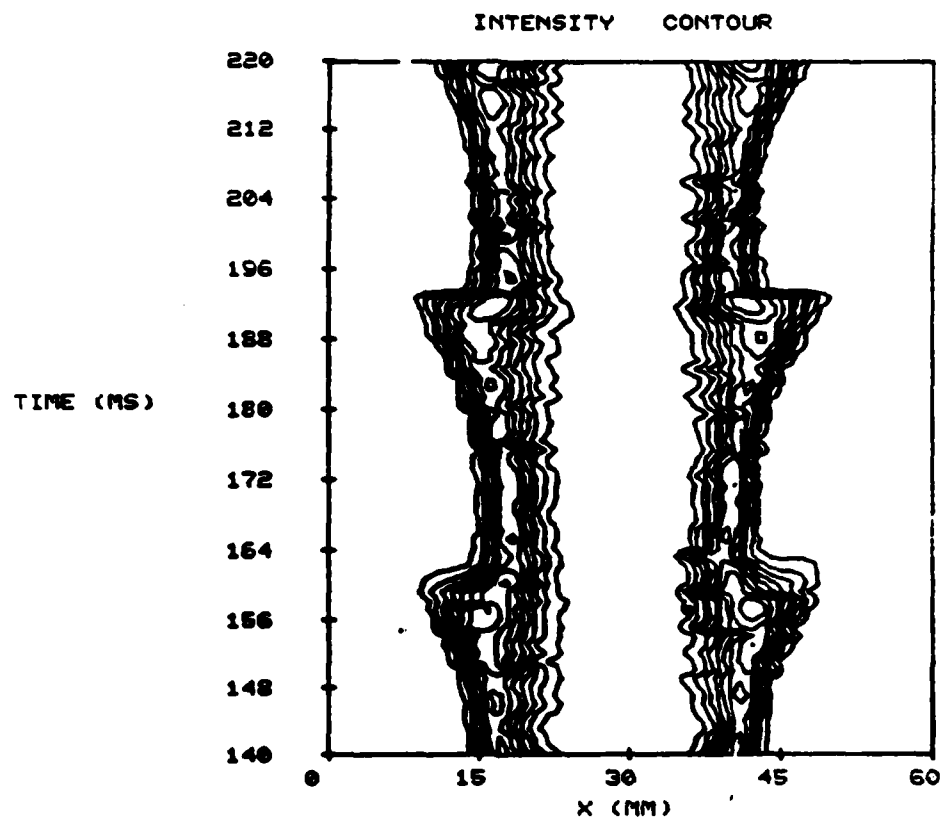


Fig. B-6 Temperature Profiles of N_2 -CO- H_2 Diffusion Flame and Intensity Contour Lines at 100 mm Axial Location, experiment E.

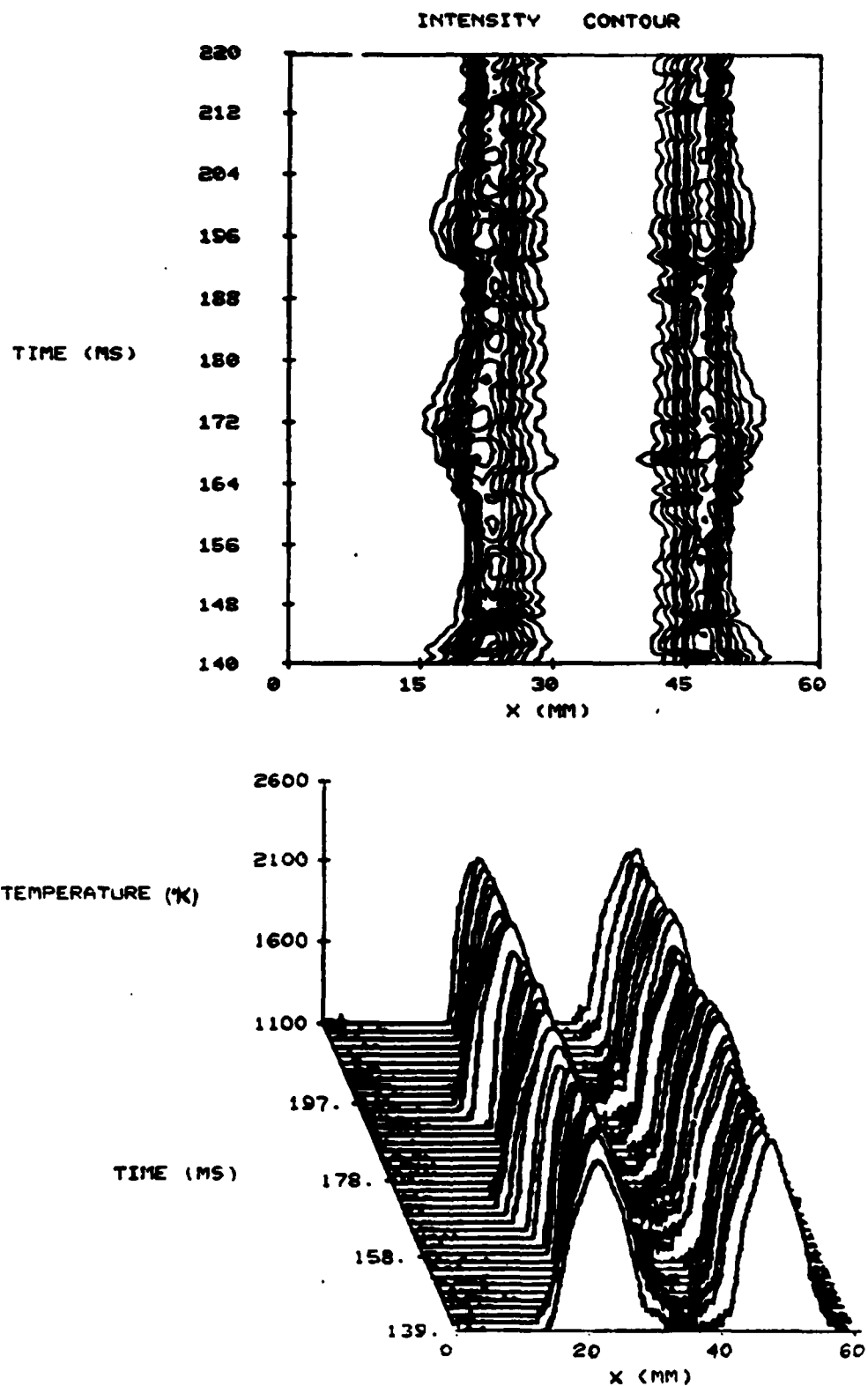


Fig. B-7 Temperature Profiles of N_2 -CO- H_2 Diffusion Flame and Intensity Contour Lines at 120 mm Axial Location, experiment E.

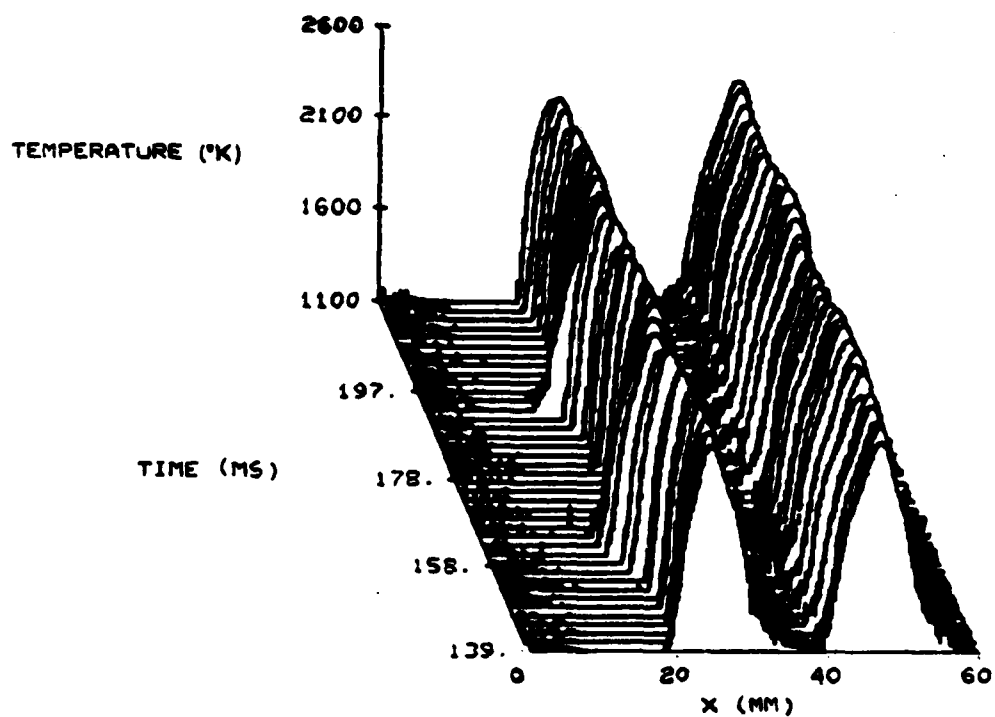
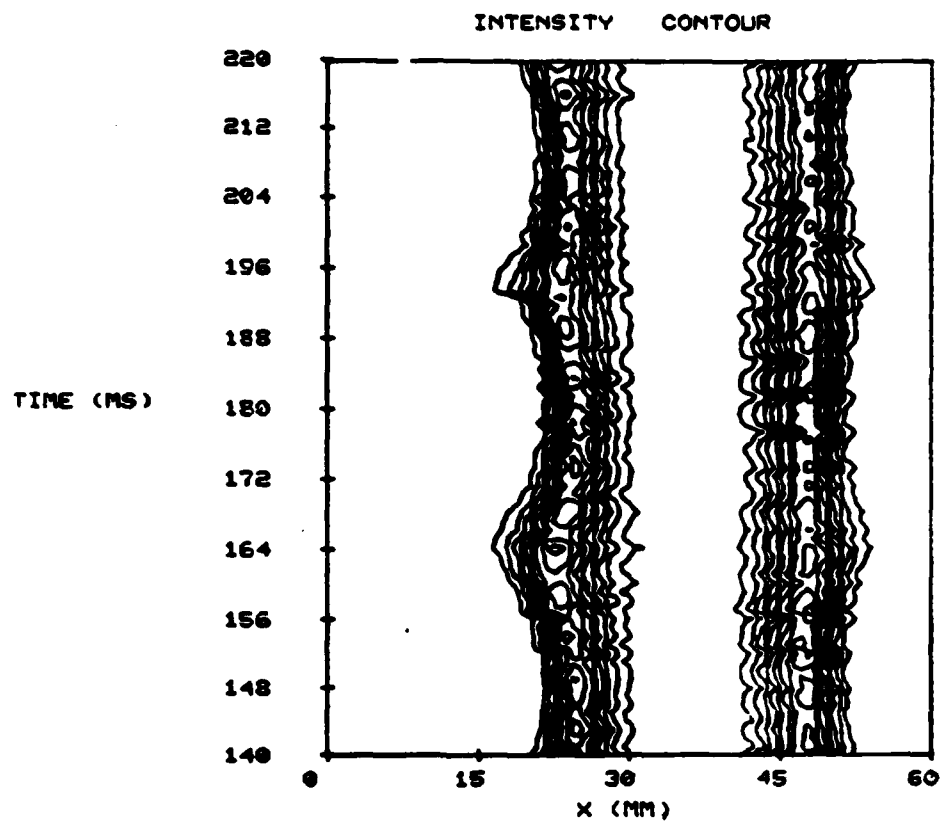


Fig. B-8 Temperature Profiles of $\text{N}_2\text{-CO-H}_2$ Diffusion Flame and Intensity Contour Lines at 140 mm Axial Location, experiment E.

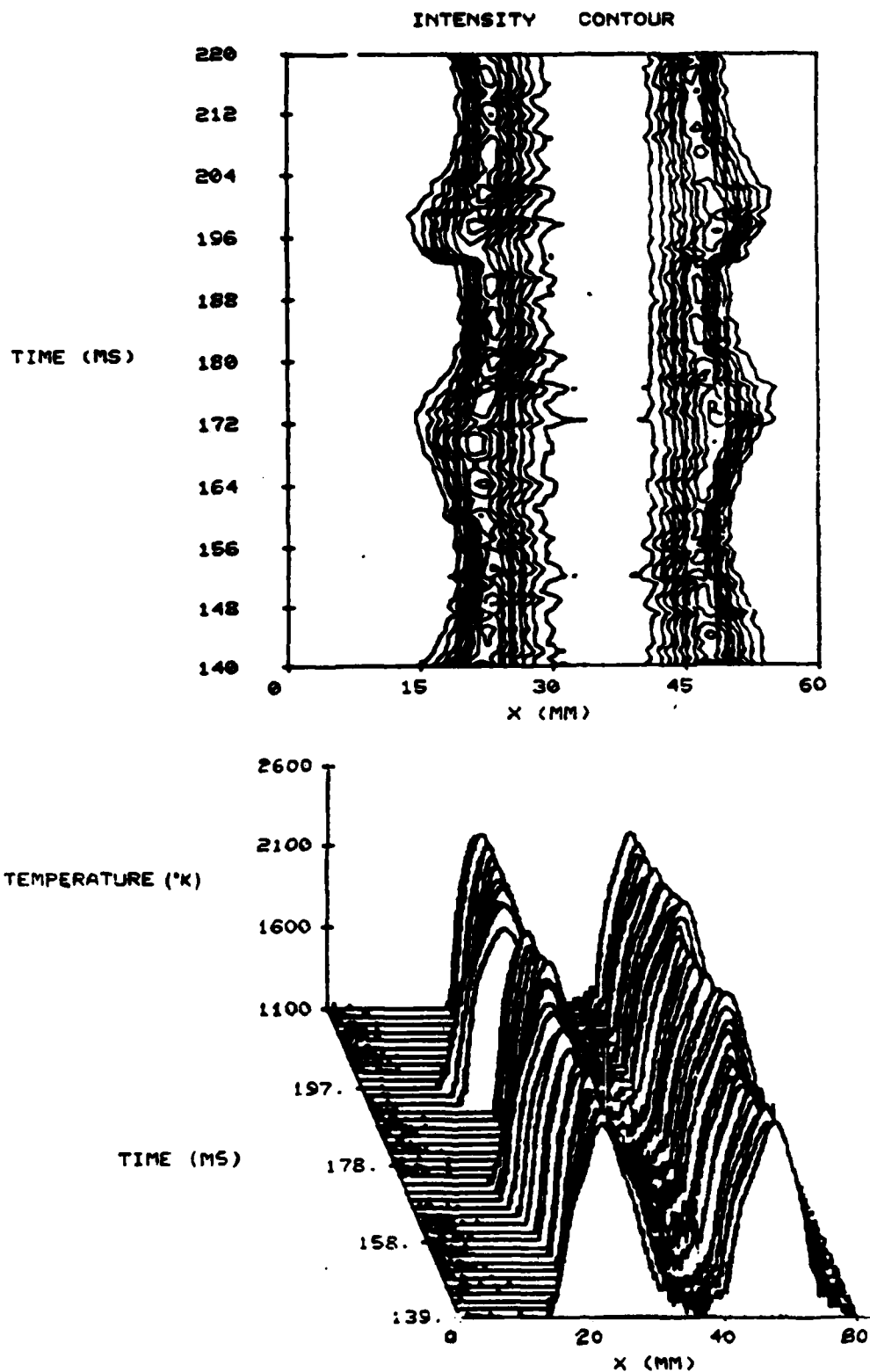


Fig. B-9 Temperature Profiles of N_2 -CO- H_2 Diffusion Flame and Intensity Contour Lines at 160 mm Axial Location, experiment E.

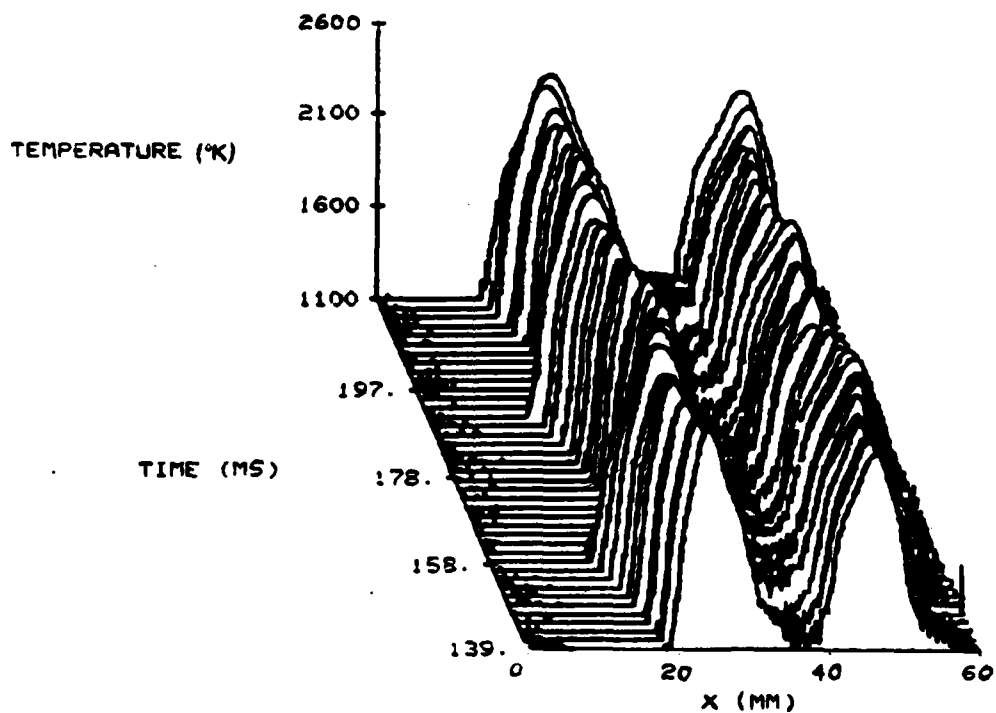
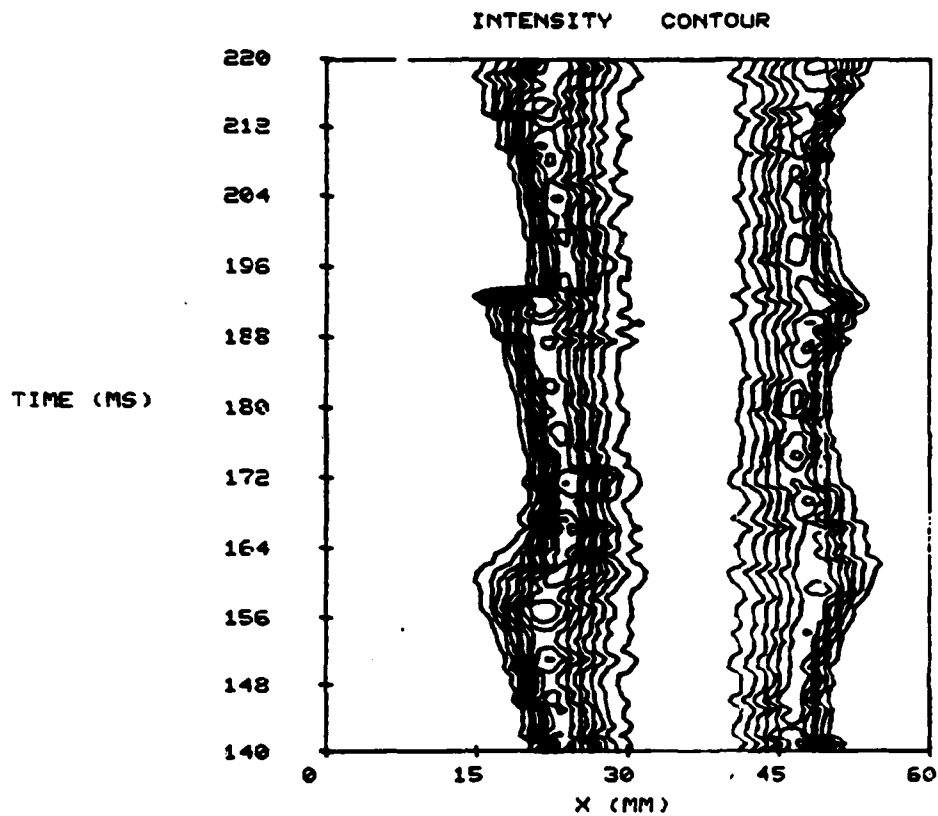


Fig. B-10 Temperature Profiles of N_2 -CO- H_2 Diffusion Flame and Intensity Contour Lines at 180 mm Axial Location, experiment E.

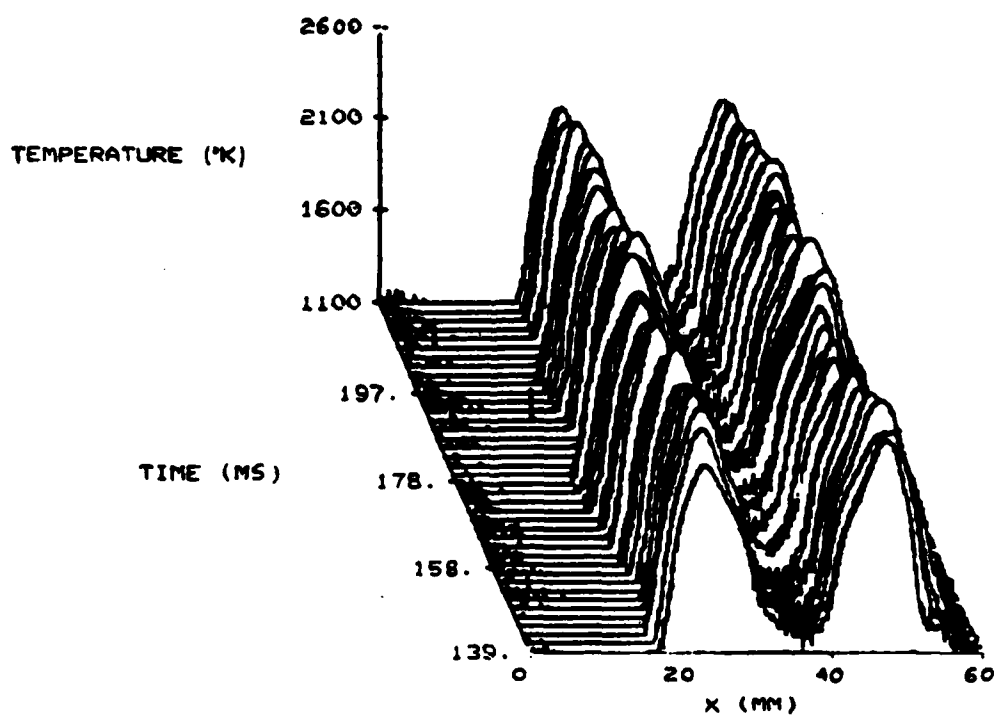
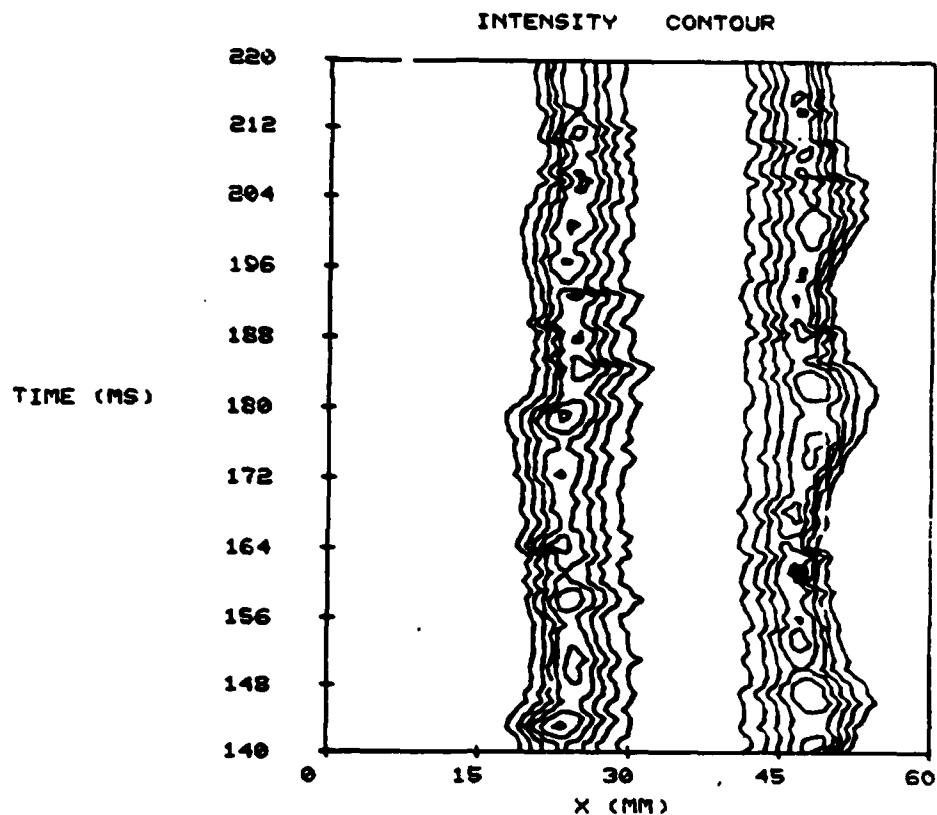


Fig. B-11 Temperature Profiles of N_2 -CO- H_2 Diffusion Flame and Intensity Contour Lines at 200 mm Axial Location, experiment E.

Appendix C: Temperature Profiles of N_2 -CO- H_2 Diffusion
Flame and Intensity Contour Lines at Various
Axial Locations; $Re = 2099$

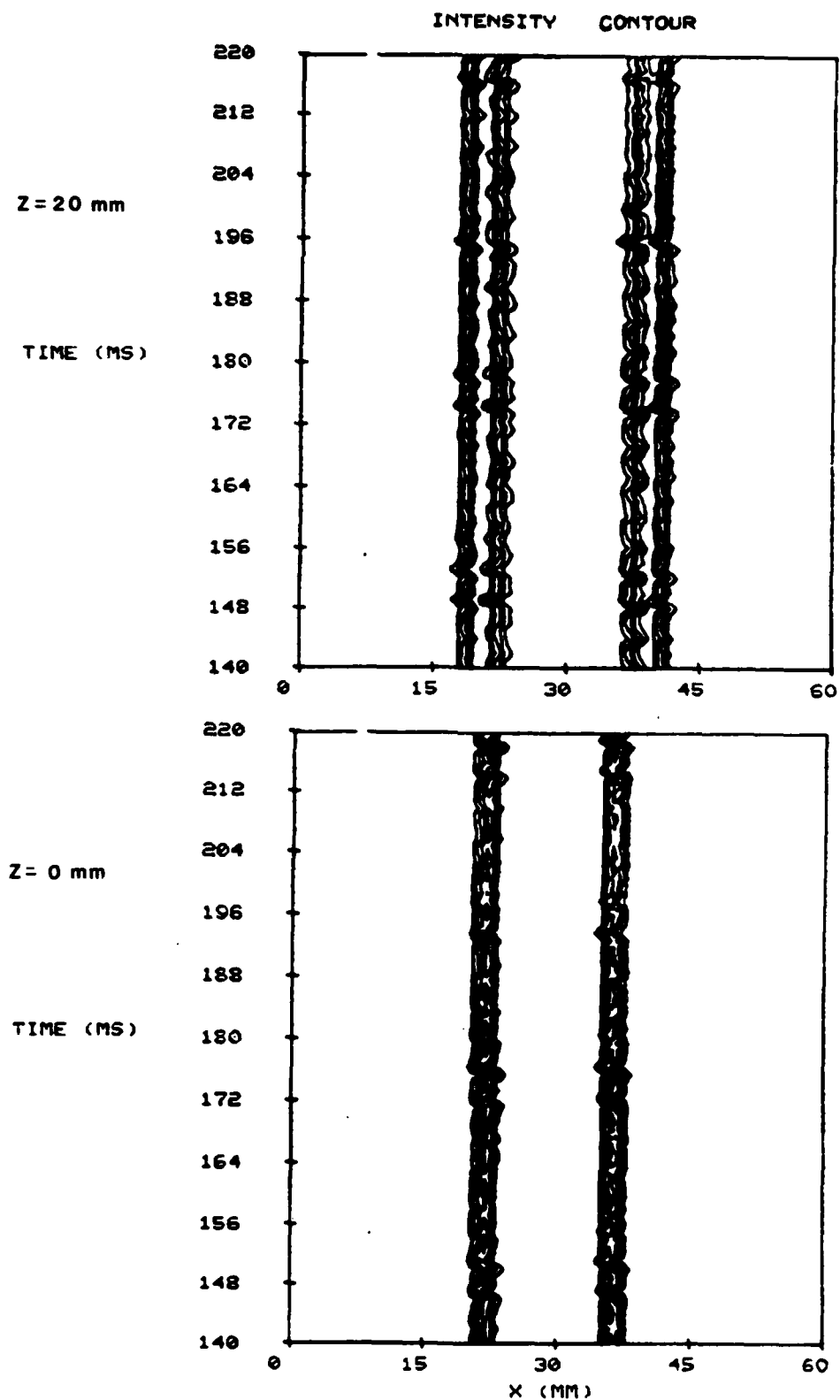


Fig. C-1 Temperature Profiles of $\text{N}_2\text{-CO-H}_2$ Diffusion Flame and Intensity Contour Lines at 0 mm and 20 mm Axial Location, experiment B.

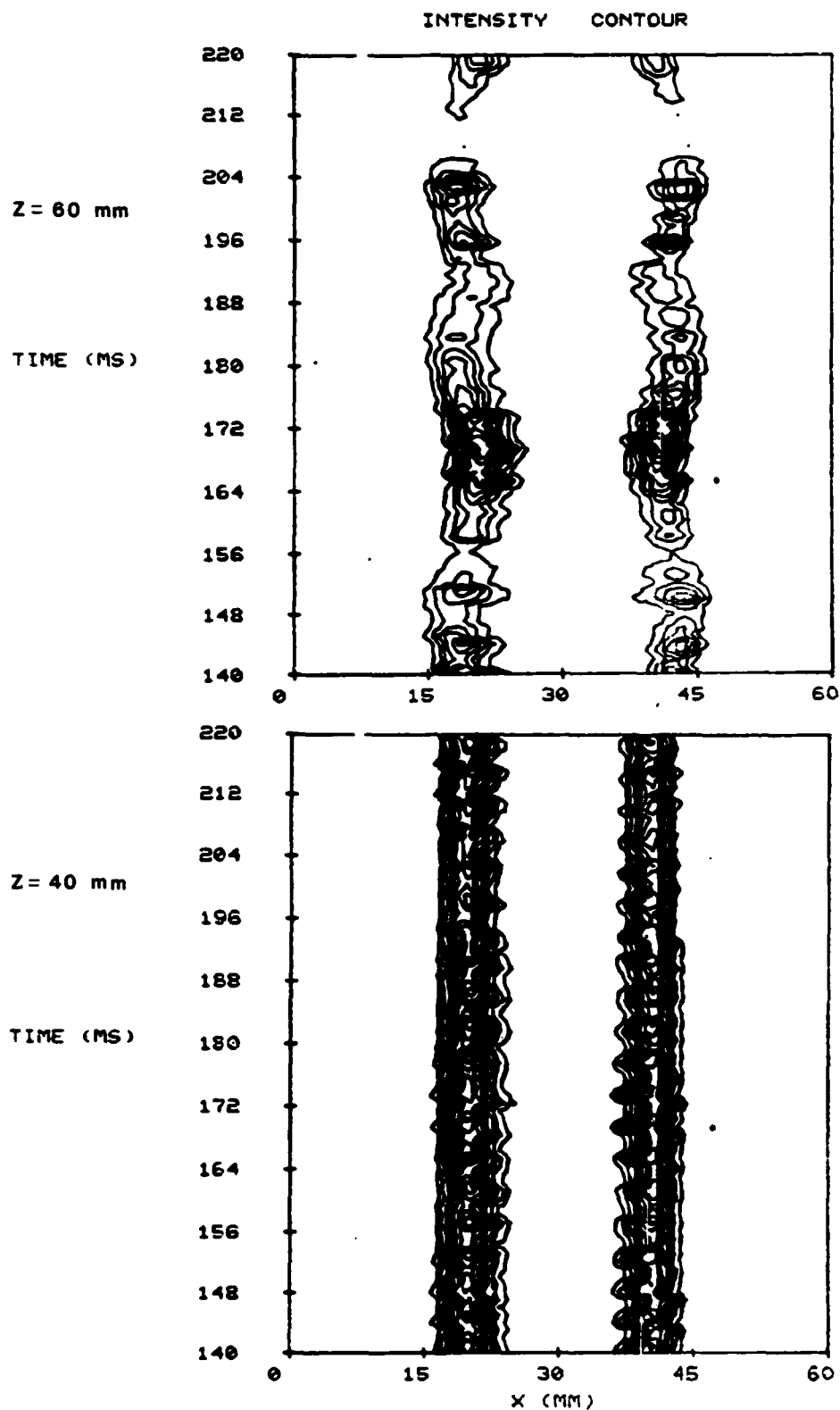


Fig. C-2 Temperature Profiles of N_2 -CO- H_2 Diffusion Flame and Intensity Contour Lines at 40 mm and 60 mm Axial Location, experiment B.

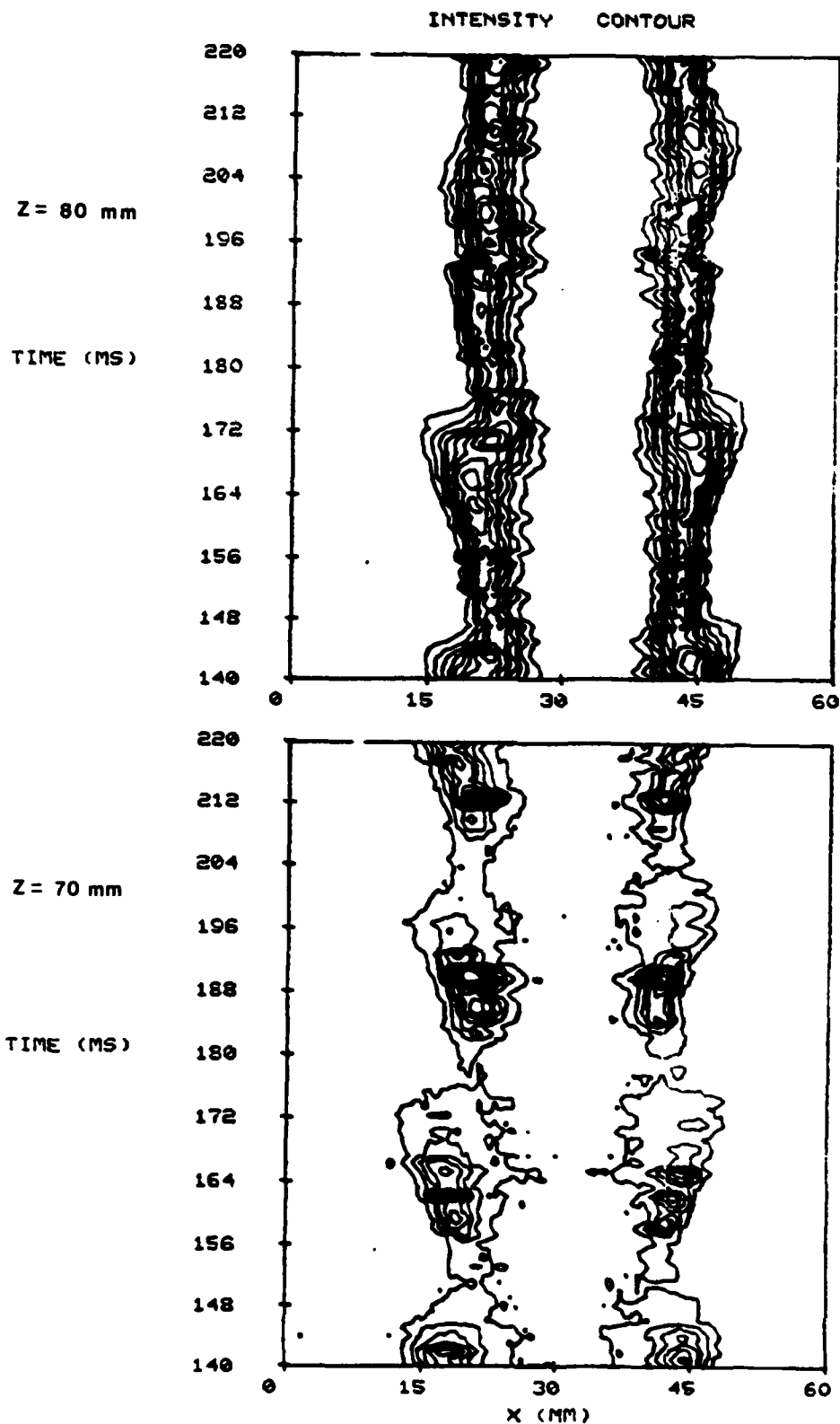


Fig. C-3 Temperature Profiles of N_2 -CO- H_2 Diffusion Flame and Intensity Contour Lines at 70 mm and 80 mm Axial Location, experiment B.

Appendix D: Temperature Profiles of N_2 -CO- H_2 Diffusion
Flame and Intensity Contour Lines at Various
Axial Locations: $\text{Re} = 1797$

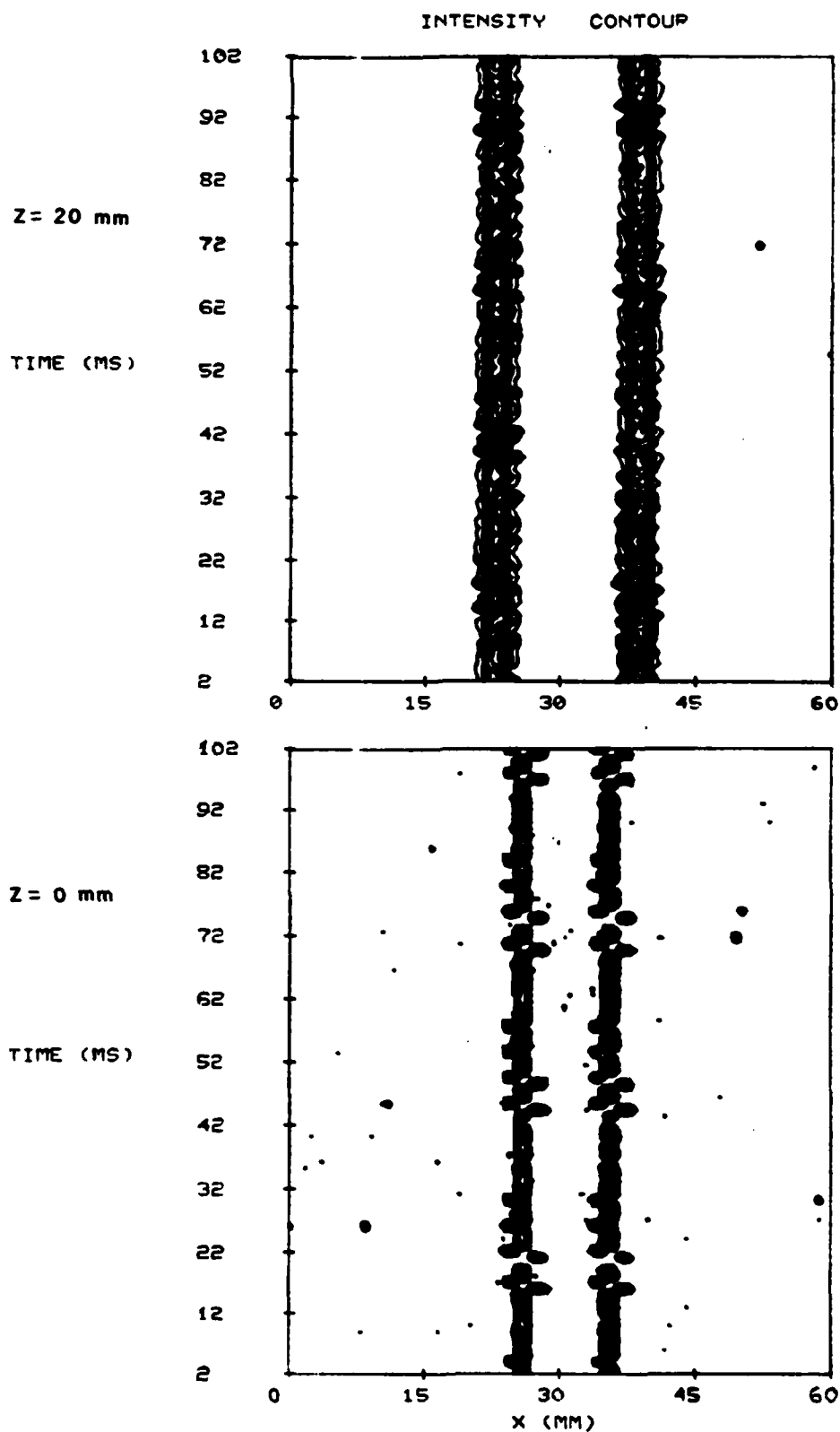


Fig. D-1 Temperature Profiles of $\text{N}_2\text{-CO-H}_2$ Diffusion Flame and Intensity Contour Lines at 0 mm and 20 mm Axial Location, experiment A.

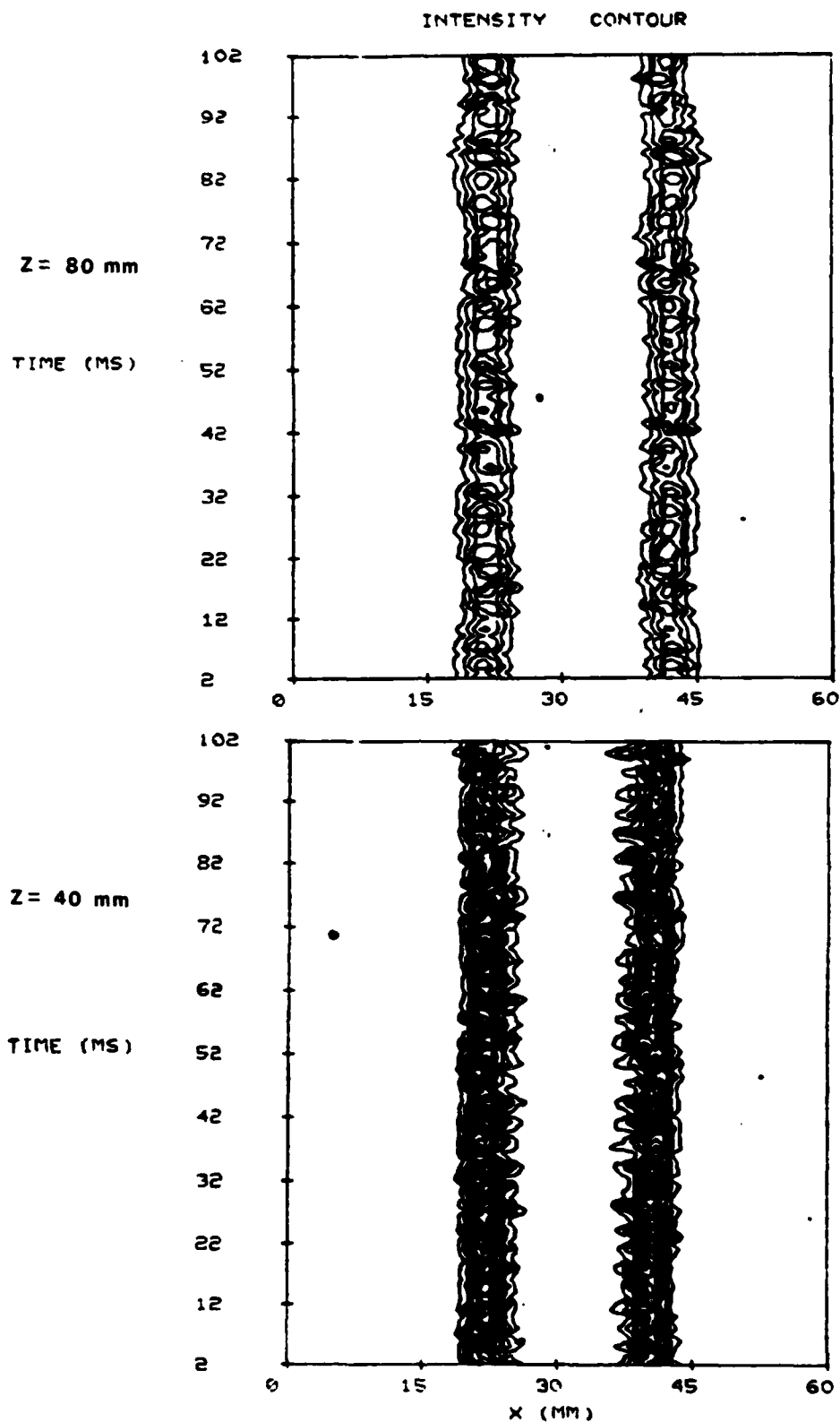


Fig. D-2 Temperature Profiles of N_2 -CO- H_2 Diffusion Flame and Intensity Contour Lines at 40 mm and 80 mm Axial Location, experiment A.

VITA

Moisés Fernández Alvaro was born on January 1, 1955, in Madrid, Spain. He graduated from High School in Madrid in 1972 and attended the Polytechnic University of Madrid, from which he received the degree of Master of Science in Aeronautical Engineering in July 1977, and in 1984 received the Master of Science in Physics. He entered Spanish Air Force in September 1978 and was assigned to the Material Command in which Quality Control, Workshop Design and Engineering Branches worked until entering the School of Engineering, Air Force Institute of Technology, in June 1986. He was promoted to major three months later.

Permanent address: Avenida Alfonso XIII, 143
28016-Madrid
Spain

UNCLASSIFIED

SECURITY CLASSIFICATION OF THIS PAGE

REPORT DOCUMENTATION PAGE

Form Approved
OMB No. 0704-0188

REPORT SECURITY CLASSIFICATION			1b. RESTRICTIVE MARKINGS		
2a. SECURITY CLASSIFICATION AUTHORITY			3. DISTRIBUTION/AVAILABILITY OF REPORT		
2b. DECLASSIFICATION/DOWNGRADING SCHEDULE			Approved for public release Distribution unlimited		
4. PERFORMING ORGANIZATION REPORT NUMBER(S)			5. MONITORING ORGANIZATION REPORT NUMBER(S)		
AFIT/GEP/ENP/87D-7					
6a. NAME OF PERFORMING ORGANIZATION	6b. OFFICE SYMBOL (if applicable)	7a. NAME OF MONITORING ORGANIZATION			
School of Engineering	AFIT/ENP				
6c. ADDRESS (City, State, and ZIP Code)			7b. ADDRESS (City, State, and ZIP Code)		
Air Force Institute of Technology Wright-Patterson AFB, OH 45433-6583					
8a. NAME OF FUNDING/SPONSORING ORGANIZATION Air Force Wright- Aero. Laboratories, Propulsion Lab	8b. OFFICE SYMBOL (if applicable) AFWAL/POOC	9. PROCUREMENT INSTRUMENT IDENTIFICATION NUMBER			
8c. ADDRESS (City, State, and ZIP Code)		10. SOURCE OF FUNDING NUMBERS			
Air Force Wright-Aero. Propulsion Lab Wright-Patterson AFB, OH 45433-6583		PROGRAM ELEMENT NO.	PROJECT NO.	TASK NO.	WORK UNIT ACCESSION NO.
11. TITLE (Include Security Classification)					
EXPERIMENTAL INVESTIGATION OF A CO-H ₂ DIFFUSION FLAME USING HIGH-FREQUENCY THERMOMETRY					
PERSONAL AUTHOR(S)					
Moises M. Fernandez Alvaro, M.S., Maj. SAF					
13a. TYPE OF REPORT	13b. TIME COVERED	14. DATE OF REPORT (Year, Month, Day)		15. PAGE COUNT	
MS Thesis	FROM _____ TO _____	December 1987		114	
16. SUPPLEMENTARY NOTATION					
17. COSATI CODES			18. SUBJECT TERMS (Continue on reverse if necessary and identify by block number)		
FIELD	GROUP	SUB-GROUP			
20	05		Atomic and molecular spectroscopy		
19. ABSTRACT (Continue on reverse if necessary and identify by block number)					
Thesis Chairman: Won B. Roh Ph.D. Professor of Physics Air Force Institute of Technology					
Approved for public release: LAW AFR 190-4. LYNN E. WOLAVER Dean for Research and Professional Development Air Force Institute of Technology (AFIT) Wright-Patterson AFB, OH 45433					
20. DISTRIBUTION/AVAILABILITY OF ABSTRACT			21. ABSTRACT SECURITY CLASSIFICATION		
<input type="checkbox"/> UNCLASSIFIED/UNLIMITED <input checked="" type="checkbox"/> SAME AS RPT <input type="checkbox"/> DTIC USERS			UNCLASSIFIED		
22a. NAME OF RESPONSIBLE INDIVIDUAL			22b. TELEPHONE (Include Area Code)	22c. OFFICE SYMBOL	
Won B. Roh Ph.D.			(513) 255 4498	AFIT/ENP	

↙

The purpose of this investigation was to measure the radial temperature profiles as a function of time in a non-sooting CO-H₂ diffusion flame at high repetition rates. Measurements were taken from the nozzle exit up to 200 mm above the nozzle in 10 mm increments. The results of such an analysis at Re=857 revealed the existence of low frequency (25-30 Hz) oscillating structures in the outside reaction layer associated with the dynamics of large scale buoyancy-driven vortices, and high frequency (300-325 Hz) oscillations believed to be associated with local instabilities of the internal jet core of the flame.

Other H₂-CO:N₂ gas mixtures (at Re=1717, 2099, and 2264) were investigated and similar high frequency oscillations were found.

In this research the novel thin filament pyrometry technique was employed; this technique relies upon the blackbody emission of a thin ceramic filament (SiC) in a combusting flowfield.

A limited Fourier Transform frequency analysis was carried out.

↖